Optimisation et caractérisation expérimentale des réseaux étendus à faible consommation d'énergie

Takwa Attia

Université Grenoble Alpes

THÈSE

Pour obtenir le grade de

DOCTEUR DE L'UNIVERSITÉ GRENOBLE ALPES

Spécialité : **Informatique**
Arrêté ministériel : 25 mai 2016

Présentée par

Takwa ATTIA

Thèse dirigée par **Martin HEUSSE**

et codirigée par **Andrzej DUDA**

Préparée au sein du **Laboratoire d'Informatique de Grenoble (LIG)**, dans **l'École Doctorale Mathématiques, Sciences et Technologies de l'Information, Informatique (EDMSTII)**.

Optimization and experimental characterization of Low Power Wide Area Networks

Thèse soutenue publiquement le **15 decembre 2021**, devant le jury composé de :

Fabrice Valois
Professeur, INSA Lyon, Rapporteur

Alexandre Guitton
Professeur, Université Clermont Auvergne, ISIMA, Rapporteur

Christelle Caillouet
Maître de Conférences, Université Côte d'Azur , Examinatrice

Didier Donsez
Professeur, Grenoble INP, Invité

Martin Heusse
Professeur, Grenoble INP, Directeur de thèse

Andrzej Duda
Professeur, Grenoble INP, Co-Directeur de thèse

Abstract

Low Power Wide Area Networks (LPWAN) are getting increased interest from academia and industry. They utterly address the Internet of Things (IoT) needs for low power and long-range networks, providing efficient connectivity over wide areas and enabling innovative applications.

This thesis focuses on the LoRa/LoRaWAN technology, a promising LPWAN candidate, which offers many advantages but presents some challenges in terms of scalability and reliability.

In the first part of this thesis, we study, evaluate, and characterize the LoRaWAN network link quality; then, we consider one of the major limitations of the technology, namely the channel access, by proposing a technique to improve the capacity of the network.

In the first contribution, we explore the actual LoRaWAN network state by monitoring all traffic on a LoRaWAN gateway and, subsequently, conducting a thorough analysis of the current practice for setting the different parameters by the ambient traffic.

In the second contribution, we evaluate and characterize the transmission quality of LoRa links by measuring the Packet Reception Rate (PRR) as a function of the payload length. We conducted extensive experiments on a test-bed in The Things Network (TTN) and investigated the resulting analysis, which shows only a slight impact on the payload length on PRR.

In the third contribution, we characterize the wireless channel experimentally, determine its behavior, and examine what factors depend on it. For both an indoor and outdoor sender, we have identified different patterns, considering the time variability of the channel at different gateways.

Finally, we address one of the major limiting factors in LoRaWAN networks, the Aloha-like access method. We study how the Message In Message (MIM) technique for LoRaWAN would have the potential to improve the network capacity. We show that while LoRaWAN with capture effect only allows reaching 23% of the channel utilization, MIM enables us to increase this utilization rate up to 35% in a single LoRaWAN cell scenario.

Résumé

Les réseaux étendus à faible consommation d'énergie (LPWAN) connaissent un élan sans précédent et suscitent un intérêt croissant de la part des universités et de l'industrie. Ils répondent parfaitement aux besoins d'un réseau à faible consommation d'énergie et à longue portée, capables de fournir une connectivité efficace dans une vaste zone pour construire l'Internet des objets (IoT) à grande échelle.

Cette thèse se concentre sur la technologie LoRa/LoRaWAN, un candidat LPWAN prometteur, qui offre de nombreux avantages mais présente quelques défis en termes d'évolutivité et de fiabilité. Pendant cette thèse, nous avons commencé par considérer l'étude, l'évaluation et la caractérisation de la qualité du lien radio du réseau LoRaWAN ; puis nous avons envisagé de remédier à une limitation majeure de la technologie, la méthode d'accès, en proposant une technique pour améliorer la capacité du réseau.

Dans un premier temps, nous explorons l'état actuel du réseau LoRaWAN en surveillant une passerelle LoRaWAN et en effectuant une analyse approfondie des différents paramètres utilisés par le traffic ambient.

Dans un second temps, nous évaluons et caractérisons la qualité de transmission des liens LoRa en mesurant le taux de réception de paquets (PRR) en fonction de la longueur de la charge utile. Nous avons mené de multiples expériences sur le réseau The Things Network (TTN). Elles ne montrent qu'un léger impact de la longueur de la charge utile sur le PRR.

Dans la troisième partie, nous caractérisons expérimentalement le canal sans fil en déterminant son comportement global et en examinant de quels facteurs ce comportement dépend. Pour un émetteur placé à l'intérieur ou à l'extérieur, nous étudions le comportement du sous-canal et concluons sur la façon dont il affecte le canal global agrégé. Enfin, nous explorons la variabilité temporelle du canal pour différentes passerelles et caractérisons les differents comportement possibles. Enfin, nous abordons l'un des principaux facteurs limitant des réseaux LoRaWAN, la méthode d'accès de type Aloha. Nous étudions comment la technologie Message In Message (MIM) pour LoRaWAN améliore la capacité du réseau en développant un modèle analytique et une simulation détaillés dans NS-3. Alors que LoRaWAN avec effet de capture ne permet d'utiliser que 23% de la capacité du canal, nous montrons que l'intégration de MIM permet d'augmenter ce taux d'utilisation jusqu'à 35% dans un scénario de cellule LoRaWAN unique.

Contents

List of Figures

List of Tables

List of Acronyms

$RSSI_m$	mean RSSI. 91
SF	Spreading Factor. 10, 11, 34, 35, 40, 43–45, 51, 53, 55, 63, 64, 68, 73, 75–84, 86–94, 96, 97, 106, 107, 116
3GPP	The 3rd Generation Partnership Project. 20, 36
ABP	Activation By Personalization. 68
ADR	Adaptative Data Rate. 21, 26, 57
BLE	Bluetooth Low Energy. 20, 33
BPSK	Binary Phase Shift Keying. 35
BW	Bandwidth. 13, 34, 35, 43–45, 68, 75
CDMA	Code Division Multiple Access. 36, 37, 39
CR	Coding Rate. 22, 34, 35, 43, 75, 84, 85
CSS	Chirp Spread Spectrum. 20, 33, 56
ETSI	European Telecommunications Standards Institute. 20, 73
FCC	Federal Communications Commission. 73
GSM	Global System for Mobile. 36
HAL	Hardware Abstraction Layer. 47, 48
IEEE	Institute of Electrical and Electronics Engineers. 20
IETF	Internet Engineering Task Force. 20
IoT	Internet of Things. 3, 5, 19, 20, 31, 33, 36, 38
ISM	Industrial, Scientific and Medical. 5, 13, 31, 34, 35, 37, 39, 41–43, 55, 56, 73

LBT Listen-Before-Talk mechanism. 37

LoRa Long Range. 5, 9, 13, 20–22, 24–26, 31, 33–35, 37–48, 53, 55, 56, 115

LoRaWAN Long Range Wide Area Network. 9, 20–26, 33–35, 37, 38, 43, 46–49, 52–55, 57, 63, 100, 102, 105, 106, 113, 115

LPWAN Low Power Wide Area Networks. 3, 13, 20, 21, 25, 26, 33–37, 39, 56, 115

LTE Long Term Evolution. 36, 38

LTE-M Long Term Evolution for Machines. 20, 34

MAC Medium Access Control. 6, 9, 13, 31, 33–35, 39, 46, 51, 52, 57

MIM Message In Message. 3, 23, 26, 115

NB-IoT Narrow Band IoT. 20, 26, 31, 33, 36–39, 115

NS-3 Network Simulator Version 3. 25–27, 100, 103–105, 113

OFDMA Orthogonal Frequency-Division Multiple Access. 36

OTAA Over The Air Activation. 68

PAN Personal Area Network. 19, 20, 33

QoS Quality of Service. 37

RFID Radio-Frequency Identification. 20

RFU Reserved for Future Use. 44, 68

RPMA Random Phase Multiple Access. 26, 31, 33, 36, 37

RSSI Received Signal Strength Indicator. 65, 73, 82, 86, 89–93, 95, 97, 101, 113

SC-FDMA Single-Carrier Frequency-Division Multiple Access. 36

SNR Signal Noise Ratio. 10, 48, 53, 54, 64, 65, 78, 80–82, 97, 116

SPI Serial Peripheral Interface. 47, 48

ToA Time on Air. 42

TP Transmission power. 10, 34, 35, 42, 44, 53, 55, 63, 75–78, 84, 91

TTN The Things Network. 21

UNB Ultra Narrow Band. 35

WWAN Wireless Wide Area Networks. 20, 33

List of Publications

- **Attia**, **T.**, Heusse, M., Tourancheau, B., & Duda, A. (2019, December). Experimental Characterization of LoRaWAN Link Quality. In 2019 IEEE Global Communications Conference (GLOBECOM) (pp. 1-6). IEEE.
- **Attia**, **T.**, Heusse, M., Tourancheau, B., & Duda, A. (2019, June). Experimental Characterization of Packet Reception Rate in LoRaWAN. In Rencontres Francophones sur la Conception de Protocoles, l'Évaluation de Performance et l'Expérimentation des Réseaux de Communication.
- Heusse, M., **Attia**, **T.**, Caillouet, C., Rousseau, F., & Duda, A. (2020, November). Capacity of a lorawan cell. In Proceedings of the 23rd International ACM Conference on Modeling, Analysis and Simulation of Wireless and Mobile Systems (pp. 131-140).
- **Attia**, **T.**, Heusse, M., & Duda, A. (2021, July). Message in Message for Improved LoRaWAN Capacity. In 2021 International Conference on Computer Communications and Networks (ICCCN) (pp. 1-9). IEEE.
- **Attia**, **T.**, Heusse, M., & Duda, A. LoRaWAN Wireless Channel Characterization: Indoor Versus Outdoor sender, to be submitted, 2022.

Introduction

0.1 Context

The proliferation of ubiquitous IoT devices and the burgeoning of cellular networks are revolutionizing our lives, providing us with a plethora of diverse and tremendous added-value services and applications. IoT services span several domains [10, 11, 12], and their application varies from one field to another; for instance, we cite smart cities, smart homes, smart grid, industrial IoT, and smart supply chain.

Billions of internet-connected devices can sense, communicate, interact, compute, make intelligent decisions and actuate. Their number is growing phenomenally; it is expected that by 2023 connected devices will be four times as numerous on Earth as humans, reaching more than 30 billion connected devices [13]. Around 18 billion out of 30 billion connected devices will be IoT-related [13]. Besides their massive number, IoT devices exist in a broad scope of varieties, comprising many capabilities and constraints. While some of these devices present the advantage of being portable, lightweight, and can be deployed in harsh environments, they are battery-powered and consequently present an energy constraint, as their batteries are required to last for years.

Building a one-size-fits-all general IoT architecture suitable for all the services is highly complex in the context of the vast scope of IoT devices and applications emergence. Consequently, diverse architectures, numerous protocols, built-in services and networks exist on the market, and each is designed to respond to specific needs and requirements. Moreover, with the ever-evolving market of IoT applications, new use cases emerge and stress the need for a network where IoT battery-powered devices are able to send short information from a long-range distance, all being energy-efficient to have the maximum battery lifetime.

However, existing legacy wireless networks such as cellular networks or Personal Area Network (PAN) do not respond to both requirements: long-range connectivity and low energy consumption.

On the one hand, while PAN like Bluetooth Low Energy (BLE), Radio-Frequency Identification (RFID), Zigbee, and 802.15.4 provide low power connectivity, the signal communication range is short, spanning only a few meters.

On the other hand, most of Wireless Wide Area Networks (WWAN), i.e., cellular networks, offer high-efficient long-range connectivity with advanced radios but at the cost of relatively high power consumption and high cost of deployment.

In this context, LPWAN emerge as a new communication paradigm [14], which complements legacy cellular and short-range wireless technologies in addressing specific IoT applications' low power and long-range requirements. Multiple organizations and standardizations entities are working toward the proposition and improvements of open standards for LPWAN like, Internet Engineering Task Force (IETF) [15], European Telecommunications Standards Institute (ETSI) [16], The 3rd Generation Partnership Project (3GPP) [17], Institute of Electrical and Electronics Engineers (IEEE). Some industrial alliances such as the LoRa alliance [18], WEIGHTLESS-SIG [19], DASH7 Alliance [20] are built around individual LPWAN technologies to develop new standards. As a result, multiple LPWAN are proposed and are under continuous improvement and evaluation. They can be divided into technologies operating in the unlicensed spectrum like LoRa or Sigfox and licensed spectrum technologies like Narrow Band IoT (NB-IoT) or Long Term Evolution for Machines (LTE-M), proposed by 3GPP, and derived from existing cellular technologies.

LPWAN employ specific modulations that ensure low power consumption while achieving long communication ranges.

Several growing IoT applications exploit LPWAN, like smart cities [21], smart buildings [22], smart island [23], smart agriculture [24], and many others.

In these applications, devices are required to send an infrequent small amount of data at a low data rate, of the order of kilobits per second, ensuring low power consumption and fair channel sharing. For the applications with low traffic, unlicensed spectrum solutions are well suited.

LoRa/LoRaWAN is one of the emerging LPWAN where LoRa defines a specific radio layer based on the Chirp Spread Spectrum (CSS) modulation [25], much different from the modulations used in other types of wireless networks. LoRaWAN [26] defines the frame formats, access and mobility procedures, security, network joining, and network architecture. The access method to the radio channel is ALOHA: the device wakes up and sends a packet to the gateway right away. CSS modulation results in good sensitivity levels enabling transmissions over long distances: a range of several kilometers outdoors and hundreds of meters indoors; this modulation is at the heart of the success of LoRa along with other factors. Indeed, among all the existing LPWAN, LoRa seems to lead the race to become the defacto standard for multiple current LPWAN applications deployment. This success drives the research community to explore and investigate its performance in

depth.

First, unlike other LPWAN, LoRaWAN offers the possibility of building and deploying an independent, self-run networks, which represents a precious and attractive opportunity to both industrial and academic communities. Consequently, academics are able to build their testbeds, evaluate and explore the network characteristics and limitations, hence fostering the improvements of the LoRaWAN protocol with research-based optimizations and propositions.

Furthermore, LoRaWAN requires simple infrastructure, making its installation affordable and low cost in a large-scale network deployment. As a result, LoRa is one of the most deployed LPWAN, present in 154 countries with the free-of-charge collaborative The Things Network (TTN) network [27]. Moreover, LoRaWAN has the benefit of being built and maintained by the LoRa alliance, a group of industrials that participate in developing the protocol. Compared to other LPWAN, LoRa manifests more flexibility within the standard as it exhibits many radio parameters that we can tune for instance to trade data rate for range. Finally, LoRaWAN has the Adaptative Data Rate (ADR) mechanism, which allows to dynamically adapt the LoRa parameters to the best ones when enabled, providing the technology with more adaptability to the environment and channel changes.

0.2 Motivations

The rise of LoRa as a promising technology and the need to effectively investigate its characteristics and evaluate its reliability are among the fundamental motivations behind the first part of our investigations and contributions of the thesis.

Due to the significant support from the LoRa alliance community, LoRaWAN benefits from many endorsements reports, sometimes skewed, and many non-confirmed assumptions often used in the performance evaluation process.

Besides that, like any growing network, studying the LoRa network's reliability and investigating its performance are of utmost interest to the industrial and research community.

Many authors have evaluated the LoRa performance and scalability with analytical modeling [28, 29], simulation [30, 31, 32, 33, 34, 35], or measurements [32, 36, 34, 37, 38, 39].

We are more interested in the experimental evaluation, as experimentation depicts realistic and accurate performance results. Besides that, experimental studies often lead to insightful findings and reveal hidden critical anomalies, fostering the design and configurations of the applications in the field.

Moreover, in previous work at Drakkar, Lone et al. [40] designed WiSH-Walt, a framework for controllable and reproducible LoRa testbeds [40]. WiSH-Walt enables easy configuration of motes

with several configuration parameters in order to run measurement experiments. They had began to investigate how reception quality depends on the main LoRa configuration parameters: Spreading Factor (SF) and Transmission Power (TP). The first part of the thesis extends and complements of the study started by Lone et al., as we conducted experiments to explore additional unstudied parameters.

However, before starting running any experiments and in order to have more rigorous experimental analysis, it seemed important to begin by investigating the actual network state by identifying the network load and exploring what is the current practice in adjusting the various parameters, we address to the following questions:

1. Are there any daily or hourly traffic patterns?
2. What are the the most used sub-bands and the central frequency channels?
3. What is the usage rate of each Data rate?
4. What are the leading LoRaWAN operators, and what are the corresponding volumes of traffic?

We have configured a monitoring set-up and performed thorough analyses, and drawn several conclusions that we considered for our following experimentations.

Further, while Lone et al. focused on SF and TP, we are interested in studying the impact of varying the payload length on the Packet Reception Rate (PRR) in the expectation of observing a strong dependency between the frame size and the PRR. Finally, we investigated the impact on PRR of two other parameters: the preamble length and the Coding Rate (CR).

One of the fundamental factors that immediately impact any wireless network reliability is the quality of the wireless link; hence, characterizing the channel is a crucial task. Moreover, most of the traffic in LoRa is uplink-oriented, resulting in no knowledge or visions regarding the packet's successful reception or not and the reasons behind its loss. In this case, identifying the channel behavior enhances the reliability and provides insights to application designers into adapting their configuration and employing adequate optimization techniques. I am interested in the identification of the overall behavior depending on various parameters: first, I focus on studying the aggregated distribution at different receiver placements, i.e., the gateways. Then, I study the impact of the set-up of the sender installation, indoor or outdoor, and how this could affect the variability of the reception power. Next, we dive deeper into the roots behind the characterization.

Finally, prompted by the conclusion from the channel study, where nodes with similar average channel gain could experience a reception power difference of more than 6 dB. We raise the following question: How can the network benefit better from the variation in received powers and foster the reception of packets with a higher power?

To this aim, we have examined the aloha-like access method of class A and the capture effect more profoundly.

Indeed, the *Class A* LoRaWAN end-device uses pure un-slotted ALOHA protocol for uplink communication: the device can transmit a packet at any moment on a radio channel chosen according to a pseudo random sequence, and provided that its duty cycle follows the frequency band regulations. After sending a packet, a device listens to a response from the gateway during two downlink receive windows. The use of the un-slotted ALOHA protocol results in the simplest access method and the lowest energy consumption. However, this comes at the cost of a low theoretical performance—the max channel utilization for ALOHA is around 18%, the result coming from the consideration that all frames overlapping in time are lost. The un-slotted ALOHA results in a high level of packet losses [41] in large-scale deployments.

The *capture effect* [42, 43, 44, 45, 46, 47] increases the theoretical channel utilization because the gateway can correctly decode a frame received with a higher power when two or more transmissions overlap. It results in an increased Packet Delivery Probability (*PDR*) and channel utilization. Haxhibeqiri et al. [34] used a simulation model based on the measurements of the interference behavior between two devices with a duty cycle of 1% to show that when their number increases to 1000 per gateway, the loss rate only increases to 32% (multiple channels, multiple SFs, and a payload size of 20 bytes). However, this level of loss rate should be considered low compared to 90% in pure unslotted ALOHA for the same load, and it results from taking into account the capture effect giving a channel utilization of around 23% [48]. MIM further improves the ratio of successful transmissions in case of collisions. In this mechanism not implemented in current LoRaWAN gateways, the receiver may switch to receiving a new stronger frame during the reception of another frame. When the receiver locks on a frame by receiving its preamble and a frame arrives with stronger power, it is beneficial to switch to the stronger frame that has higher probability of correct decoding. Several authors successfully applied MIM to 802.11 or 802.15.4 wireless LANs and showed its benefit of improving transmission reliability [45, 49, 50, 51, 52].

0.3 Contributions & publications

The contributions of the thesis are grouped into two categories: experimental and simulation studies.

- **Contribution 1:** we have studied and identified the current state of the LoRaWAN network by configuring a monitoring system made up of a Kerlink gateway installed on the roof of the IMAG building. The gateway forwards all the received traffic to a server. We have logged in real-time the traffic and saved it into a data set for future processing. The aim in the first

place is to examine the daily or hourly traffic and identify if there is a particular pattern. The resulting analysis shows that no particular pattern emerges. Then, we performed an analysis to examine the most used sub-bands and central frequencies, where we found that the h1 sub-band is more used than h2. Furthermore, we have determined the most used data rates for all aggregated frequencies and by sub-frequencies. We found that data rate 0, which corresponds to Spreading Factor 12 and bandwidth of 125 kHz, is dominant. Finally, we display a table of the LoRaWAN networks and operators during our experiment and show which operators were generating most of the load and how many devices were operating that time.

- **Contribution 2:** We have investigated the LoRaWAN link quality by examining the impact of some of the LoRa physical parameters on the packet reception rate. Our purpose is to evaluate and characterize the transmission quality of LoRa links by measuring PRR as a function of the payload length. Moreover, we aim to examine the different factors affecting PRR and evaluate how they could influence the probability of correct frame reception. To this aim, we have conducted extensive experiments for several months on a test-bed in the TTN [27], a public LoRa network. The result reveals a fundamental finding: there is only a slight impact of the payload length on PRR so that the constant bit error rate does not strongly influence packet reception probability.

  The successful frame reception considerably depends on favorable conditions of the entire frame reception process (the preamble, the header, and the payload). Conditions favorable to successful decoding are the following: no collisions nor strong attenuation during the transmission, which will foster the *preamble detection and time synchronization* success at the gateway resulting in the rest of the packet being successfully received.

  Finally, we conclude that the these findings present significant insights for LoRaWAN application designers in the sense that devices need to consider *packet retransmissions* in order to achieve high levels of data delivery and to face frame losses because of the ALOHA access method and the channel variability. As larger frames have similar PRR as smaller ones, we recommend that *retransmitting data aggregated in larger frames* is not only more efficient in terms of overhead but it also significantly improves the data delivery rate, as long as the duty cycle limit is met.

- **Contribution 3:** In the third part, we investigate the characterization of the wireless channel experimentally and answer the following questions: what is the behavior of the LoRaWAN wireless channel? On what it depends? And why it exhibits this behavior? To do so, we have configured two set-ups with an indoor and outdoor sender and analyzed the

results.

The result of the measurements shows that the LoRa channel for links of several kilometers behaves like a *slow fading Rayleigh Channel*—each transmission faces an exponentially distributed Rayleigh channel gain that remains mostly constant during the transmission. Our analysis also proves that the frequency hopping policy, i.e., changing the central frequency for every transmission, results in the Rayleigh fading channel behavior. We conclude that there is a significant channel gain difference between indoor and outdoor sender, which should be considered while designing any application. Finally, the measures confirm that the channel gains are always variable and that even for nodes with similar average channel gains, it would be very common to witness reception powers with a difference of 6 dB. In this case, the capture effect allows the gateway to receive one of the colliding frames.

- **Contribution 4:** In this contribution, we propose a technique to enhance the reception process of the LoRaWAN gateways so that channel utilization can reach values up to 35% in a single LoRaWAN cell. We investigate the benefits of concurrent and preemptive reception at the gateways: the capture effect allows to receive a frame even if it collides with a later frame, whereas Message in Message (MIM) reception allows the gateway to drop the current reception and switch to a new, more powerful frame. We examine Message In Message for LoRaWAN and evaluate the extent of improvement it can bring to its capacity. An implementation in the NS-3 simulator allows us to assess the gains of this approach through extensive simulations. We provided detailed simulations in NS-3 for an analytical model for channel utilization in LoRaWAN under multiple concurrent frames. System analysis shows that MIM improves channel utilization up to 35% in a single LoRaWAN cell scenario, representing a noticeable improvement considering the channel utilization of 23% for LoRaWAN with capture effect and 18% for LoRaWAN without capture effect. Finally, macro-diversity through the deployment of multiple gateways in a cell significantly improves the capacity, with the channel utilization reaching over 40% with two gateways and 60% with four gateways.

0.4 Thesis Structure

The thesis consists of three chapters presented in two parts; part one describes a state-of-the-art, including the LPWAN, LoRa and LoRaWAN. Part two encompasses the contributions divided by themes in two chapters. The first chapter describes all the conducted experiments with the finding and analysis, and Chapter two presents the proposed improvement and its implementation on Network Simulator Version 3 (NS-3).

Part I, Chapter1: LPWAN and LoRa.

In Chapter 1, we overview LPWAN and LoRa/LoRaWAN networks. Then, we describe the following LPWAN: LoRa, Sigfox, NB-IoT, and Ingenu Random Phase Multiple Access (RPMA). We provide a comparison table of these networks followed by a discussion referring to cost, quality of service, network coverage, flexibility, and adaptability. Then, we report the LoRa physical layer details, including the LoRa modulation, the physical layer parameters, the LoRa frame structure, interference, and collisions in LoRa. Next, we describe the LoRaWAN architecture, LoRaWAN classes, MAC frame format, and ADR. Finally, we present some of the main properties of LoRa and several identified issues. Finally, we illustrate some of the essential advantages and the open issues of the technology.

Part II, Chapter2: Experimental Evaluation and Characterization of LoRaWAN Link Quality.

We start by describing the traffic monitoring set-up followed by an analysis of the daily traffic density, sub-band utilization rate, data rate density, and finally, traffic by operator. Next, we provide a presentation of the experimental test-bed and a description of the STM board. Then, we show the experimental set-up and configurations for the study of the impact of the payload length on PRR. We present the experimental result of the conducted experiments followed by an anomaly explication and analysis; we explain the preamble detection and time synchronization mechanism at the gateway side and the impact of channel attenuation on synchronization probability P_s. Next, we vary the preamble length and the coding rate, and study their impact on PRR. In the third part of this chapter, we perform a thorough investigation of the channel. We start by presenting the experimental set-up and configuration, where we run two types of experiments from an indoor and outdoor sender. We investigate the overall behavior, then the difference in channel gain between indoor and outdoor. Finally, we observe the variability through time and frequency.

Part II, Chapter3: Message in Message for Improved LoRaWAN Capacity.

We investigate the capture effect and MIM: we present the five reception schemes: collisions, simple capture, advanced capture, physical capture, and introduce the MIM mechanism in general. Then, we describe how collision schemes are represented in LoRaWAN and how MIM could be implemented in real LoRaWAN gateway hardware. In the second part, we present the NS-3 simulator. Next, we investigate the capture schemes in LoRaWAN and how we have implemented

them in NS-3 through presenting their pseudo-codes. We describe the simulation setup and parameters. Then, we present the simulator validation followed by the simulations results for different reception schemes and configurations, when the nodes are in the same place and when they are fixed, in several distance configurations.

The final chapter concludes the thesis with a recall of the contributions and a presentation of perspectives.

Part I

State of the Art

Chapter 1

LPWAN and LoRa

Contents

Introduction

This chapter provides an overview of the LPWAN networks by presenting LoRa, Sigfox, NB-IoT, and Ingenu RPMA, followed by a comparative study. Then, it describes the LoRa physical layer and its different parameters and the CSS modulation technique, followed by an illustration of the LoRaWAN MAC layer. Finally, we discuss the open issues in LoRa networks.

1.1 IoT, Wireless technologies, and LPWAN

1.1.1 IoT and wireless networks

The ambition of the Internet of Things is to enable a plethora of services by means of integrating billions of internet-connected devices. By 2023, around 18 billion out of 30 billion connected devices will be IoT-related according to cisco white paper [13]. IoT devices may be equipped with various communication technologies and sensors; they can be with or without energy constraints, have advanced or basic computation capabilities, can be mobile or static, and easy, or hard to reach [53], [12]; they can be connected to the Internet through various wireless telecommunication networks, cellular and non-cellular networks. Figure 1.1 presents existing wireless IoT networks in terms of range, speed, and power consumption. While PAN like BLE, Thread, or Zigbee ensure low power connectivity but a short range [54], WWAN, i.e., cellular networks, provide long-range, high speed but at the cost of high power consumption. However, none of these technologies are suitable for long-range and low-power IoT applications. LPWAN emerge as a new communication paradigm, which complements conventional cellular and short-range wireless technologies in addressing low power and long-range requirements of a broad range of IoT applications.

1.1.2 LPWAN

LPWAN is a low-power and long-range network dedicated to constrained IoT devices that could be deployed in harsh environments [14]. It relies on a robust modulation and simple star of stars architecture to achieve long-range and ensures low power consumption at the cost of low bandwidth and speed. It exploits unlicensed sub-gigahertz frequency bands with duty cycle restrictions. In LPWAN applications, end-devices send a small amount of data infrequently at a low data rate, ensuring low power consumption and fair sharing of the channel. More specifically, LPWAN corresponds to fault-tolerant, low cost, low data rate, and low power consumption IoT applications. Moreover, end devices in an LPWAN context are typically low-cost, hardware-constrained, and battery-powered. LPWAN Networks include unlicenced spectrum LPWAN like LoRa and Sigfox or licensed spectrum technologies that are derived from popular cellular WWAN like NB-IoT

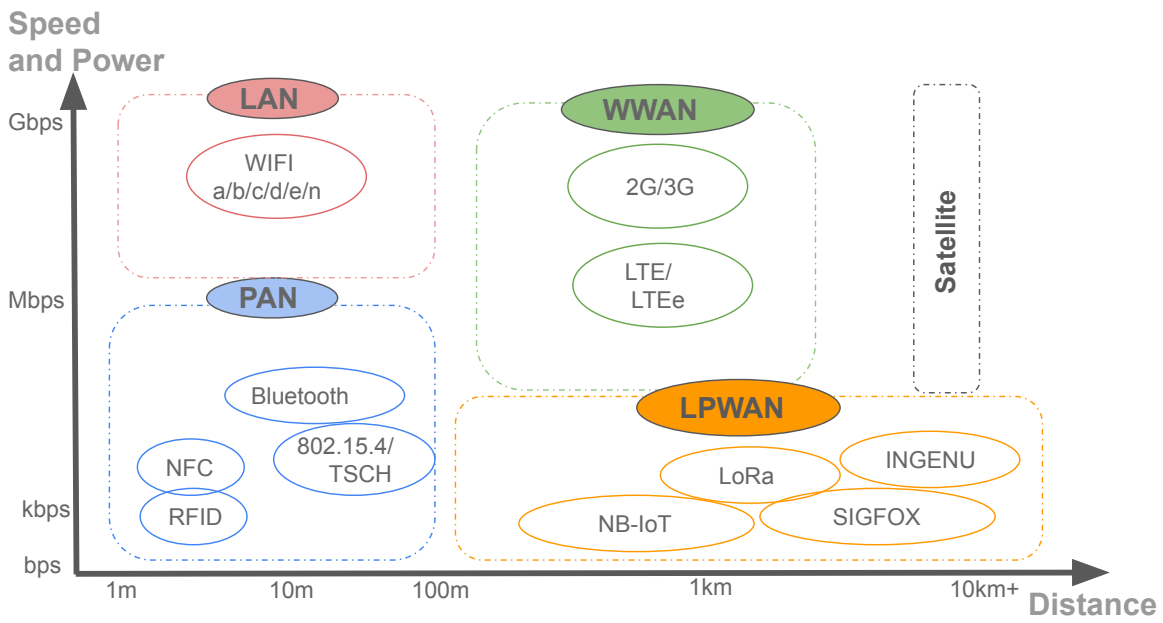

Figure 1.1 – Wireless networks

or LTE-M. In the following, I will provide a brief description of each LPWAN technology.

1.1.2.1 LoRa

LoRa is an emerging LPWAN based on a patented physical layer by Semtech [55]. It uses the CHIRP Spread Spectrum (CSS) modulation at the physical layer [25] and the MAC layer LoRaWAN [56]. CSS modulation uses frequency ramps with cyclic shifts to encode the information with a variable spreading factor. This type of modulation is robust against interference and Doppler effect and can reach long ranges.

LoRa uses unlicensed ISM bands: initially, the EU863-870 MHz and the EU433 MHz Sub-GHz bands in Europe and some countries in Africa and the Middle East. Recently, it has begin to use the 2.4 GHz band.

We can tune several parameters of the physical layer of LoRa, enabling the system designer to trade data rate for range or power and, therefore, optimize the parameter selection for a given scenario. These parameters include the *SF*, TP, CR, and BW. These parameters influence the effective bitrate of the modulation, its robustness against interference and noise, and its ease of decoding. The choice of the *SF* is a trade-off between data rate and communication range. Indeed, high *SF*s reach long ranges but deliver low data rates, and low *SF*s achieve high data rates but short ranges. The BW can take values from 7.8125kHz to 500 kHz. Larger bandwidth enables a higher data rate but results in lower sensitivity. The CR corresponds to the rate of Forward Error Correction (FEC) applied to enhance the packet error rate in the existence of noise and interference. A lower CR provides better robustness but increases the transmission time and energy consumption. The LoRa

link budget depends mainly on *SF*, TP, BW, CR of the nodes and allows communication ranges of about kilometers (typically 5-15 km). The LoRa packet size depends on the *SF* with a maximum size between 59-230 bytes. The data rate depends on the *SF*, the BW, and the CR and ranges from 290 b/s to 37.5 kb/s.

LoRaWAN is a MAC protocol proposed by the LoRa Alliance [56] over the LoRa physical layer. It defines the network architecture, the radio access method, and the MAC frame structure. LoRaWAN defines a star topology network composed of end devices and gateways connected through the Internet to a network server.

LoRaWAN defines three types of devices, namely *Class A*, *B*, and *C*. *Class A* devices use pure unslotted ALOHA protocol for the uplink: the device can send a packet at any instant on a chosen radio channel provided its duty cycle follows the frequency band regulations. After sending a packet, a device listens to a response from the gateway during two downlink receive windows. *Class A* results in the lowest energy consumption and longest battery lifetime. End devices have to respect the regulatory restrictions with a duty cycle of less than, e.g., 1% in each European (EU) 868 MHz band. LoRa enables bidirectional communications where uplink traffic is predominant. A LoRa gateway can simultaneously receive many packets using different spreading factors. LoRa can use several channels, i.e., frequency diversity.

1.1.2.2 Sigfox

Sigfox is a dedicated wireless network provider for LPWAN [57]. It offers end-to-end connectivity based on a patented technology, through implementing its own gateways [58]. It uses unlicensed ISM bands: 868-878.6 MHz band in Europe. Sigfox is mainly uplink-based traffic with limited downlink capability. Its data rate is limited to 100 b/s, which is potentially restricting the use cases. At the beginning, Sigfox supported only uplink communications, but then, it allowed bidirectional asymmetric communication. Downlink communications are limited to 4 messages of 8 bytes per day. It uses a Binary Phase Shift Keying (BPSK) modulation in a Ultra Narrow Band (UNB) of 100 Hz. With an ultra narrow band, noise levels are low, receiver sensitivity is high, and energy consumption is low. The Sigfox link budget allows a communication range of tens of kilometers depending on the environment (e.g., 3-10 km and 30-50 km in urban and rural environments, respectively). The packet size is limited to 12 bytes in the uplink direction. In Europe, the duty cycle is 1% limiting the number of uplink messages per day to 140. The Sigfox network is based on a star topology. The access protocol in Sigfox is also ALOHA, operating in a range of random frequency and time without channel sensing or listen before talk [58]. Redundant transmissions and time-frequency diversity, i.e., transmitting multiple times over randomly selected channels, enhances reliability wherea acknowledgments are not supported. The Sigfox infrastructure is closed, which

limits the opportunities for the IoT community to optimize its performance.

1.1.2.3 NB-IoT

Narrow-band Internet of Things (NB-IoT) is a cellular technology introduced and standardized by 3GPP Release 13 for bringing wide-area coverage to IoT. It is designed to coexist with legacy Global System for Mobile (GSM) and Long Term Evolution (LTE) technologies in licensed frequency bands [59]. NB-IoT supports three modes of operation: i) Stand-alone: using a stand-alone carrier, e.g. it can occupy a single GSM carrier (200 kHz), ii) Guard band: occupying the unused resource blocks within an LTE carrier's guard-band, iii) In-band: using resource blocks within a normal LTE carrier of 180 kHz [60]. NB-IoT adopts a significant part of the LTE design, comprising downlink Orthogonal Frequency-Division Multiple Access (OFDMA), uplink Single-Carrier Frequency-Division Multiple Access (SC-FDMA), channel coding, rate matching, interleaving [61], which reduces the time and effort for full specification development. Moreover, it uses SC-FDMA in uplink and OFDMA in downlink. The NB-IoT network consists of a star topology. It needs a software upgrade on top of existing LTE infrastructure to be supported or it can be deployed as a standalone network in a dedicated licensed spectrum.
Its data rate is limited to 250 kbps for the multi-tone downlink communication and to 20 kbps for the single-tone uplink communication, the maximum transmission power is fixed to 20 dBm, transmission power control and data rate adaptation are possible with NB-IoT. The link budget can reach up to 164 dBm for long coverage and the communication range depends on the environment (e.g., 1-5 km and 10-15 km in urban and rural environments, respectively). The packet size is 125 bytes for uplink and 85 bytes for downlink. The simplification of the protocol design and the reduction of the data rate and bandwidth requirements (needing only 180 kHz) significantly decreases NB-IoT's cost and energy consumption compared to legacy LTE. Enhancement of NB-IoT continues with new releases by 3GPP. Improvements with better handling of mobility, multicast services, and localization are planned.

1.1.2.4 Ingenu RPMA

Ingenu, previously On-Ramp Wireless, introduced a proprietary LPWAN technology based on a patented physical access scheme named RPMA [62]. RPMA is a variation of Code Division Multiple Access (CDMA), enabling multiple transmitters to share a single time slot. RPMA first raises the time slot duration of traditional CDMA and then adds a random offset delay for each transmitter scattering the channel access, which decreases transmitted signals' overlap and enhances the signal to interference ratio [63], [64]. Ingenu provides bidirectional communication, but with a meager link asymmetry, it uses RPMA for uplink communication. For downlink communica-

tion, base stations spread the signals for dedicated end devices and then broadcast them using CDMA. The base stations utilize multiple demodulators to decode signals that arrive at different timing within a slot at the reception side. Ingenu operates in the 2.4 GHz ISM, where it benefits from relaxed regulation on the spectrum use across different regions [63], but at the cost of more interference in the band and not as good propagation properties as in the sub GHz band. RPMA can reach up to -142 dBm receiver sensitivity and 168 dB link budget [62, 64], enabling communication ranges to reach up to 1-3 km in an urban environment and 25-50 km in rural environments. Transmission power values can reach up to 20 dBm, and end devices can tune their transmit power to reach the closest base station and limit interference to nearby devices. Ingenu drives efforts to standardize the physical layer specifications under IEEE 802.15.4k standard. Therefore, it is made compliant with the IEEE 802.15.4k specifications.

A single RPMA channel uses 1 MHz and supports up to 40 channels simultaneously [64]. The packet size varies from 6 bytes to 10 kbytes. The data rate is 624 kb/s for uplink and 156 kb/s for downlink per sector. Ingenu is a star topology and can be enlarged to tree topology by adding an RPMA extender. Ingenu adopts the Listen-Before-Talk mechanism (LBT) as an access procedure.

1.1.2.5 LPWAN Comparaison

LPWAN network principal aim is to provide low-power and long-range connectivity. While some LPWAN technologies provide better power consumption and low cost, others afford better Quality of Service (QoS) [65, 66]. Table 1.1 shows the principal differences and similarities between the previously describes LPWAN networks.

- **Power consumption and battery life:** Many factors condition power consumption and consequently, the battery lifetime of an end device. The most impactful is the access method: LoRaWAN class A and Sigfox use simple Aloha, where nodes are in sleep mode most of the time, resulting in the lowest power consumption and, therefore, longer battery lifetime. However, NB-IoT and Ingenu use more complex and synchronized access methods, which require higher power consumption.

- **Cost:** The cost of an LPWAN network includes the cost of the network deployment (base stations), the cost of the spectrum if it is licensed, and finally, the cost of end devices. LoRa and Sigfox present the advantage of being less expensive because they use unlicensed spectrum and less expensive gateways and end-devices.

- **Payload size:** NB-IoT supports data transmission up to 1600 bytes, and the Ingenu packet size varies from 6 bytes to 10 kbytes. for LoRaWAN, the packet length varies from 0 to 259

bytes depending on the Spreading Factor, however Sigfox proposes the lowest and fixed payload length of 12 bytes, which potentially limits its use for diverse IoT applications that need sending more data.

- **Quality of Service(QoS):** NB-IoT uses the licensed spectrum and LTE-based synchronous protocol, which results in a high packet reception ratio and consequently guarantees better reliability to the network. On the other hand, Sigfox, Ingenu, and LoRaWAN use license-free sub-GHz bands, relying on the solid physical layer properties that are immune against interference and fading. However, their use of the ALOHA protocol leads to higher packet collision rate and, therefore, affects the networks' reliability and scalability. Techniques such as retransmission and spatial diversity can improve their efficiency.

- **Network coverage:** Ingenu and NB-IoT provide the highest Link Budget (168 dB and 164 dB), reaching 1-5 km in urban and 10-50 km in rural areas. LoRa and Sigfox provide 150 dB and 156 dB of Link Budget covering 2-10 km in urban and 15-50 km in rural areas.

- **Flexibility:** Although LoRaWAN is based on the patented technology, it is still an open-source standard, encouraging researchers and developers to build their networks and contribute to the LoRaWAN evaluation and enhancement. Moreover, Knight has developed an SDR solution [67] based on reversing the LoRa physical layer and giving more access to open source developers to explore the technologies and optimize them.

  On the other side, other technologies are purely private like Sigfox and Ingenu, or cellular like NB-IoT allowing only to subscribe to the network provider and test it.

Table 1.1 – LPWAN Comparaison.

Standard	**LoRa**	**Sigfox**	**NB-IoT**	ingenu
Modulation	CSS	UNB DBPSK, GFSK	QPSK	RPMA-DSSS ,
Bandwidth	250kHz, 125kHz, 500kHz	100kHz	200kHz	
Frequency band	Sub-GHz ISM: EU (433 MHz, 868 MHz), US (915 MHz), Asia (430 MHz) ISM 2.4 GHz	Sub-GHz ISM: EU (868 MHz), US (902 MHz)	Licensed 700–900 MHz	ISM 2.4 GHz
Data rate	03–37.5 kbps (LoRa), 50 kbps (FSK)	100 bps (UL), 600 bps (DL)	158.5 kbps (UL), 106 kbps (DL)	78 kbps (UL), 19.5 kbps (DL)
Coverage	5 km (urban), 15 km (rural)	10 km (urban), 50 km (rural)	15 km	15 km (urban), 500 km line LOS
Payload length	up to 250 B	12 B (UL), 8 B (DL)	125 B (UL),85 B (DL)	10 KB
Deployment model	Private and Operator-based	Operator-based	Operator-based	Private
Bidirectional	Yes/half-duplex	Limited/half-duplex	Yes/half-duplex	Limited/half-duple
Adaptative Data Rate	CDMA Yes	No	No	No
MAC layer	pure ALOHA	pure ALOHA	FDMA/OFDMA	CDMA-like
Topology	star of stars	star of stars	star of stars	star, tree

1.2 LoRa Physical layer

The LoRa physical layer, patented by Semtech [7, 68], includes the process of digital data modulation into an RF signal and then its transmission over the air. It specifies the physical modulation, physical parameters, and physical frame structure. It operates in the ISM bands, 433-MHz, 868-MHz or 915-MHz ISM bands, depending on the region in which it is deployed, with duty cycle restrictions.

1.2.1 LoRa modulations

LoRa modulation is a proprietary spread spectrum modulation based on CHIRP Spread Spectrum (CSS) [25]. CSS spreads the signal in a larger bandwidth to form what we refer to as a chirp. A

chirp is a signal where the frequency increases/decreases linearly with time sweeping the entire bandwidth. Figure 1.2a) shows a raw up-chirp, where the frequency increases linearly from $f_c - \frac{BW}{2}$ to $f_c + \frac{BW}{2}$ sweeping the bandwidth, and Figure 1.2b) depicts a raw down-chirp, where the frequency decreases over time. f_c is the central frequency.

CSS encodes information on frequency ramps while cyclically shifting the base up-chirp, representing a LoRa symbol. Figure 1.3 and 1.4 demonstrates a modulated shifted LoRa chirp.

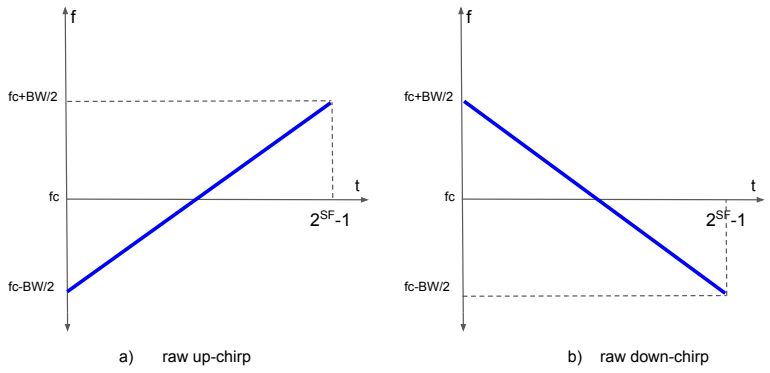

Figure 1.2 – a) Raw up-chirp b) Raw down-chirp

Each LoRa symbol is 2^{SF} chips long; therefore, there are 2^{SF} possible shifts for each SF, i.e., 2^{SF} code words. The chip rate is equal to the modulation bandwidth (chip-per-second-per-Hertz) and takes values of 125, 250, or 500 kHz. The LoRa symbol duration T_{symb} is defined as:

$$T_{symb} = \frac{2^{SF}}{BW}. \tag{1.1}$$

T_{symb} doubles each time we increase SF by one unit, thus, larger SF results in longer chirps, as illustrated in Figure 1.5. Each symbol encodes SF bits, i.e., for $SF = 12$, it carries 12 bits in a single LoRa symbol and the symbol rate is $R_s = \frac{BW}{2^{SF}}$ and the bit rate is $R_b = SF * \frac{BW}{2^{SF}}$.

At the receiver, the demodulation process consists of determining the frequency shifts of the received chirp. For this, the receiver, after locking into the signal, multiplies each symbol with a down chirp, and computes the FFT of this multiplication to get the position of the peaks, which represent the shifts, and determine the corresponding LoRa symbol. Figure 1.4 shows raw up-chirps used in the preamble, two down chirps representing the sync word, and different LoRa symbols with different frequency shifts, representing the code words. LoRa modulation is resistant against multipath fading and the Doppler effect. The receiver's sensitivity is enhanced because of the respective processing gain of the spread spectrum technology, providing tolerance to the frequency mismatch between a transmitter and a receiver.

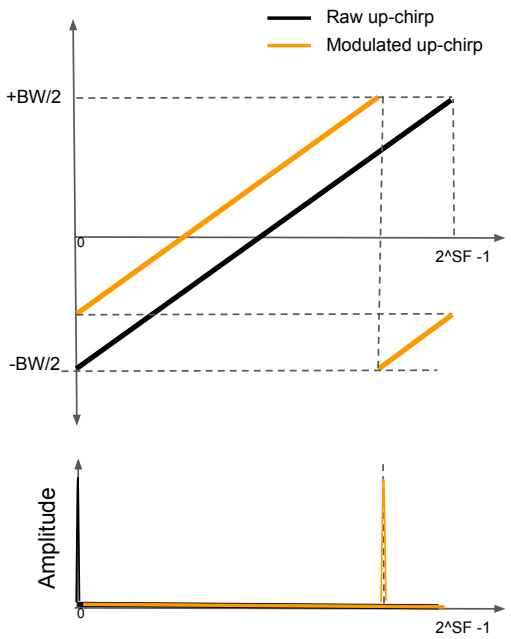

Figure 1.3 – Encoding chirp

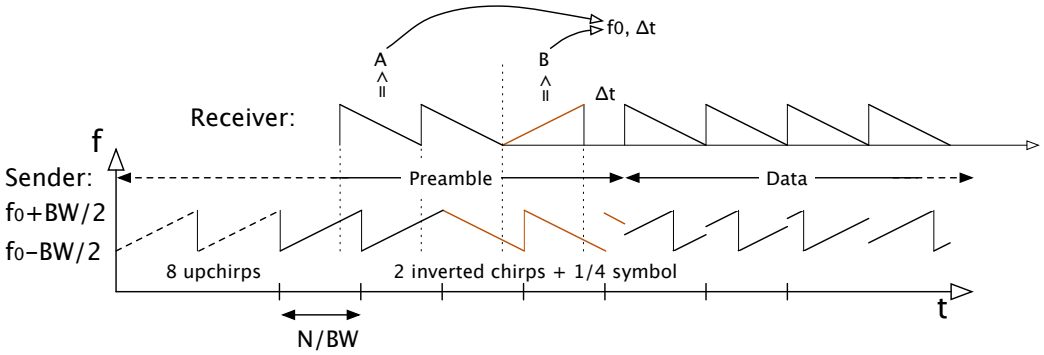

Figure 1.4 – Modulation and demodulation of Physical LoRa frame

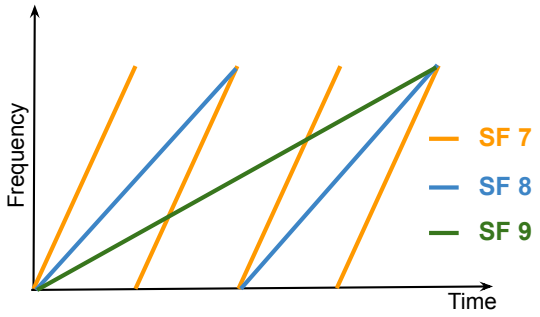

Figure 1.5 – Raw up-chirp for different Spreading factor.

1.2.2 Sub-GHz ISM bands

LoRa was initially configured to work only in the sub-GHz ISM band, but recently it has been extended to work in the 2.4 Ghz bands.

The use of the sub-GHz band offers robust and reliable communication at low power budgets.

Compared to the 2.4 GHz band, lower frequencies face less attenuation created by obstacles and solid surfaces.

Moreover, the sub-GHz band is less congested than 2.4 GHz, a band used by most popular wireless technologies, e.g., Wi-Fi, Bluetooth, ZigBee, and other home appliances, causing higher interference.

The sub-GHz ISM bands are free, which results in difficulty controlling and limiting the number of devices operating within them.

As a result, regional and national regulatory groups have created policies and regulations to monitor usage within these bands and protect them from becoming overused and saturated.

Two principal regulations are to be considered by any user of these bands: maximum transmission power and duty cycle. The first regulation sets a limit on the maximum transmission (Tx) power of the device. This limit is sub-band and region-dependent For instance, in Europe, the maximum is 14 dBm (25 milliwatts), and in the US, the limit on TP power is 24 dBm; Table 1.2 details the power limit per sub-band.

The second regulation is the duty cycle restriction: a duty cycle is defined as the fraction of time a device is busy transmitting in the band. For example, a duty cycle of 1 % indicates that a device can transmit 1 % of the time. In LoRa, we define T_{off}, a time during it a device cannot send a packet after being active for Time on Air (ToA) seconds:

$$T_{off} = \frac{1 - ToA}{100} \tag{1.2}$$

The ISM bands used by LoRa are regions dependent. For instance, in Europe, LoRa uses the h1.4 and h1.5 sub-bands in uplink and h1.6 in the downlink.

Moreover, the duty cycle is per sub-band and is region and frequency-dependent. Duty cycles are computed per sub-band: a device may consume 1% in H1.1 or in h1.5, 10% in h1.7, 1% in h1.9, during the same hour. h1.7 is used by the GW to respond to the devices (cf. RX2) Table 1.2 shows the duty cyle percentage for each sub-band in the 868 MHz band [6]. Devices can adopt alternative policies such as Listen Before Talk and sensing the channel mechanism. The use of frequency hopping can be an alternative for users to increase their duty cycle as the % of restriction is per sub-band, which forces the radio technology to use different sub-channels within a band to prevent one channel from being saturated.

LoRa added the support to exploit the 2.4 GHz band because it offers more relaxed spectrum regulations on the radio duty cycle and allows higher maximum transmission power in this band across multiple regions.

In the rest of the thesis, we focus on the the Sub-GHz ISM band.

Table 1.2 – ERC Recommendation for ISM bands [6].

Sub-band	Frequency. (MHz)	Transmission Power	Duty cycle
h1.1	**865-868**	14 dBm	1%
h1.2	863-870	14 dBm	0.1%
h1.5	**868-868.6**	14 dBm	**1%**
h1.6	868.7-869.2	14 dBm	0.1%
h1.7	869.4-869.65	27 dBm	10%
h1.8	869.7-870	7 dBm	100%
h1.9	869.7-870	14 dBm	1 %

1.2.3 Parameters of the LoRa Physical Layer

LoRa provides the ability to customize the physical layer by tuning many physical parameters, they can be pre-configured by the developer, or optimized to meet some objective output or constraints. The physical layer of LoRa defines several parameters [69]: Spreading Factor (SF), Transmission Power (TP), Carrier Frequency(CF), Bandwidh (BW) and Coding Rate (CR).

Bandwidth (*BW*): it is the width of the frequency band occupied by the transmission symbols, or CHIRPs. We can configure the bandwidth between 7.8 kHz and 500 kHz. Larger bandwidth allows for a higher data rate, but results in lower sensitivity.

Spreading Factor (*SF*) characterizes the number of bits carried by a CHIRP: *SF* bits are mapped to one of 2^{SF} possible frequency shifts. *SF* varies between 6 (7 in practice) and 12 with *SF12* resulting in the best sensitivity and range, at the cost of achieving the lowest data rate and worst energy consumption. Decreasing the *SF* by 1 unit roughly doubles the transmission rate and divides by 2 the transmission duration as well as energy consumption.

Coding Rate (*CR*): it corresponds to the rate of Forward Error Correction (FEC) applied to improve packet error rate in presence of noise and interference. A lower coding rate results in better robustness, but increases the transmission time and energy consumption. The possible values are: 4/5, 4/6, 4/7, and 4/8.

Transmission Power (*TP*): LoRaWAN defines the following values of *P* for the EU 863-870 MHz band: 2 dBm, 5 dBm, 8 dBm, 11 dBm and 14 dBm. The achievable data rates depend on the chosen bandwidth, spreading factor, and coding rate: a higher bit rate results from lower *SF*, higher BW, and CR of 4/5, at the cost of lower sensitivity and range. The bit rates range from 250 b/s to 11 kb/s: 250 b/s corresponds to *SF*12 for BW of 125 kHz, whereas 11 kb/s results from *SF*7 over BW of 250

kHz. Devices can also use the FSK modulation to reach a higher data rate of 50 kb/s. In h.7, the TP can take values up to 27 dBm.

Table 1.3 – Data Rate configuration and notation.

Data Rate	**Configurations**	**Indicative physical bit rate[bits/s]**
0	LoRa: *SF*12 /125kHz	250
1	LoRa: *SF*11 /125kHz	440
2	LoRa: *SF*10 /125kHz	980
3	LoRa: *SF*9 /125kHz	1760
4	LoRa: *SF*8 /125kHz	3125
5	LoRa: *SF*7 /125kHz	5470
6	LoRa: *SF*7 /250kHz	11000
7	FSK: 50kbps	50000
8..15	Reserved for Future Use (RFU)	

Theses parameters influence the effective bit rate (R_b) of the modulation, its resistance to interference noise and its ease of decoding. Indeed, Semtech [70] has defined the effective bit rate of LoRa as:

$$R_b = CR * \frac{SF}{2^{SF}} * BW \tag{1.3}$$

R_b depends on *CR*, *BW* and *SF*. We note that an increase of the BW results in an increase in the bit rate, on the contrary, an increase of the *SF* results in an decrease in the date bit rate. Table 1.5 depicts R_b for several values of *SF* and *BW*.

Table 1.4 – Transmission power configuration and notation.

TXPower	**Configuration**
0	20 dBm(if supported)
1	14 dBm
2	11 dBm
3	8 dBm
4	5 dBm
5	2 dBm
6..15	RFU

Table 1.5 – LoRa Data bit Rate R_b in kb/s for different Bandwidth and Spreading Factors.

	BW=125kHz	BW=250kHz	BW=500kHz
SF=6	9.38	18.75	37.50
SF=7	5.47	10.94	21.88
SF=8	3.13	6.25	12.5
SF=9	1.76	3.52	7.03
SF=10	0.98	1.95	3.91
SF=11	0.54	1.07	2.15
SF=12	0.29	0.59	1.17

Table 1.6 – Receiver sensitivity in dBm of Semtech SX1276 [7] for different Bandwidth and Spreading Factors.

	SF=7	*SF*=8	*SF*=9	*SF*=10	*SF*=11	*SF*=12
BW=125kHz	-123	-126	-129	-132	-133	-136
BW=250kHz	-120	-123	-125	-128	-130	-133
BW=500kH	-116	-119	-122	-125	-128	-130

The sensitivity of the receiver is an important parameter to consider, it is defined as [70]:

$$S = -174 + 10\log(BW) + NF + SNR_r \tag{1.4}$$

where -174 is the thermal noise, BW is the receiver bandwidth, NF is the noise factor that depends on the hardware, and the SNR_r is the minimum Signal to Noise Ratio required to decode a signal with a given *SF*. Table 1.7 shows the SNR_r values for several SFs. SNR_r strongly depends on *SF*, an increase of *SF* results in a better SNR_r and consequently better sensitivity, also an increase in BW, results in a decrease in *S*. Table 1.6 shows sensitivity for different *SF* and *BW*.

Table 1.7 – LoRa parameters for 125 kHz BW.

SF	Chirps/ symbol	SNR_r	Airtime	Bit rate	PL_{max}
7	128	-7.5 dB	56 ms	5469 b/s	230 B
8	256	-10 dB	103 ms	3125 b/s	230 B
9	512	-12.5 dB	205 ms	1758 b/s	123 B
10	1024	-15 dB	371 ms	977 b/s	59 B
11	2048	-17.5 dB	741 ms	537 b/s	59 B
12	4096	-20 dB	1483 ms	293 b/s	59 B

1.2.4 LoRa frame structure

LoRa frame starts with a preamble followed by the explicit PHDR header (protected by PHDR_-CRC). The frame contains the payload (LoRaWAN MAC frame) protected by the payload CRC [68] (see Figure 1.6). In explicit mode used in uplink frames, the explicit header contains the information about the payload: its length, *CR*, and the information whether CRC is used or not.

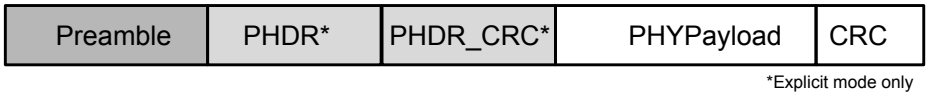

Figure 1.6 – LoRa frame structure.

The preamble length n_{pr} is programmable from 6 to 65535 symbols (by default, 8 symbols). The LoRa modem adds 4.25 symbols representing the synchronization word. The preamble duration τ_{pr} is defined as [71]:

$$\tau_{\text{pr}} = (n_{\text{pr}} + 4.25) * T_s \tag{1.5}$$

where T_s is the LoRa symbol duration:

$$T_s = \frac{2^{SF}}{BW}. \tag{1.6}$$

τ_j, the total frame duration (airtime) at rate DRj is the sum of τ_{pr} and the payload duration τ_{pa}:

$$\tau_j = \tau_{\text{pr}} + \tau_{\text{pa}} \tag{1.7}$$

where

$$\tau_{\text{pa}} = n_{\text{pa}} * T_{sym} \tag{1.8}$$

and n_{pa} is defined as:

$$n_{\text{pa}} = 8 + \max(\text{ceil}(\frac{8PL - 4SF + 28 + 16 - 20H}{4(SF - 2DE)})(CR + 4), 0), \tag{1.9}$$

where PL is the number of payload bytes, $H = 0$ when the header is enabled and $H = 1$ when there is no header, and $DE = 1$ means low data rate optimization enabled, or disabled ($DE = 0$).

1.3 LoRaWAN

LoRaWAN is a MAC protocol proposed by the LoRa Alliance [56] over the LoRa physical layer. It defines the network architecture, the network stack, the radio access method, and the MAC frame structure.

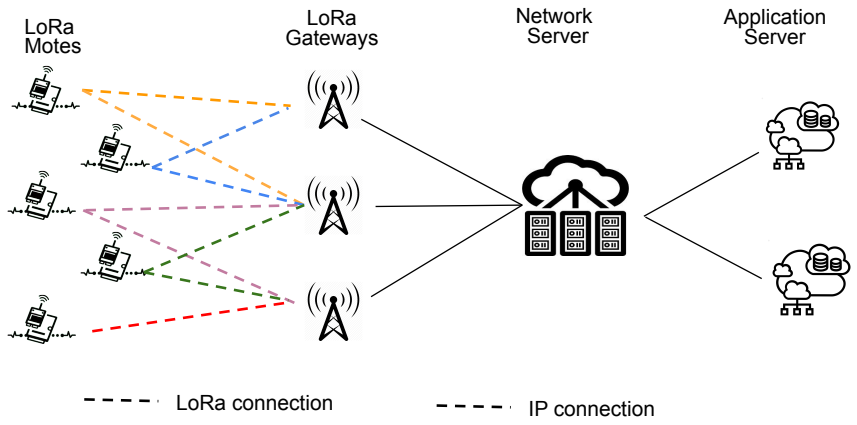

Figure 1.7 – LoRa architecture.

1.3.1 Architecture

LoRaWAN is a star of stars topology network composed of end-devices, gateways, network servers, and application servers.
LoRaWAN defines 4 entities in the network:

- **End-devices:** Electronic devices equipped with sensors, connected to one or many gateways via single-hop LoRa radio links.
- **Gateways:** Concentrators that relay messages between the end-devices and the Network Server, using LoRa radio link with end-devices and the Internet to the Network server.
- **Network server:** The central entity, which manages the entire network through multiple functions:
  - End device activation
  - Packets deduplication
  - Packet routing and acknowledgment
  - Radio resource management
  - Security
- **Application server:** The software programs that run on the network server to get statistics from collected data and perform other tasks.

Figure 1.7 depicts the topology of the networks, where the end devices communicate with the gateways through a single-hop LoRa link, and gateways forward correctly received packets to the network server using the IP protocol stack. Figure 1.8 shows the LoRa protocol stack at the end device, gateway, and the network server [1]. The node consists of an SX127x transceiver, a microcontroller that encapsulates a Serial Peripheral Interface (SPI), Hardware Abstraction Layer

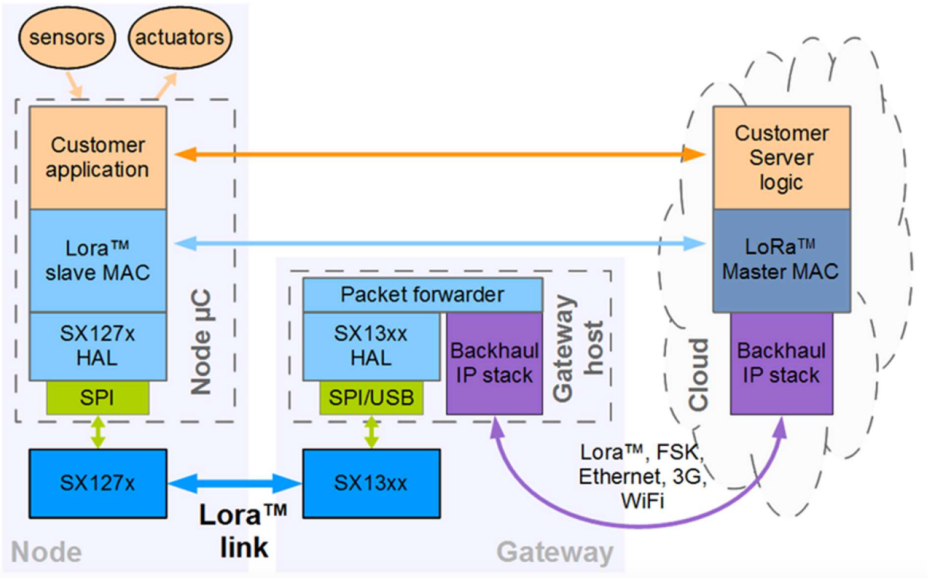

Figure 1.8 – LoRaWAN protocol stack [1].

(HAL) SX127X, a LoRa slave MAC, and a customer application. The gateways are equipped with an SX13xx transceiver, a gateway host that encapsulates a SPI, a SX13xx HAL, a packet forwarder, and a Backhaul Internet Protocol (IP) stack.

A cloud-based LoRaWAN master server comprises a Backhaul IP stack, a LoRa Master MAC and a customer server logic.

Each packet can be received by multiple gateways, i.e., LoRaWAN implements macro-diversity, which greatly increases the network's reliability. The gateway checks the correctness of the packet through a CRC check, adds additional information about the quality of the received signals, reception timing, and then forwards it to the network server the successfully decoded packets. The network server performs deduplication, filters the unwanted packets, and chooses one of the gateway in-range for downlink, according to some criteria (usually the one with best SNR or best radio link.).

Moreover, the macro-diversity of LoRaWAN combined with the spread spectrum of the LoRa CSS modulation, enables the network to geo-localize end-devices with no additional cost nor additional processing power, which is greatly beneficial to a wide range of applications requiring location determination [72].

Traffic in LoRaWAN is bidirectional, but uplink communication is predominant. LoRa gateways can process in parallel up to nine LoRa channels, where a channel is identified by the central-channel frequency and spreading factor couple.

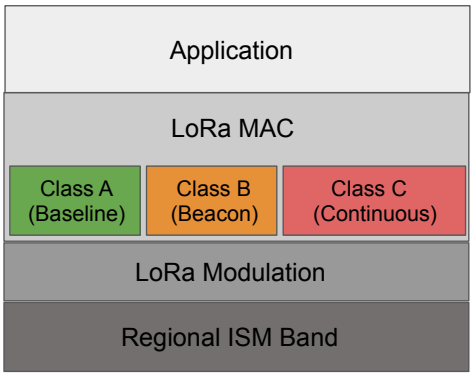

Figure 1.9 – LoRaWAN stack.

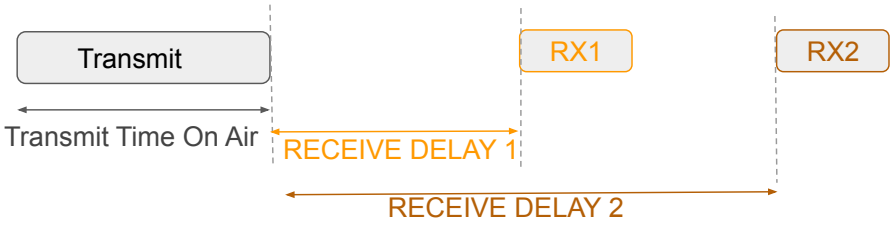

Figure 1.10 – Class A End-device receive slot timing.

1.3.2 LoRaWAN classes

LoRaWAN defines three types of devices, namely Class A, B, and C.

1.3.2.1 Class A

A stands for "All" end devices, which is the default mode of operation, before switching to another class type (B or C) with server coordination. Class A provides bi-directional communication [73, 26]. End-devices use pure un-slotted ALOHA protocol for the uplink: a device wakes up and sends a packet according to its communication needs on a chosen radio channel, provided that its duty cycle follows the frequency band regulations. Usually, the choice of the channel is pseudo-random to enable frequency diversity, alleviating potential wireless channel fades. After the packet transmission, a device listens to the gateway during two downlink receive windows. After finishing packet sending, the end device waits for a delay, usually fixed to one second and +/- 20 μs and referred to as the receive delay, then opens the first receive window. If the gateway is available and can send downlink to the end devices in the first receive window, it will send a downlink packet with the same frequency and data rate as in the uplink. Otherwise, the node will wait for another receive delay and opens a second receive window; this time, frequency and data rate are pre-configured for the end-device and the gateway. Figure 1.10 shows the receive slot diagram for class A. Downlink messages from the Network Server at any other time have to stand by until the next scheduled uplink. Class A results in the lowest energy consumption and the longest battery lifetime.

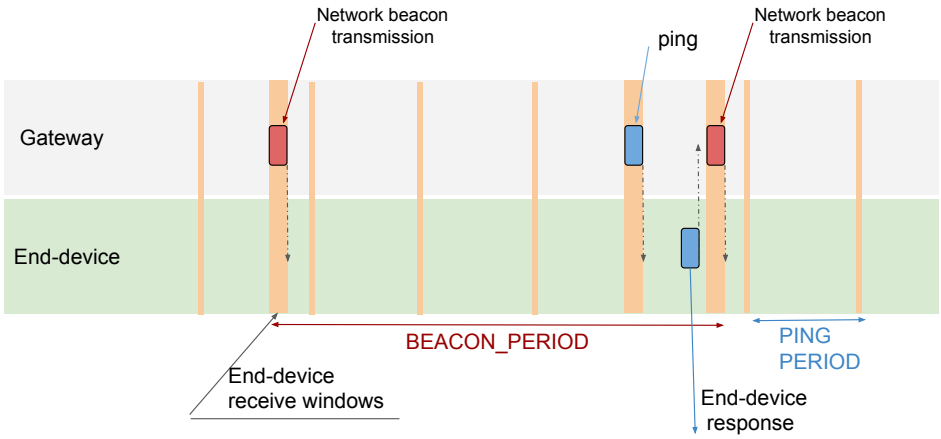

Figure 1.11 – Class B Beacon and ping slots timing.

1.3.2.2 Class B

B stands for Beacon; Class B allows bi-directional communication with scheduled receive slots, in addition to the receive windows that open whenever a Class A-style uplink is sent to the server [74]. In Class B, end-devices open extra receive windows at scheduled times relative to Beacons sent by the gateway. Class B enables the reception of downlink packets from the server at any time.

Figure 1.11 shows the time-synchronized beacon communication process between the gateway and an end device of class B.

By periodically receiving one of the beacons, the end device will adjust its internal clock with the network. Therefore, it will open receive windows (ping slots) periodically based on the beacon timing reference. The network can initiate a downlink communication using one of the ping slots.

1.3.2.3 Class C

C stands for continuously receiving. In Class C, end-devices open in continuity receive windows, only closed when it is transmitting [75]. Figure 1.12 shows the receive windows of the class C end device.

Class A devices may switch to Class C for a few minutes at a given time to get a firmware update over-the-air (FUOTA) broadcast. When the broadcast of the update is accomplished, the device can switch to its default Class A. Class C end devices open the same two receive windows as Class A devices, but they do not close the RX2 window; they keep it open until the next transmission is sent. As a result, they can receive a downlink in the RX2 window at any time. The end device also opens a short window with the same frequency and data rate of RX2, between the end of the last transmission and the beginning of the RX1 receive window [75].

Class C offers the lowest latency for end-device to server communication but at the cost of the

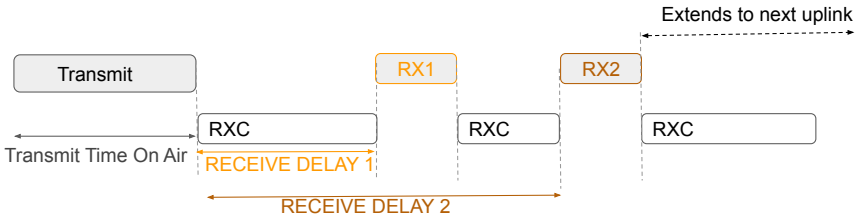

Figure 1.12 – Class C end-device receive windows.

highest power consumption compared to classes A and B.

1.3.3 MAC Frame format

The MAC frame is encapsulated inside the PHYPayload field in the Physical frame format, as specified in Figure 1.13. The MAC frame is composed of a single-octet MAC Header (MHDR), followed by the MAC payload (MACPayload) field that the size is the region and *SF* specific, and ending with message integrity code (MIC) of 4-octet size. The MAC header indicates the message type (MType) with three bits and the major version (Major) for the frame encoding with 2 bits. The three bits that rest are maintained for future usage. **MACPayload.** The MAC payload includes a frame header (**FHDR**) of 7 to 22 bytes succeeded by an optional port field (**FPort**) and an optional frame payload field (**FRMPayload**). A frame without Fport nor FRMPayload and only valid FHDR is considered as a correct frame.

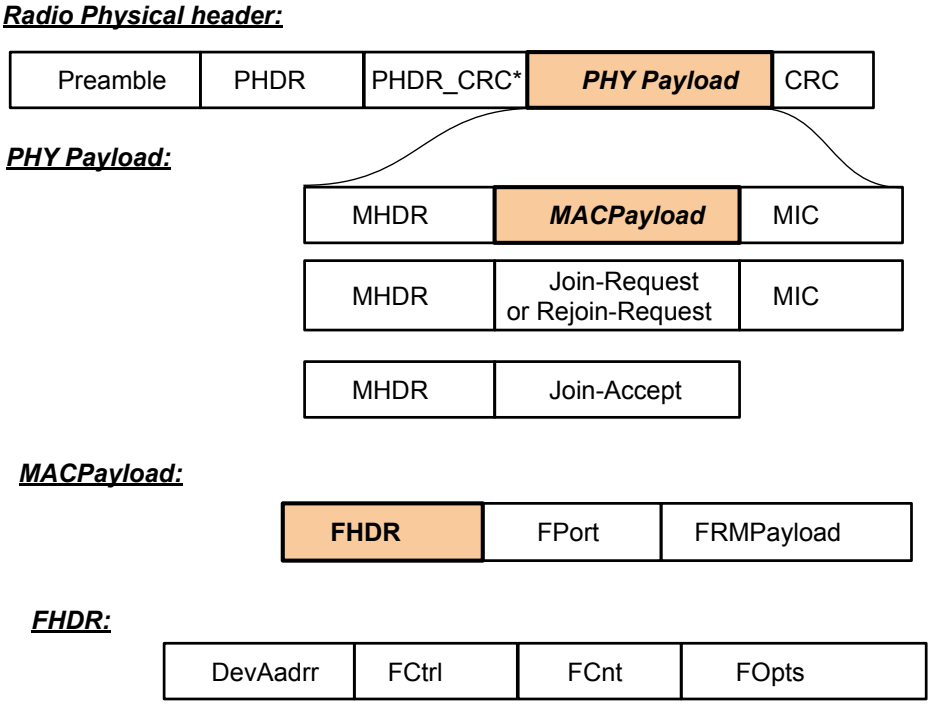

Figure 1.13 – MAC frame format.

The MAC frame is constituted of a single-octet MAC Header (MHDR), followed by the MAC payload (MACPayload) field,for which the size is the region and *SF* specific, and ending with mes-

Table 1.8 – MAC message types.

Mtype	Description
000	Join Request
001	Join Accept
010	Unconfirmed Data Up
011	Unconfirmed Data Down
100	Confirmed Data Up
101	Confirmed Data Down
110	RFU
111	Proprietary

sage integrity code (MIC) of 4-octet size. The MAC header indicates the message type (MType) with three bits and the major version (Major) for the frame encoding with 2 bits. The remaining three bits are reserved for future use.

LoRaWAN defines eight different MAC message types presented in Table 1.8, where:

- **Join-request, rejoin-request, and join-accept:** used for over-the-air activation procedure.
- **Unconfirmed data up/down:** frames that do require any acknowledgment.
- **Confirmed data up/down:** frames that must be acknowledged.
- **Proprietary protocol messages:** used to fulfill non-standard message formats.

Figure 1.14 shows the Frame header format, where it encloses the short device address of the end-device (**DevAddr**), a frame control octet (**FCtrl**), a 2-octets frame counter (**FCnt**), and up to 15 octets of frame options (**FOpts**) used for MAC commands transportation [26].

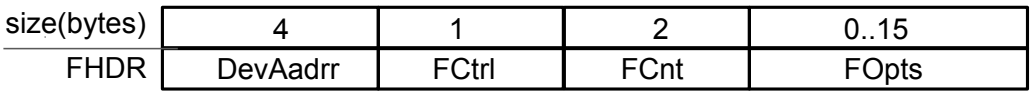

Figure 1.14 – Frame Header.

The **FCtrl** content for downlink and uplink frames are presented in Figure 1.15 and Figure 1.16, respectively, where:

- **ADR:** the ADR bit.
- **ADRACKReq:** the ADR acknowledgment request bit.
- **ACK:** the acknowledgement bit
- **ClassB:** The Class B bit.

- **FPending** The frame pending bit.
- **FOptsLen:** The frame-options length field.

Bit#	7	6	5	4	[3..0]
FCtrl bits	ADR	ADRACKReq	ACK	ClassB	FOptsLen

Figure 1.15 – Uplink fcnlt.

Bit#	7	6	5	4	[3..0]
FCtrl bits	ADR	RFU	ACK	FPending	FOptsLen

Figure 1.16 – Downlink fcnlt.

1.3.4 ADR

In the LoRa network, the end devices can use any of the possibles data rates and transmission power, which can be optimized for the end device and overall network reliability.

LoRaWAN proposes ADR to provide reliable and battery-optimized connectivity by automatically adapting *SF* and TP to the link conditions. When an ED notices that a downlink response from the network does not follow many consecutive uplink transmissions, it considers it a loss of connectivity. Consequently, it starts increasing the TP by one step (2 dBm) up to the maximum value before doing the same for *SF*. These steps progressively improve the robustness of the link.

Figure 1.17 shows the flow-chart of how an ED adapts its TP and *SF* according to LoRaWAN Specifications v1.1. [2, 26]. ADR_ACK_LIMIT andADR_ACK_DELAY are two parameters that manage the number of uplink messages. When a downlink response is not received, the ED will increase TP or *SF*. The ED adapts its communication settings to establish reliable but not necessarily energy-efficient communication with the network.

ED can request the server to control the uplink reception quality based on past stored measurements. The NS calculates the link quality measure, SNR, based on the last N packets and compares it to the minimum receiver sensitivity threshold required to decode the packet successfully; if it is too high, the network sends commands to reduce *SF* and/or TP. The newly set of *SF* and TP values ensures that the expected SNR of the future packets is above the minimum receiver sensitivity threshold with a pre-defined margin. Decreasing *SF* (high data rate) and TP allows faster transmissions, which consumes less energy and increases network capacity. Semtech provides recommendations for implementing the network-side of the ADR algorithm, adopted by various operators, including, The Things Network, a popular crowd-sourcing LoRaWAN network. In the recommended algorithm, they use the 20 last received frames (N = 20) with their respective maximum signal to noise ratios (SNR max) Figure 1.18 shows the ADR mechanism at the network.

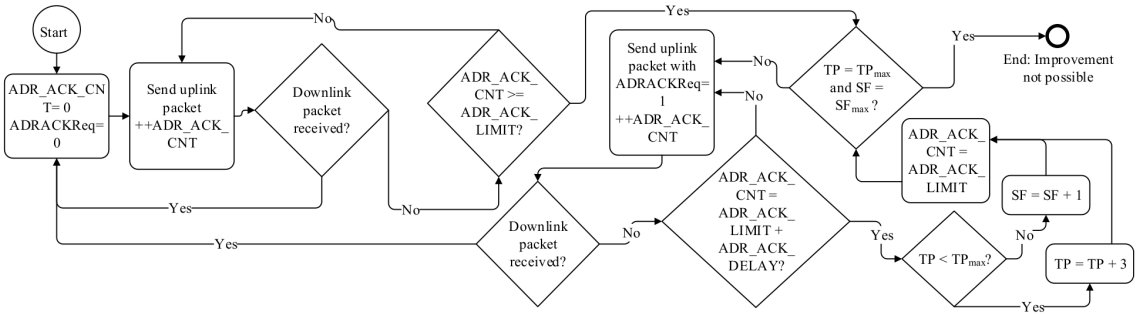

Figure 1.17 – ADR mechanism at the end-device [2].

Adaptive Data Rate control is not supported when the radio channel attenuation is highly variable. Thus, the network server cannot control the data rate, so the device application layer will control it with the aim to minimize the aggregated air time according to the network conditions.

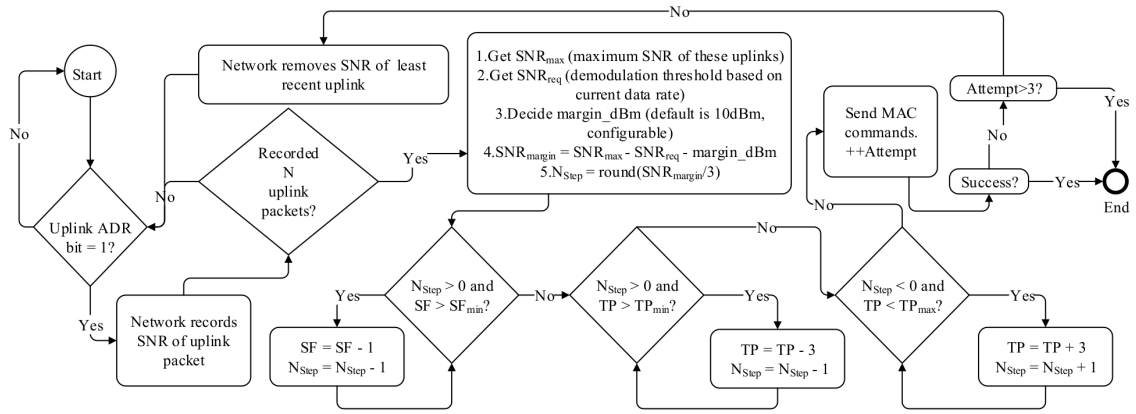

(b) ADR mechanism on network side

Fig. 1: ADR algorithm

Figure 1.18 – ADR mechanism in the network [2].

1.4 Open Issues

Numerous studies investigated the capacity issue of LoRaWAN network by identifying the factors behind many limitations. We discuss below the main limitations that impact scalability of the network:

1.4.0.1 Aloha-like MAC access

This choice of a simple access method highly impacts the reliability of LoRaWAN and its scalability to a large number of devices—the theoretical channel utilization for ALOHA with fixed packet sizes is around 18%. It results in a high level of packet loss due to collisions as the number of devices

increases. Even if we take into account the *capture effect*[1], which increases the packet reception probability in case of collisions, the access method strongly limits the capacity of the network to scale.

1.4.0.2 Downlink traffic & Duty cycle

In LoRaWAN, while most of the traffic is uplink-oriented, reliability can be enhanced through frame acknowledgments (ACK) in the downlink process. However, the downlink process dramatically impacts scalability of the network in a large-scale network due to two limitations at the gateway [76], [77], [78], [79], the first one is the hardware nature of the gateway being half-duplex, and the second one is the duty cycle limitation. Indeed, a half-duplex gateway cannot receive and send simultaneously; as a result, during the process of sending a downlink frame, the gateways are blind regarding all the received frames, which results in dropping all the received packets at that instant and causes a high packet loss.

Moreover, since the LoRaWAN operates in the ISM bands, a duty cycle restriction is applied when not using a "Listen before Talk" mechanism for channel access. When the limitation of the duty cycle is reached at the gateway side, a downlink frame cannot be sent immediately following an uplink frame. Indeed, a gateway should send an acknowledgment exactly in the first or the second "receive window" of the end device; otherwise, the ACK will not be received, and the corresponding frame will be lost; in this case, the end device will proceed to a re-transmission of the frame or an increase of its transmission parameters such as *SF* and TP, thus increasing contention.

1.4.0.3 Interference

Many papers investigated the interference impact on the reliability of the network [80] [81], [82], [83], [84] [85]. They considered both inter-network interference and intra-network interference. They stressed the network coexistence interference impact, especially in the case of dense deployment networks, and how this should be more investigated and taken into account in the management of the spectrum sharing. Goursaud et al. [8] investigated the inter-network interference caused by LoRa packets with several *SF*, although it is often assumed that the *SF* are orthogonal, they show that it is not the case but the impact of the interference from packets that have different SF_j to the packet of interest that has SF_i is negligible. Table 1.9 shows the theoretical co-channel rejection for all combinations of the desired signal.

Moreover, Groce et al. [9] investigated the imperfect orthogonality between the various SF experimentally. They also show that SFs are not perfectly orthogonal. They computed the Signal to Interference Ratio SIR threshold under it, inter SF errors occur. Table 1.10 shows the SIR thresholds

[1]The *capture effect* refers to the capacity of correctly receiving a significant fraction of colliding frames [45].

Table 1.9 – Co-rejection matrix [8].

SF_d/SF_i	6	7	8	9	10	11	12
6	-6	12	14	16	16	26	18
7	21	-6	16	18	19	19	20
8	24	24	-6	20	22	22	22
9	27	27	27	-6	23	25	25
10	30	30	30	30	-6	26	28
11	33	33	33	33	33	-6	29
12	36	36	36	36	36	36	-6

Table 1.10 – SIR Thresholds with SX1272 transciever [9].

SF_d/SF_{int}	7	8	9	10	11	12
7	-1	8	9	9	9	9
8	11	-1	11	12	13	13
9	15	13	-1	13	14	15
10	19	18	17	-1	17	18
11	22	22	21	20	-1	20
12	25	25	25	24	23	-1

for correct demodulation resulting from their conducted experiments with an SX1272 transceiver. The table shows that the SIR thresholds differ from the values shown in [8], over 10 dB–an order of magnitude lower.

Conclusion

This chapter considers the study and description of the LPWAN network in the first part, where we presented the motivation behind the rise of LPWAN, we described LoRa, NB-IoT, Sigfox, and Ingenu LPWAN and, we provided a comparative study of these LPWAN networks in terms of power consumption, cost of deployment, payload size, quality of service, network coverage and flexibility. We conclude that, while LoRa and Sigfox are suitable for applications that require low-cost deployments, long coverage, and long battery lifetimes, NB-IoT is suitable for applications that require very low latency and high quality of service.

Then we provided a detailed description of the LoRa physical layer: the CSS modulation, the sub-GHz ISM bands, the parameters of the physical layer, and finally the physical LoRa frame structure.

For LoRaWAN, we presented the LoRaWAN architecture and described the various entities of

the network: end-devices, gateways, network server, and application server. LoRaWAN defines three classes, we detailed each of them. Then, we presented the MAC Frame format and the ADR mechanism.

Finally, we discussed some of the open issues related to the emerging network.

Part II

Contributions

Chapter 2

Experimental Evaluation and Characterization of LoRaWAN Link Quality

Contents

Introduction

As LoRaWAN is one of the new emerging LPWAN technology, it is crucial to investigate its performance in terms of transmission quality and ability to scale. Many authors have addressed the issue of evaluating LoRa performance and scalability through analytical modeling [28, 29], simulation [30, 31, 32, 33, 34, 35], or measurements [32, 36, 34, 37, 38, 39]. In previous work of our team, Lone et al. [40] designed WiSH-Walt, a framework for controllable and reproducible LoRa testbeds. They have investigated how the quality of reception depends on the two LoRa parameters:*SF* and TP.

This chapter aims to experimentally study, evaluate, and characterize the LoRaWAN network reliability through studying LoRaWAN link quality by measuring PRR as a function of a collection of parameters and then characterizing the LoRaWAN wireless channel in several configurations.

In the first part of this chapter, I will present experiments with traffic monitoring on a LoRaWAN Kerlink gateway. The experiments lead to preliminary analysis and consideration of the actual state of the network with the aim of answering to the following questions:

1. Is there any daily or hourly traffic patterns?
2. What are the sub-bands and the central frequencies the most used?
3. What is the usage rate of each Data rate?
4. What are the leading LoRaWAN operators, and what is their usage of the traffic?

The resulting statistics determine which parameters to privilege in the following experiments to avoid collisions and have more reliable results.

In the second section of the chapter, we report on the results of extensive experiments on the WiSH-WalT testbed with The Things Network (TTN), a public LoRa network [27] during several months. The goal of the conducted experiments is to characterize the transmission quality of LoRa links by measuring PRR as a function of the payload length. Several factors may impact PRR and we wanted to evaluate how they influence the probability of correct frame reception.

Our main finding is that there is only a slight impact of the payload length on PRR, which means that a constant bit error rate does not strongly influence the probability of packet reception. Successful reception rather depends on favorable conditions for receiving the whole frame (the preamble, the header, and the payload): no collisions as well as no strong attenuation during the transmission so that *preamble detection and time synchronization* succeeds at the gateway and then, the rest of the packet is successfully received.

We quantify successful reception with probability P_s of being (or not) in a favorable condition for each frame reception: once the frame preamble is received, there is great chance that the whole frame is correctly received. We estimate probability P_s and show that it depends on *SF* and SNR, and often becomes a dominant factor of successful reception depending on the signal strength at a gateway.

These findings have important implications for LoRaWAN application designers: to achieve high levels of data delivery, devices need to consider *packet retransmissions* because they have to cope with frame losses not only due to the ALOHA access method, but also to the channel variability. As larger frames have similar PRR as smaller ones, *retransmitting data aggregated in larger frames* is not only more efficient in terms of overhead but it also significantly improves the data delivery rate, as long as the duty cycle limit is met.

In the third part, we investigate the characterization of the wireless channel experimentally and answer the following questions: what is the behavior of the LoRaWAN wireless channel? On what does it depend? And why does it exhibit this behavior? With this aim, we have configured two set-ups with an indoor and outdoor sender and analyzed the results.

The result of the measurements shows that the LoRa channel for links of several kilometers behaves like a *slow fading Rayleigh channel*—the reception power of each transmission is affected by an exponentially distributed Rayleigh channel gain that remains mostly constant during the transmission. Our analysis also shows that the frequency hopping policy, i.e., changing the central frequency for every transmission, results in the Rayleigh fading channel behavior. We conclude a significant channel gain difference between indoor and outdoor sender, which should be considered while designing any application.

Finally, the measures confirm that the channel gains are always variable and that even for nodes with similar average channel gains, it would be very common to witness reception powers with a difference of 6 dB. In this case, the capture effect allows the gateway to receive one of the colliding frames.

2.1 Real World Traffic Monitoring

This part aims to analyze the received traffic by one gateway during a period of time and study its density, the sub-frequency usage, the data rate percentage, and determine if a pattern emerges from the statistics. We show in the first paragraph the overall daily traffic during one month, followed by hourly traffic analysis. In the second paragraph, we illustrate sub-band utilization and data rate density. Finally we show the traffic by operator

2.1.1 Traffic Monitoring Set-up

The traffic sniffing set-up consists of a Kerlink gateway [3], Figure 2.1, an outdoor LoRaWAN gateway installed on top of the roof of the IMAG building in Grenoble. The gateway listens to and receives all LoRa-type packets regardless of their network, then redirects the traffic to a server where we install a client to get all saved traffic for processing.
The analyzed dataset consists of more than 1M received packets over one month by the Kerlink gateway. The dataset includes all the meta-data corresponding to each received packet, such as data rate, carrier frequency, sub-band, SNR, Received Signal Strength Indicator (RSSI), timestamp, and coding rate. For the experiments presented further, we needed to determine the sub-band, central frequency usage and channel utilization. Learning the most used data rate is also essential to make the appropriate choice of the experiments data rate to eliminate as much as possible any potential collisions that could affect the reliability of the future results and analysis.

2.1.2 Daily Traffic Density

Figure 2.2 outlines the total number of daily received packets by the gateway from the 26th of October 2018 to the 24th of November 2018. Figure 2.2 shows a significant variability of the traffic. For instance, the number of packets increases during the first week to reach almost 35000 received

Figure 2.1 – Kerlink gateway [3].

packets on the 1^{st} of November, which was a day-off. Then the traffic decreases to less than 20000 on the 11^{th} of November, which was also a day-off, increased and decreased again; we observe that no particular pattern emerges.

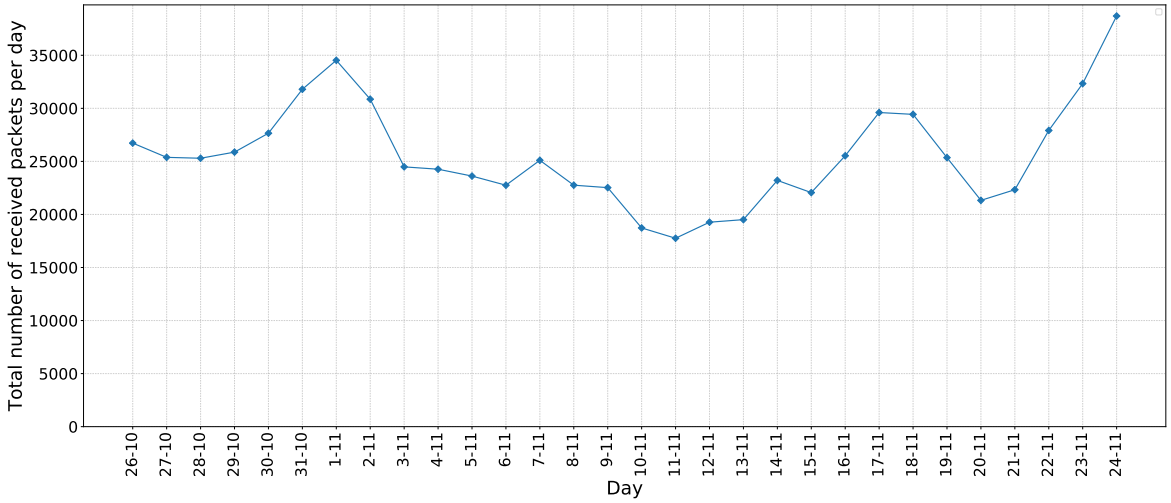

Figure 2.2 – Overall daily traffic received by an outdoor Kerlink Gateway for one month.

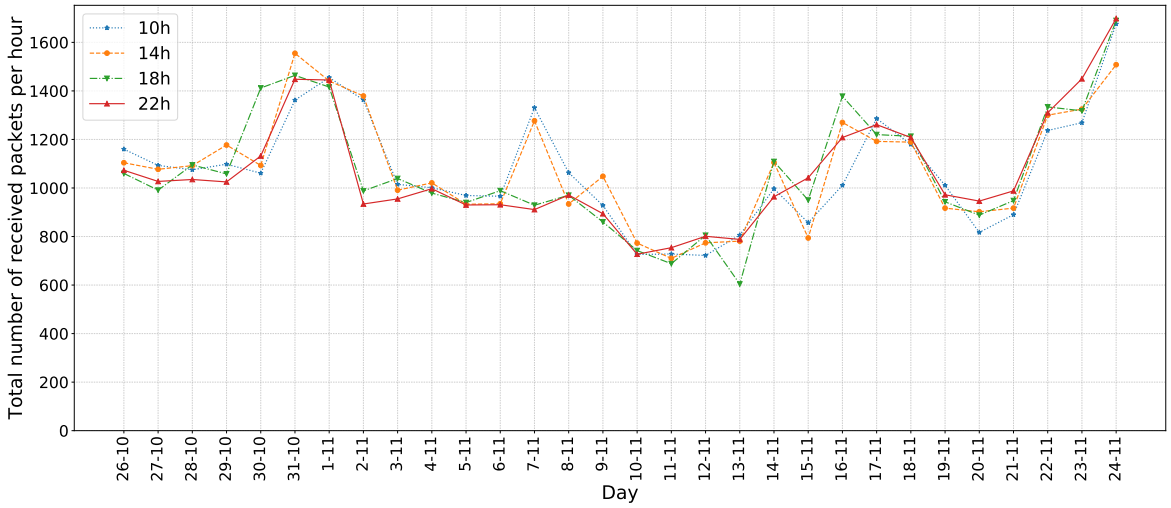

Figure 2.3 – Received traffic by hour.

Figure 2.3 shows the daily traffic variation for the same period at specific hours 10h, 14h, 18h, and 22h. Figure 2.4 illustrates the received packet variation throughout the day hours for several days. These analyses study the traffic dependency at any hour of the day. Figure 2.3 reveals that the traffic for all the shown hours follows the overall curve in Figure 2.2 when it increases or decreases with slight shifts. More precisely, the plot curve at 10h is shifted more or less to the right and on top for some days compared to the 22h.

Figure 2.4 illustrates that the traffic is almost constant throughout of the day, with various levels for each day, confirming that the traffic is more day-dependent than hour-dependent.

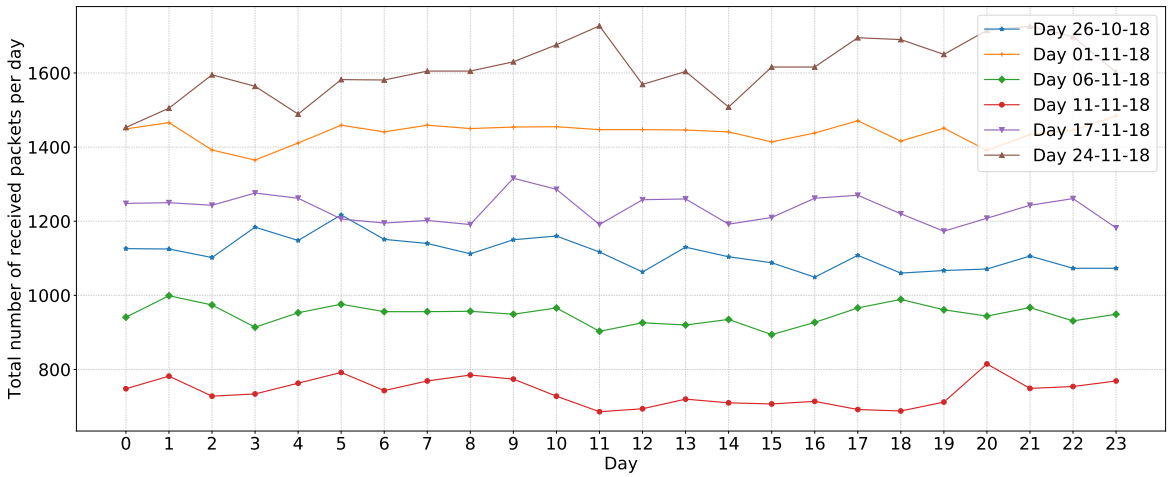

Figure 2.4 – Total number of received packets per hour for several days.

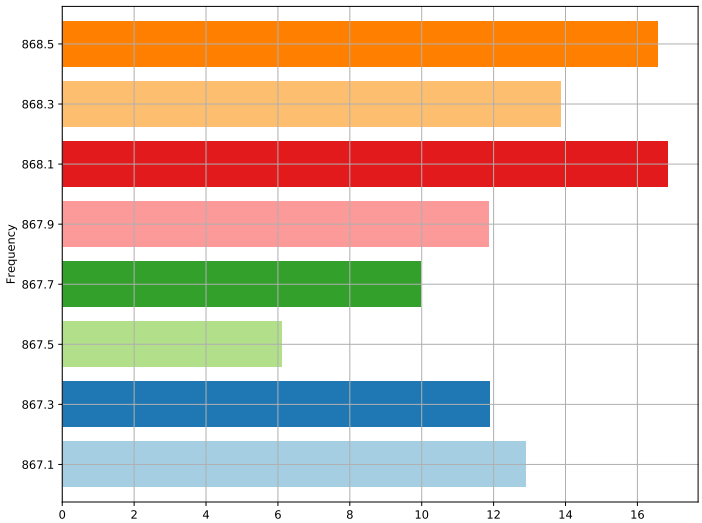

Figure 2.5 – Average channel usage.

Table 2.1 – Data Rate configuration and notation.

Data Rate	**Configurations**	**Indicative physical bit rate[bits/s]**
0	LoRa: *SF*12 /125kHz	250
1	LoRa: *SF*11 /125kHz	440
2	LoRa: *SF*10 /125kHz	980
3	LoRa: *SF*9 /125kHz	1760
4	LoRa: *SF*8 /125kHz	3125
5	LoRa: *SF*7 /125kHz	5470
6	LoRa: *SF*7 /250kHz	11000
7	FSK: 50kbps	50000
8..15	RFU	

2.1.3 Sub-Band Utilization

Figure 2.5 displays the average channel usage for the available frequency channels.

Overall, we note that the three frequencies of the h1.5 sub-band 868.1, 868.3, and 868.5 with channel load of 17%, 14%, and 17%, respectively, are more loaded than the five frequencies of the h1.1 sub-band 867.1, 867.3, 867.5, 867.7, 867.9 Mhz with the loads of 13%, 12%, 6%, 10%, and 12%, respectively.

In fact, h1.5 is the sub-band to use by default for all LoRaWAN class-A devices in Europe. Otherwise configured, nodes will only send packets on these frequencies. Nodes must use frequencies of h1.5 to join the network, either through Over The Air Activation (OTAA) or Activation By Personalization (ABP). Finally, STM boards used in our experiments use a pseudo-random policy, for choosing the sub-band on which the next transmission will happen, it alternates between sub-bands h1.5 and h1.1, randomly picks one sub-frequency from that sub-band, which explains the results.

2.1.4 Data Rate Density

Figure 2.6 represents the bar and the pie charts of received traffic in terms of the number of received packets per data rate and their respective percentages. Overall, data rate 0(DR0: *SF*=12, BW=125 Khz) is the most used data rate compared to other DR with over 500000 packets over 1Million, which corresponds to 56% of the overall received traffic. DR3, DR4, and DR5 get almost the same traffic quantity with 11%. Finally, DR2 represents 7%, DR1 3%, and DR6 2%.

We can explain that *SF* 12 represents the largest *SF* by the fact that it offers the best sensitivity, is more resilient to noise, and reaches longer distances, especially when nodes are indoor, more

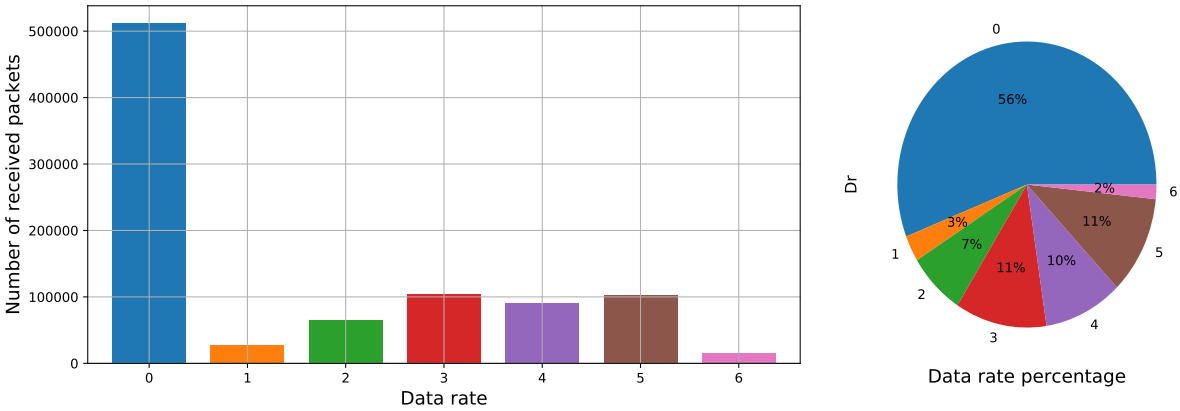

Figure 2.6 – Received packets by data rate.

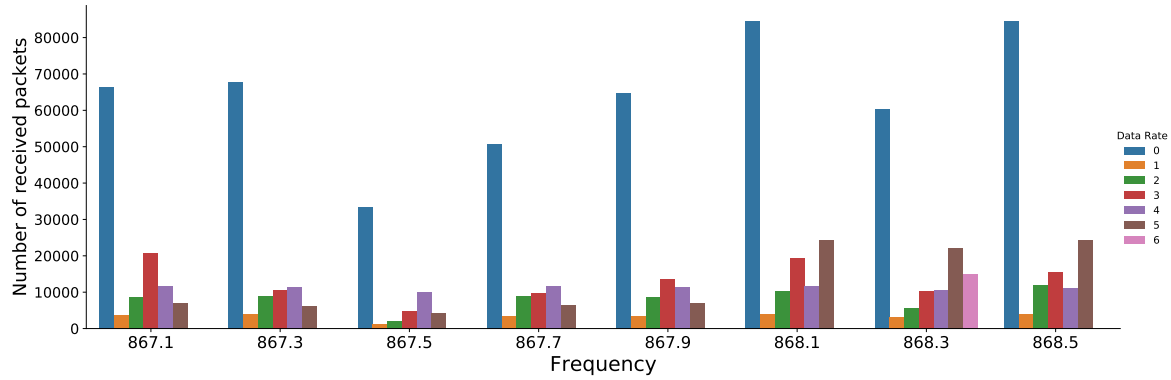

Figure 2.7 – Received packets by data rate for each sub-channel frequency

probably explain the significant difference between the usage of the several data rates.

Figure 2.7 provides more detailed information regarding data rate usage by sub-channel. For all the sub-channels, data rate 0 is significantly more employed. The other data rates usage varies from sub-channel to the other, while data rate 5 is the second most used for the carrier frequencies of the h5 sub-band, i.e., 868,1, 868.3, and 868.5Mhz; for others, like 867.1, data rate 3 is the second most used one.

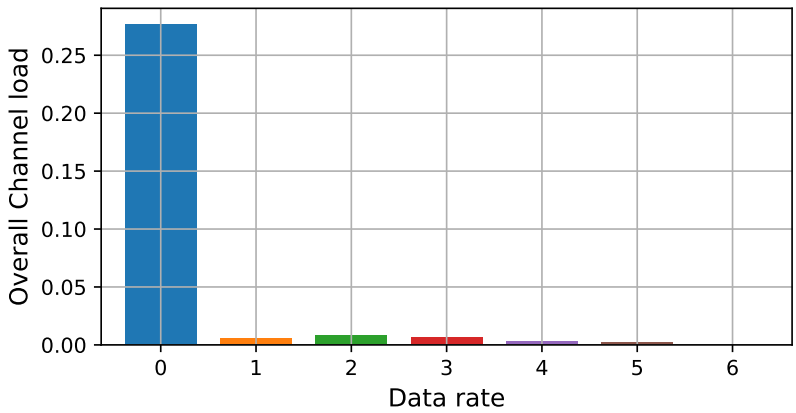

Figure 2.8 – Overall channel load by data rate.

Although Figures 2.6 and 2.7 provide information about data rate usage, the illustration is only

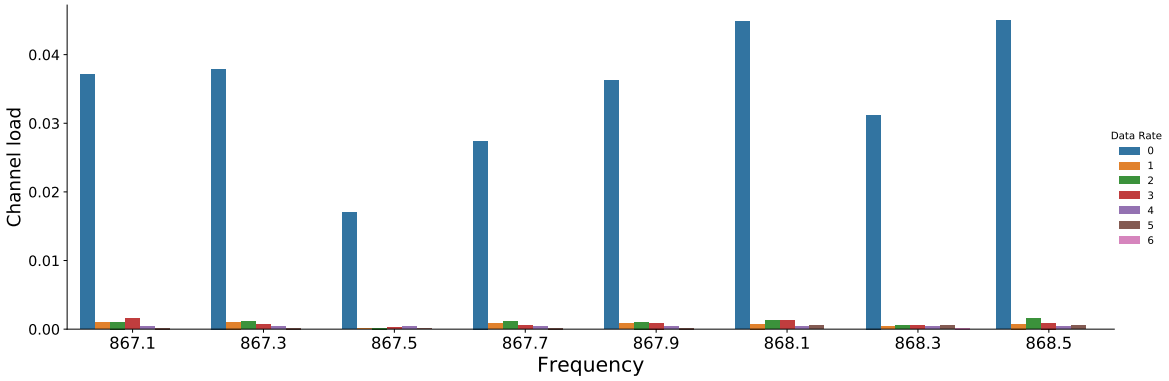

Figure 2.9 – Channel load by data rate by data rate for each sub-channel frequency

in terms of the number of received packets, which is only a reflection on the utilization of the channel and whether the wireless channels are saturated. To get more insights into the load of the channel, we have plotted the offered traffic percentage for all aggregated data rate and by sub-channel frequency in Figures 2.8 and 2.9, respectively.

The offered load of the aggregated data rate 0 reaches almost 0.25 of the channel capacity; this load is the sum load for the eight available used frequencies from both h1 and g1. For more accurate analysis, in terms of channel load by each central frequency, the channel load of data rate 0 is around 0.045% for all the sub-channel frequencies, considering that the channel is aloha-like, in which the channel saturates at 0.5 loads. As a result, we can conclude the channel is not yet saturated. Still, we note that the load of DR0 is predominant.

2.1.5 Traffic by operator

Table 2.2 presents the list of the LoRaWAN operators and networks from whom the gateway received packets. It also shows, for each identified network, the total number of received packets, the number of devices, the percentage of traffic compared to overall traffic, and finally, traffic by device.

While we recognize local LoRaWAN operators like TTN, Orange France, and Bouygues Telecom, we notice equally a number of private networks, experimental networks, some foreign operators like Swiss Led, Swisscom, and an unknown network. For the sake of clarity, we have merged networks with meager traffic into one set labeled "others".

Figure 2.10 shows the bar plots of the overall traffic, the number of devices, and traffic by one device for each network. On the one hand, most of the traffic is mainly distributed between 5 networks, Xnet with over 47%, The Things network with 15.5%, Orange France with 12.4%, Bouygues Telecom with 6.3%, and Experimental with 4.1%. On the other hand, Orange France has the highest number of devices with 578 nodes, followed by Bouygues with 303, then TTN with 160, and Experimental with 49. Surprisingly, Xnet that sent almost half of the overall traffic, has only 16 de-

Table 2.2 – LoRaWAN operators.

Operator	Overall traffic	Number of Devices	Percentage of traffic	Traffic by device
Actility	3144	22	0.358	143
Bouygues Telecom	63388	303	7.226	210
Comsol Networks	229	2	0.026	115
ER-Telecom Holding	99	1	0.011	99
Experimental	40649	49	4.633	830
Gemalto	334	2	0.038	167
Gimasi	132	6	0.015	22
Inmarsat	567	2	0.064	283
Kerlink	56	7	0.006	8
Loriot	18	4	0.002	5
Orange France	123611	578	14.09	214
Patavina Technologies	498	1	0.056	498
SENET	1	1	0.0001	1
SoftBank	479	2	0.054	239
Swiss Led	1	1	0.0001	1
Swisscom	1	1	0.0001	1
The Things Network	154817	160	17.64	967
TrackNet	8	1	0.0009	8
Unknown	15650	15	1.780	1043
xnet	473524	16	53.98	29595

vices. By computing the number of packets by device, we discovered that Xnet sent almost 30000 packets per mote, while TTN sent 967, Orange 214, and Bouygues 210. For the total number of monitoring, we get 41 packets sent per hour per mote for Xnet, which is relatively high.

We raise the question about the network's reliability and security if many networks do not respect the duty cycle restrictions or in case of a DDoS attack. The latter would immediately affect the collision rate in an aloha-based network, a sensitive access method to the collision. Then, do entities like ANFR (Agence Nationale des Fréquences) in France verify if the rules about duty cycle are respected?

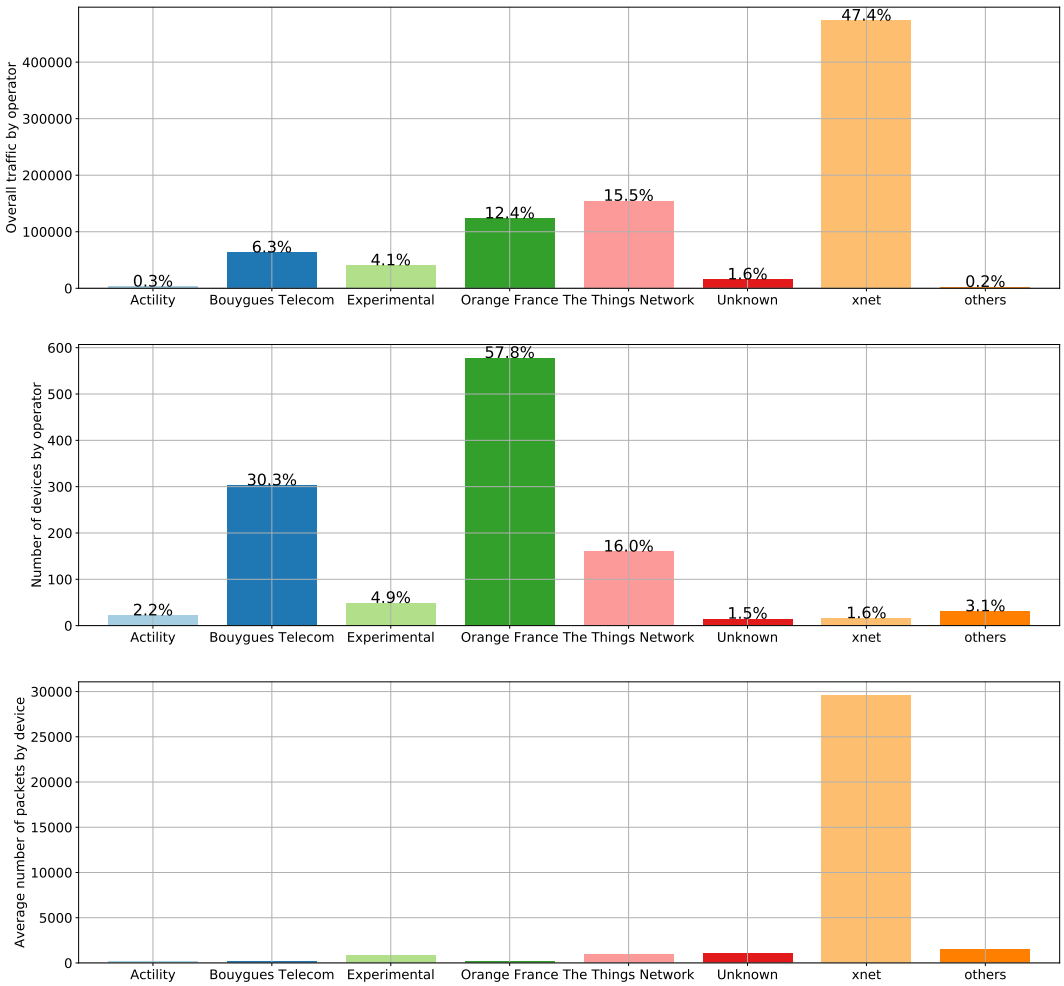

Figure 2.10 – LoRa traffic by operator

2.2 Experimental Test-bed

Our testbed consists of five STMicroelectronics motes [86] that operate under the WiSH-WalT framework [40] in the TTN network, a collaborative LoRaWAN network [27]. Its gateways forward traffic to the EU TTN server from which we collect data for characterizing transmission quality. WiSH-WalT enables easy configuration of motes with several parameters and running experiments. Each gateway performs a CRC check: if the CRC is valid, the gateway forwards the packet to the TTN server, otherwise, it drops the packet. The number of gateways correctly decoding a given packet mainly depends on *SF* of each transmission, since higher *SF* trades data rate for transmission robustness to reach larger distances. Up to 13 gateways were receiving the traffic from our motes.

2.2.1 STM boards

We have adopted in our experimentations the STMicroelectronics motes of type B-L072Z-LRWAN1 [86, 4]. The B-L072Z-LRWAN1 kit supports LoRa, Sigfox, and FSK/OOK technologies, and is commanded by an STM32L072CZ microcontroller and SX1276 transceiver [87]. The mote comprises an ST-LINK/V2-1 embedded debug tool interface, antenna, push-buttons, LEDs, Arduino™ Uno V3 connectors. It has support for LoRaWAN Class A, Class B, and Class C.

It includes a CMWX1ZZABZ-091 LoRa®/Sigfox™ module, which is equiped with an embedded ultra-low-power STM32L072CZ MCU, based on Arm® Cortex®-M0+ core, with 192 Kbytes of Flash memory, 20 Kbytes of RAM, 20 Kbytes of EEPROM It supports the frequency range: 860 MHz - 930 MHz, and has a 157 dB maximum link budget, a high sensitivity: down to -137 dBm and a 127 dB+ dynamic range RSSI. It benefits from a programmable bit rate up to 300 kbit/s, a preamble detection and sync word recognition [4].

STM provides the I-CUBE-LRWAN firmware package, presented in Figure 2.12, to debug, modify, run and flash the mote [5]. The I-CUBE-LRWAN Expansion Package includes a set of libraries and application examples for STM32L0 Series, STM 32L1 Series, and STM32L4 Series microcontrollers operating as end devices. The package includes an application running on the B-L072Z-LRWAN1 embedding the CMWX1ZZABZ-091 LoRa® module (Murata).

It is compliant with the LoRaWAN® version it has support for bidirectional end devices with class-A, class-B, and class-C. It works on the EU 868 MHz ISM band ETSI, EU 433 MHz ISM band ETSI and US 915 MHz ISM band Federal Communications Commission (FCC). It supports end-device activation either through OTAA (over-the-air activation) or ABP (Activation by Personalization) and it has support for adaptive data rate.

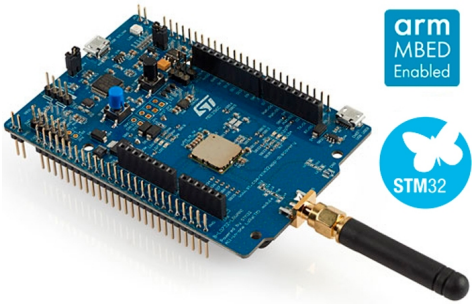

Figure 2.11 – STM [4].

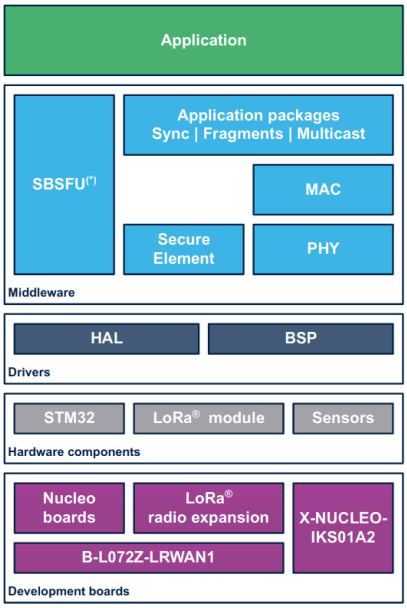

Figure 2.12 – I-CUBE-LRWAN firmware [5].

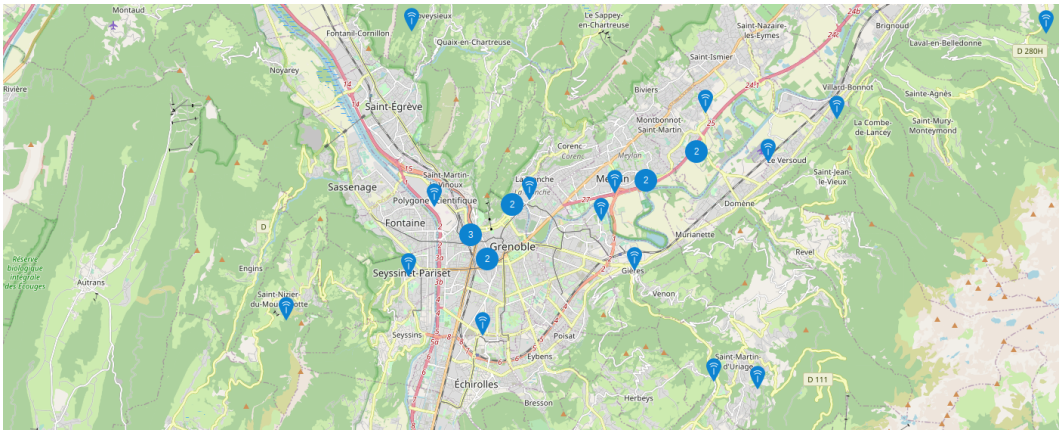

Figure 2.13 – TTN gateways in the Grenoble area.

2.3 Influence of Payload Length on Packet Reception

2.3.1 Experimental set-up

In the experiment, the STM mote periodically sends packets with varying payload length (PL) from 0 to PL_{max} with 1% of duty cycle and respecting the limitations given in Table 1.7. The mote sends a packet while following a pseudo-random policy: it alternates each time between the two bands. It randomly picks one frequency from each band, resulting in doubling the duty cycle, reminding that it is by sub-band. We performed experiments in three configurations:

- CONF-A: $SF = 9$, TP = 14 dBm, and we vary the payload length from 0 to 120 bytes.
- CONF-B: same as CONF-A, but we alternate between TP = 10 dBm and TP = 2 dBm.
- CONF-C: TP = 14 dBm, we vary the payload length from 0 to 55 bytes, and alternate between $SF = 11$, $SF = 9$, and $SF = 7$.

We set BW to 125 kHz and CR to 4/5 in all configurations.

Table 2.3 – Altitude of the gateways and distance to them ordered by reception quality.

Id.	Altitude (m)	Distance (km)
Gw1	220	0.01
Gw2	240	0.03
Gw3	220	2.4
Gw4	-	-
Gw5	253	3.9
Gw6	233	4.4
Gw7	246	2.9
Gw8	210	1.7
Gw9	249	5.2
Gw10	256	5.5
Gw11	244	5.7
Gw12	238	7.1
Gw13	2253	18.3

Table 2.4 gives, when available based on the GPS location, the altitude of the gateways collecting packets during the experiments and the distance from our motes to them. We number the gateways in the order of the reception quality to make the figures more readable.

2.3.2 Data Collection

We ran a background script that saves all generated traffic through an MQTT client.

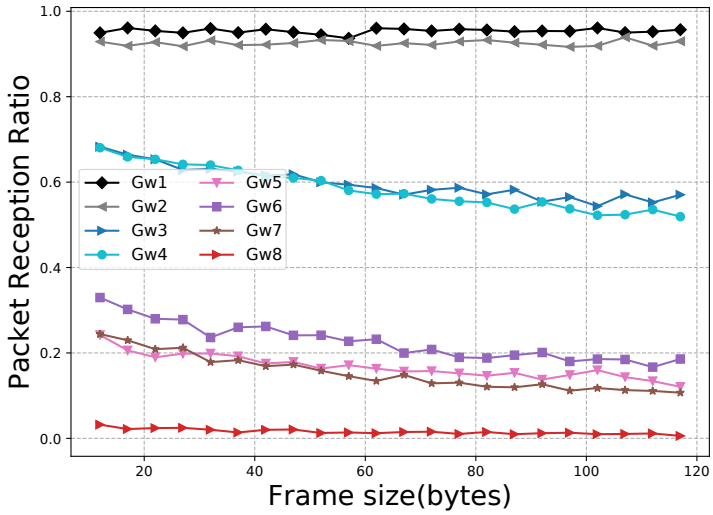

(a)

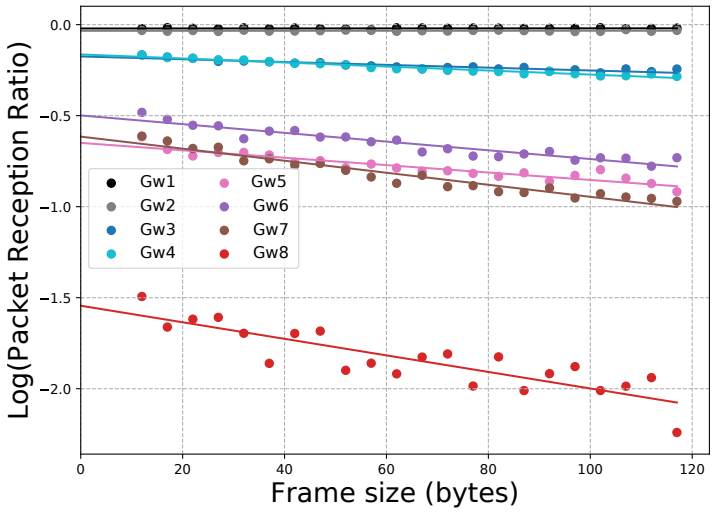

(b)

Figure 2.14 – a) PRR vs. frame size for *SF*9, TP = 14 dBm. b) log(PRR) vs. frame size for SF9.

2.4 Experimental Results

Packet Reception Rate (PRR) is a key metric that measures the reliability of transmissions. Figure 2.14a presents PRR as a function of the frame size for CONF-A. Notice that a mandatory explicit LoRaWAN frame header of 13 bytes is added to the frame—this is why we plot the result as a function of the frame size observed at gateways.

We can notice that the PRR curves are almost flat, which demonstrates only a slight impact of PL on the frame reception. The important finding is the fact that the curves do not tend to 1 for the frame size going to 0, which shows that the packet reception is not only affected by constant BER. To observe the shape of the curves better, Figure 2.14b presents the same data in the log scale with a linear regression function to show the limit behavior of PRR when the frame size goes to 0. We provide more in-depth analyses of this behavior in Section 2.5.

We also notice that the shape of PRR curves is slightly different for each gateway depending on

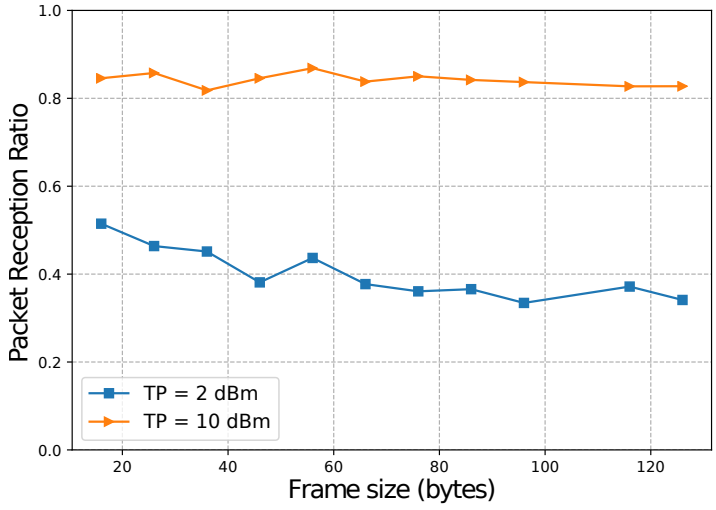

(a)

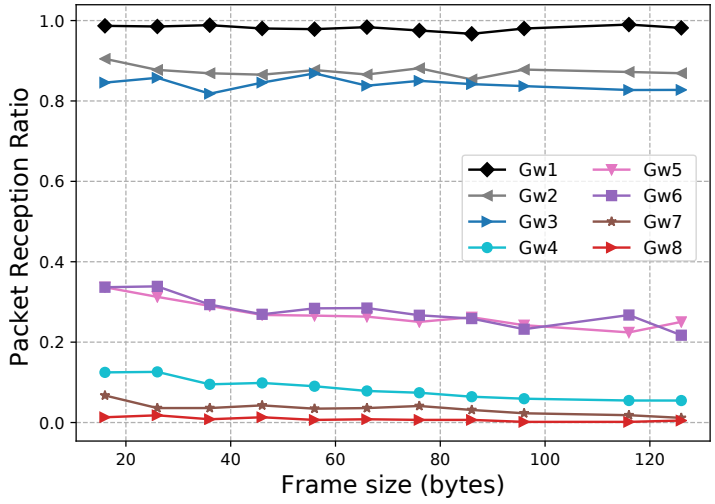

(b)

Figure 2.15 – a) PRR vs. frame size for Gw3. b) PRR vs. frame size, TP = 10 dBm, *SF*9.

its position as described in Table 2.4, which strongly impacts channel quality. Moreover, although the distance that separates our mote from both Gw1 and Gw2 is almost the same, PRR of Gw1 is better then Gw2. This effect probably comes from the fact that Gw2 is outdoor on a higher altitude so it captures more traffic, which means more possibility of collisions with our packets. The marginal difference incidentally shows that there are relatively few collisions for the selected channels and *SF*. This conjecture is corroborated by the fact that longer frames, which are more likely to collide at some instant during their reception, are only slightly more likely to be dropped. We ran many other configurations with different values of *SF* and the results were similar to CONF-A, for which PRR is only slightly impacted by PL.

Figure 2.15a shows PRR for CONF-B for Gw3, as a function of the frame size for TP = 2 dBm and TP = 10 dBm, and Figure 2.15b presents PRR as a function of the frame size for all gateways when TP = 10 dBm. We observe the same behavior—only a slight impact of the payload length on

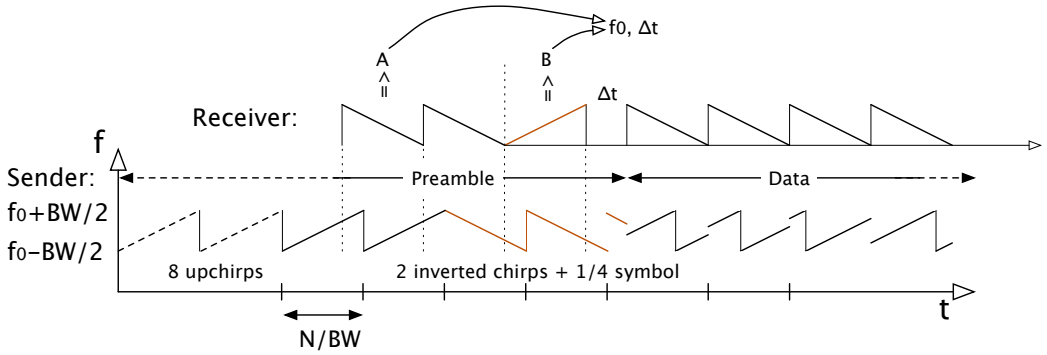

Figure 2.16 – Receiver synchronization with preamble.

PRR: when we increase TP, PRR increases, but it keeps the same almost flat shape.

2.5 Analysis of PRR Anomaly

In general, on wireless channels, Packet Reception Rate PRR is a function of Bit Error Rate BER and packet length PL:

$$\mathrm{PRR} = (1 - \mathrm{BER})^{\mathrm{PL}}. \tag{2.1}$$

When the PL value approaches 0, PRR increases to 1. We would therefore expect that the PRR value of each gateway starts close to 1 and then drops when PL increases. However, our results shown in all figures strongly differ from this expected theoretical PRR dependence on the packet size.

To investigate further the effect, we propose to introduce an extra multiplicative factor that represents its impact on PRR in addition to SNR, PL, and *SF* through probability P_s, which accounts for the uncertainty of successfully initiating the reception. Toward this goal, we apply the log function on the PRR formula. Since the majority of the curves are linear, we perform linear regression:

$$\log(\mathrm{PRR}) = \mathrm{PL} \times \log(1 - \mathrm{BER}) + \log(P_s). \tag{2.2}$$

When we vary the payload of the LoRa packets between 0 and 120 bytes, the frame size changes from 13 to 133 bytes because of an additional 13 byte overhead corresponding to the mandatory LoRaWAN header. By extending the regression function to the payload size of 0, we obtain the value characterizing the multiplicative factor as shown in Figure 2.14.

Successful reception of a frame mainly depends on three conditions: i) absence of collisions, ii) preamble detection and time synchronization with the gateway, and iii) valid decoding. Assuming low traffic, so rare collisions, we investigate the effects of channel variability on packet reception.

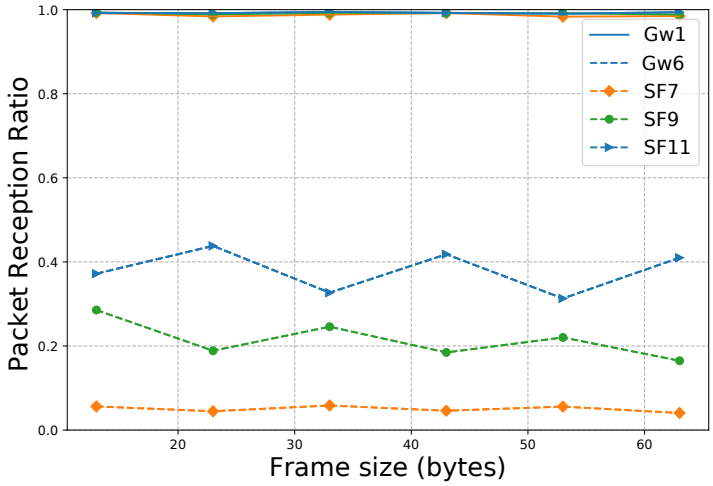

Figure 2.17 – Gw1 and Gw6: PRR as a function of the frame size for several *SF*.

2.5.1 Preamble detection and time synchronization

To correctly receive a frame, the gateway need to first detect the frame preamble and synchronize with it. As the CSS modulation is sensitive to synchronization issues between the received packet and the reception process at the gateway, errors may occur during the preamble detection process. If the preamble is not correctly detected by the receiver, the complete frame is lost.

Figure 2.16 illustrates the process of receiver synchronization: a sender transmits a preamble of 8 upchirps followed by 2 inverted chirps (downchirps) and 1/4 of a symbol. The receiver multiplies the upchirps by downchirps so it can find two unknown variables: precise transmitter frequency f_0 and relative time reference Δt between the sender and the receiver, to decode correctly further symbols that encode data. If the synchronization process fails, the receiver cannot receive the frame. Note that for low values of *SF* (e.g., *SF*7), chirps are short and they double their duration for each increment of *SF*. So, the synchronization process is more vulnerable for *SF*7 and becomes more reliable for larger *SF*.

2.5.2 Channel attenuation

To characterize further P_s, we have run experiments in the CONF-C configuration in which we varied the frame size cyclically and alternated between *SF* 7, 9, and 11 for two weeks. Then, we determined P_s for each gateway and each *SF* with the following method:

- for each couple (Gwi, *SF*), we plot PRR vs. frame size like in Figure 2.17 (we give the data for Gw1 and Gw6 as an example, we skip other gateways, Gwi, due to the lack of space).
- we apply log(PRR) and perform the linear regression to obtain the value of $\log(P_s)$ for PL= 0 for each pair (Gwi, *SF*).

Figure 2.18 presents the data for P_s in function of *SF* for gateways 1 to 3, 5, 6, 8, and 13 (there are

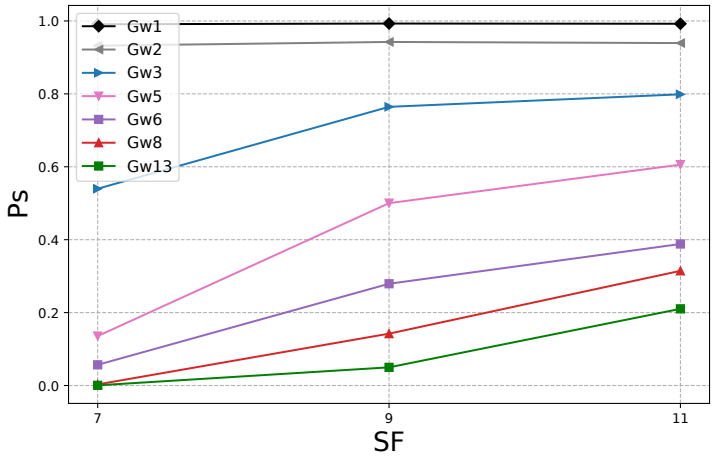

Figure 2.18 – P_s as a function of *SF*.

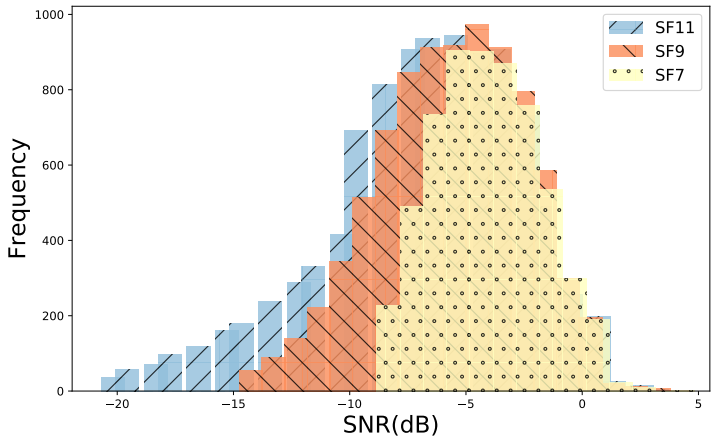

Figure 2.19 – SNR distribution at Gw3 for CONF-C.

seven gateways that receive packets for three configured values of *SF*: 7, 9, and 11). We can notice in this figure that, as expected, P_s depends on *SF*: P_s increases for larger *SF*. Nevertheless, the improvement is relatively limited between *SF*9 and *SF*11: there is no threshold *SF* (or transmission power) above which PRR would notably rise. This behavior bears similarity with what is expected for a slowly varying Rayleigh channel.

So, we represent in Figure 2.19 the measured SNR distributions. We can observe that they closely follow the distribution of the Rayleigh channel gains for *SF*11. For smaller *SF*s, the distribution is truncated to the left because the corresponding packets are simply not received. In essence, each transmission faces an exponentially distributed Rayleigh channel gain, which remains mostly constant during the transmission.

Figure 2.20 presents P_s as a function of mean SNR for each couple (Gwi, *SF*). To understand the curves, we need to explain how we compute mean SNR—it is the mean of the SNR values computed for all received packets at each *SF* so it does not take into account the packets that are lost. Mean SNR grows for smaller *SF*, since only the packets with higher SNR are effectively received for less robust modulations, whereas for greater *SF*, the packets with smaller SNR are included in the mean. For instance, mean SNR for Gw13 is computed only on a small fraction of

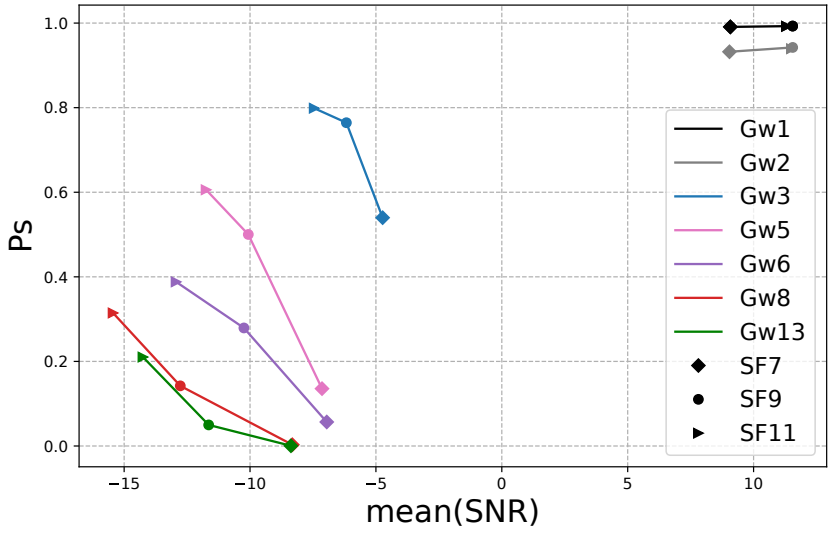

Figure 2.20 – P_s as a function of mean SNR.

packets that made it through.

In the figure, we do not observe a clear relationship between measured SNR and *SF* to use: there is approximately 5 dB of SNR difference between Gw3 and Gw5, which should theoretically be compensated by using *SF*11 instead of *SF*9, as each *SF* step brings 2.5 dB of the coding gain. This is what we see with similar PRR between Gw5 at *SF*9 and Gw3 at *SF*7. However, at *SF*11, Gw5 is still well below PRR of Gw3 at *SF*9. In other words, PRR reaches a plateau above which switching to higher *SF* brings little improvement.

PRR at Gw6 stands out: it is below the general PRR vs. SNR trend. This gateway also shows an unusual behavior in Figure 2.14 with even less influence of the packet size than the other gateways. We have not identified the reason that makes this gateway special, but the investigation into its behavior helped us to identify the limiting factor for PRR.

2.5.3 Related Work

Several authors experimentally evaluated LoRa performance with the focus on different parameters, types of hardware, and various network characteristics. Augustin et al. [32] measured LoRa packet loss rate on a LoRa testbed showing: i) less than 10% of loss rate over a distance of 2 km for *SF* 9-12 and ii) more than 60% of loss rate over 3.4 km for *SF*12.

Haxhibeqiri et al. [34] studied LoRa scalability. Their simulation model based on the measurements of the interference behavior between two nodes shows that when the number of nodes with the duty cycle of 1% increases to 1000 per gateway, the loss ratio increases to 32%, which is low compared to 90% in pure ALOHA for the same load. This difference comes from taking into account the capture effect.

Petrić et al. [36] observed a highly variable packet error rate (between 3% and 90%) for the range of 3 km from a gateway under the following conditions: bandwidth of 125 kHz, coding rate

of 4/5, transmission power of 14 dBm, and spreading factor *SF* 7, 9, and 11.

Mikhaylov et al. [38] studied the variation of the payload length, however, in a synthetic setup based on motes connected by cables and involving an artificial interferer, therefore, the results are not representative for real operational traffic.

Blenn et al. [39] provided statistics of the TTN traffic based on global TTN logs: number of received frames, number of gateways, number of devices etc. They reported on the probability density function of RSSI and SNR, and presented the histograms of the payload length and spreading factors. They used the observed parameter in simulations to estimate collision probability as a function of the traffic intensity.

To the best of our knowledge, our work is the first one to study the impact of the payload size on PRR measured in an operational LoRaWAN network and reveal the behavior different from other types of wireless networks. We also point out the influence of the attenuation of a slow fading Rayleigh channel and receiver synchronization on successful packet reception.

2.6 Preamble Length and Coding Rate Variation

2.6.1 Preamble Length Variation

Preamble detection is a fundamental task in the process of correct reception of the packet. The gateway should first detect the frame preamble and synchronize the reception process to receive a frame correctly. If the receiver does not correctly detect the preamble, the complete frame is lost. We wanted to study the variation of the preamble length and its impact on the overall PRR. The preamble length is programmable, and it can take values from 4 to 65535. The mote datasheet mentions that when changing the preamble length, the gateway needs to be re-configured. As we do not control the TTN gateways, we suppose they can receive packets with different preamble lengths. The following results show that packets sent with various preamble lengths were correctly received.

We have run experiments according to three configurations: in the first one, the node alternates between the values of the preamble length: 8, 12, and 16 using one of the available sub-frequencies in a pseudo-random policy:

In the second one, the node alternates between 8, 12, and 16 as a preamble length using one frequency of 868.5. The last experiment is like the first one but with different values of preamble length; the mote alternates between 6, 34, 48, and 62. Figures 2.21, 2.22, and 2.23 show the PRR for various preamble length values at several gateways for the three scenarios, 1, 2 and 3 respectively.

Overall, we notice a negligible variation in the PRR; while it slightly increases for gw2 and gw6, it decreases, then increases for gateways 3, 5 and 7 increases, and then decreases for others; results

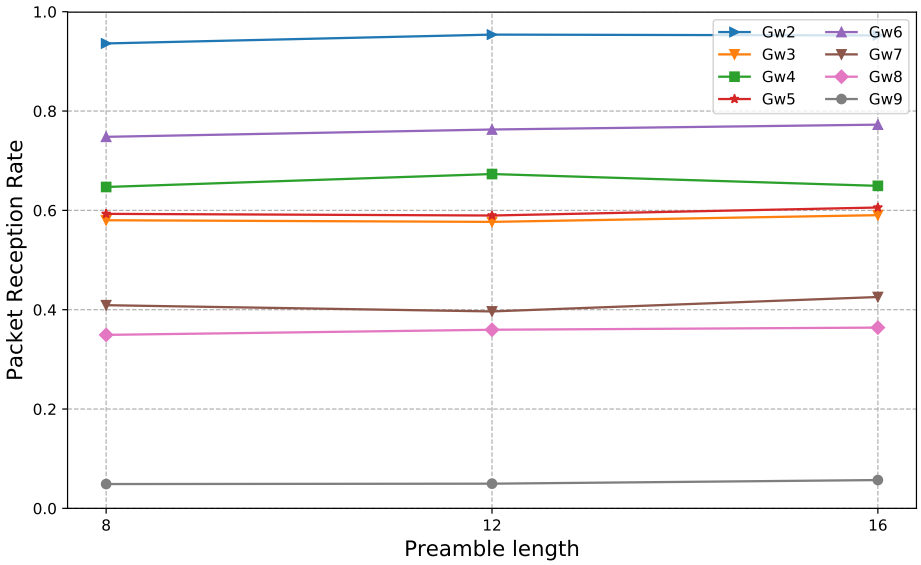

Figure 2.21 – PRR versus preamble length with frequency hopping, transmission power 14 dBm, *SF*12.

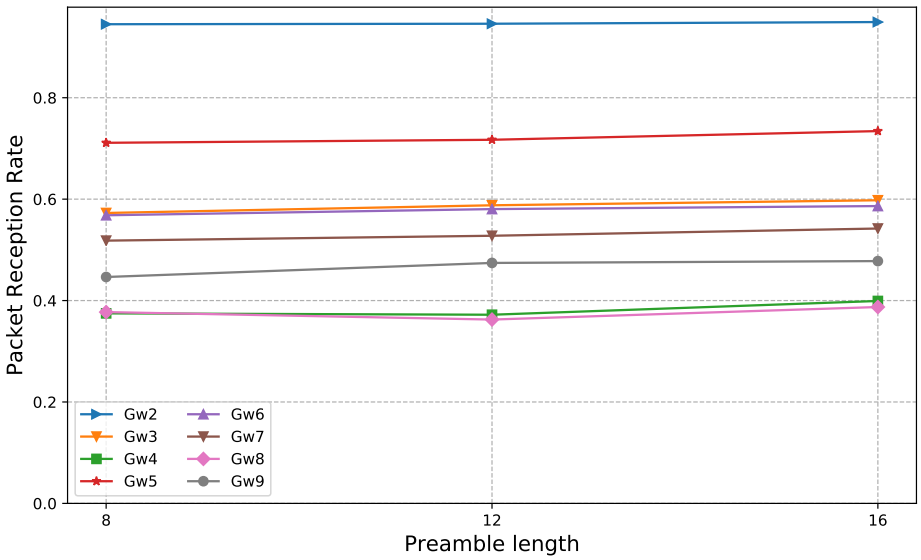

Figure 2.22 – PRR versus preamble length with fixed frequency=868.5, transmission power 14 dBm, *SF*12.

are similar with higher values of preamble length.

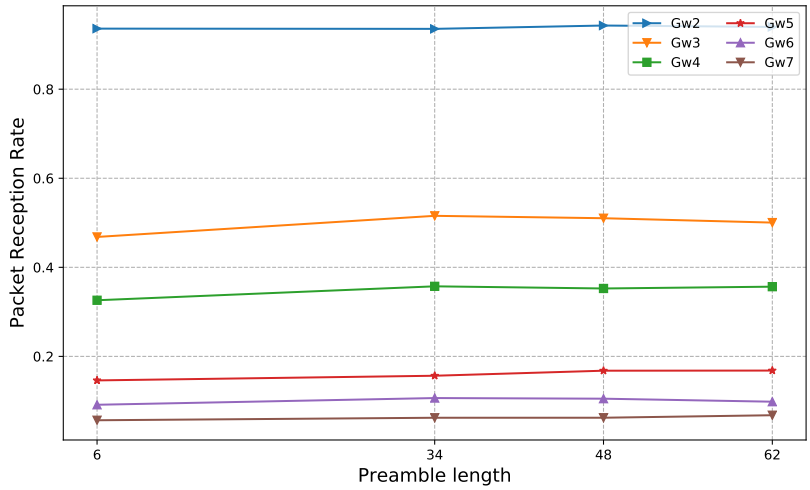

Figure 2.23 – PRR versus preamble length with frequency hopping, transmission power 14 dBm, *SF*12.

2.6.2 Coding Rate Variation

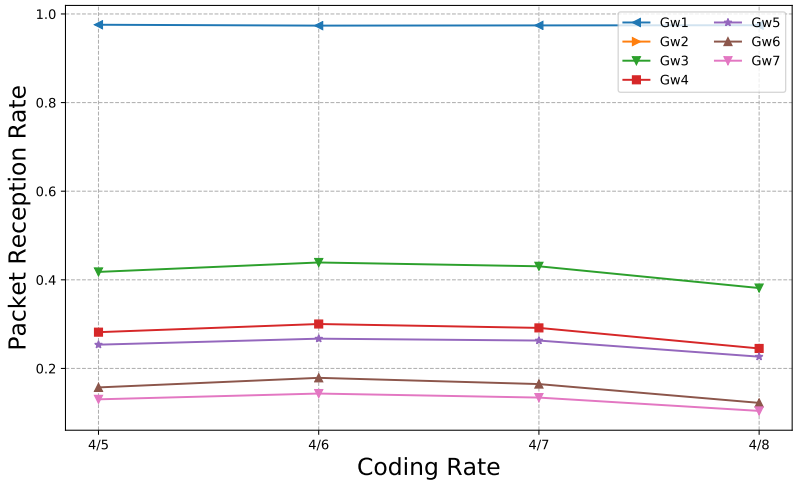

Figure 2.24 – PRR versus coding rate transmission power 14 dBm, *SF*11.

The Coding Rate (CR) corresponds to the Forward Error Correction (FEC) rate applied to improve the packet error rate in the presence of noise and interference. It takes values from 4/5, 4/6, 4/7, and 4/8. The implementation of CR is done by encoding 4-bit data with redundancies into 5-bit, 6-bit, 7-bit, or 8-bit. As a result, a lower CR provides better robustness but increases the transmission time and energy consumption.

In this paragraph, we wanted to study the impact of increasing the Coding Rate on the PRR. We run experiments with the following configuration, the mote alternates between 4/5, 4/6, 4/7, 4/8 values, using one of the eight available sub-frequencies in pseudo-random policy, with *SF*=11 and TP=14 dBm.

Figure 2.24 presents the PRR versus CR for gateways 1, 3, 4, 5, 6, and 7. We note that the PRR increases for the coding rate $4/6$ then decreases for coding rate $4/7$ and $4/8$ for gateways from 3 to 7. for gateway 1, there is no apparent effect. We can conclude that increasing the CR to $4/6$ or $4/7$ is slightly beneficial for improved PRR.

2.7 Experimental Channel Characterization

Wireless channel link quality is one of the significant determinants that affect wireless network reliability in many aspects. The application designer and network optimizer need to understand and know the channel behavior to assess the network parameter in an optimum way to have better performance.

One of the main characteristics of the wireless channel communication is fading—deviation of the attenuation affecting a signal over certain propagation media: a signal faces two types of fading, large scale fading, and small scale fading.

Many papers assume a Rayleigh fading channel. This assumption is quite usual, except in rare cases [88], but we draw attention to the fact that it was originally a model for mobile nodes. In the case of LPWAN networks, we consider mostly static nodes so that it would also be reasonable to assume less variability of the channel gain.

2.7.1 Experimental Set-Up

To get insight on how the channel gain behaves in the real world, we have run long-term experiments using an STMicroelectronics mote [86] and several gateways of The Things Network (TTN), a public LoRa network [27]. We have generated traffic and gathered statistics for three months to get the RSSI distributions and other graphs describing the channel.

We have configured two types of experiments, one where the node is indoor inside the office and one where it is outdoor. We send at $SF11$ with a transmission power of 14 dBm. The transmissions alternate between 8 different frequency channels. All histograms from the indoor sender are non-line-of-sight links in a suburban environment. For the outdoor histograms, some are non-line of sight, and some are line of sight. The total number of receiving gateways is 13 for the indoor and 16 for the outdoor.

2.7.2 Channel behavior: Indoor and outdoor

Figure 2.25 represents the expected fading gain (in dB) distribution for a Rayleigh channel, where the received signal power is affected by a multiplicative random variable with an exponential distribution of the unit mean.

Figure 2.26 shows the RSSI distributions of the received packets at six gateways, 2.4 km, 2.9 km, 3.7 km, 3.9 km, 4.4 km, and 5.2 km from the end-device, corresponding to gateways 3, 4, 5, 6, 7, and 9, for two types of senders: indoor, hatched figures and outdoor, dotted and hatched figures.

Figure 2.27 depicts the Packet Reception Rate (PRR) at the same selected gateways 3, 4, 5, 6, 7, and 9 from the indoor sender, hatched bars, and from an outdoor sender, dotted and hatched bars.

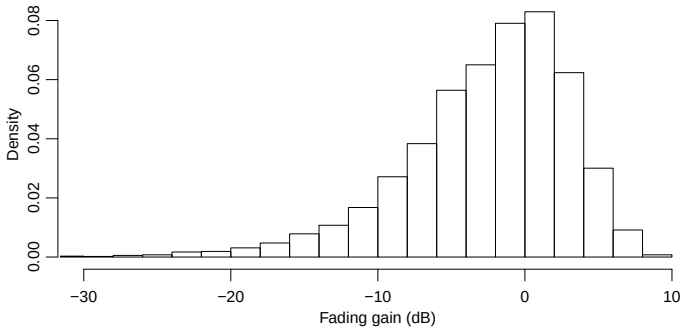

Figure 2.25 – Expected fading gain (in dB) distribution for a Rayleigh channel

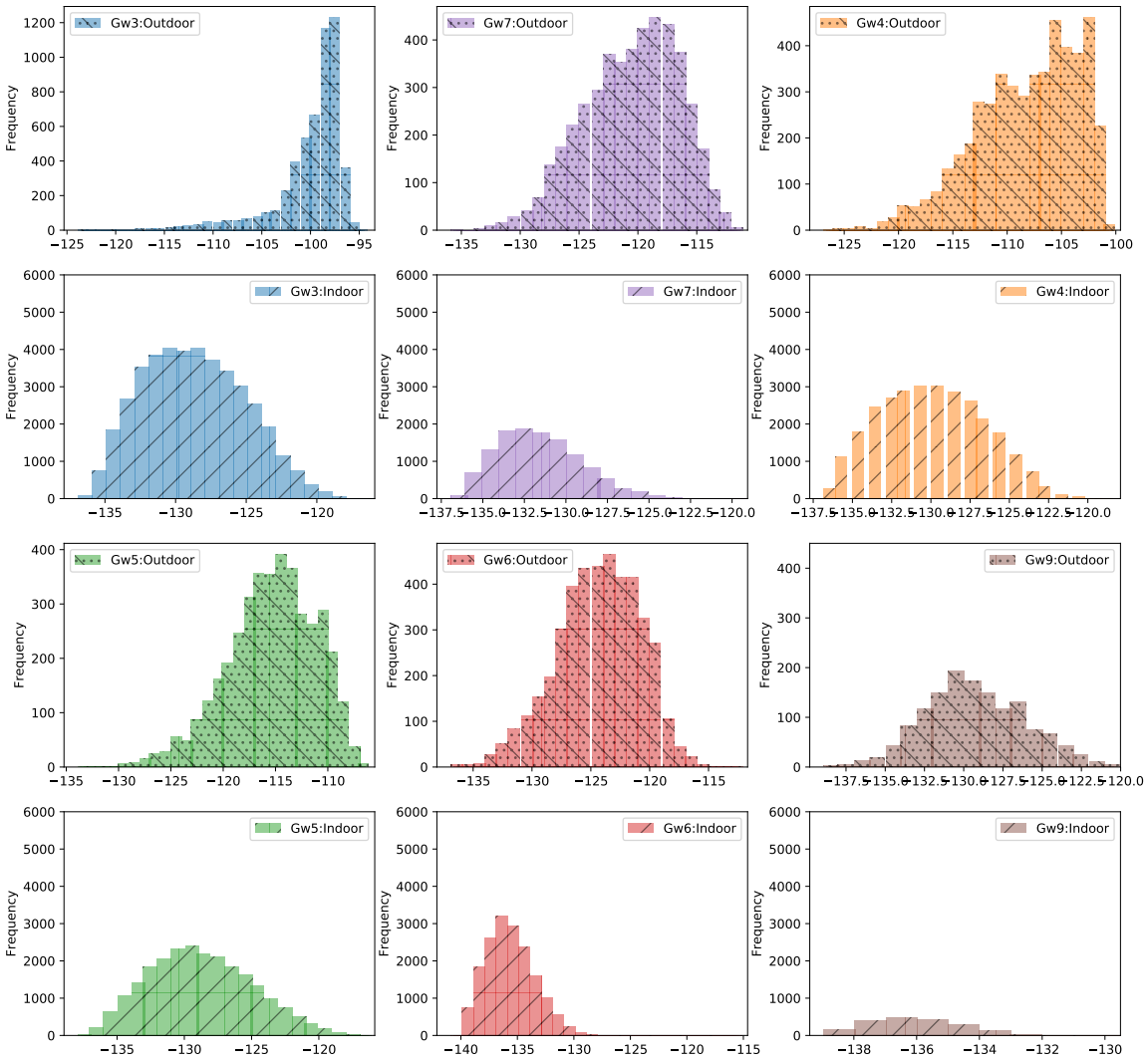

Figure 2.26 – Measured RSSI distribution at gateways 3, 7, 4, 5, 6, and 9 from an outdoor sender (hatched and dotted), and indoor sender (hatched), transmission power 14dBm, *SF*11.

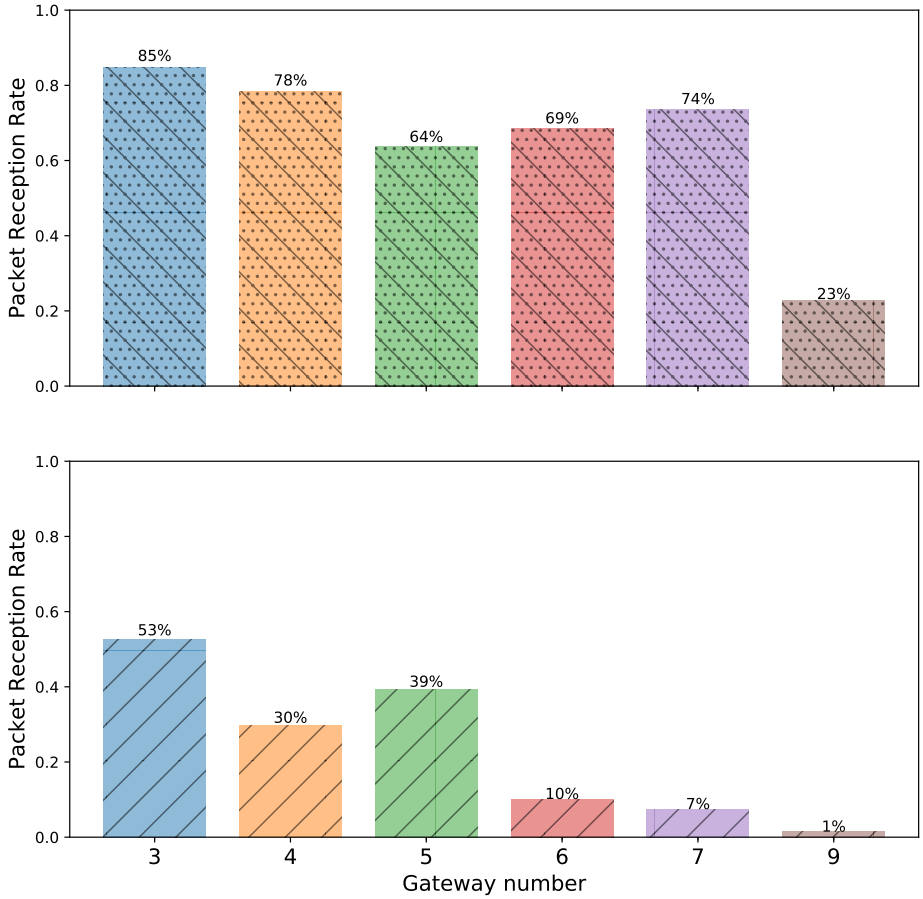

Figure 2.27 – Packet Reception Rate at gateways 3, 4, 5, 6, 7, and 9 from an outdoor sender (hatched and dotted), and indoor sender (hatched), transmission power 14dBm, *SF*11.

Table 2.4 – Altitude of the gateways and distance to them ordered by reception quality.

Id.	Altitude (m)	Distance (km)
Gw0	220	0.005
Gw1	220	0.01
Gw2	240	0.03
Gw3	220	2.4
Gw4	248	3.7
Gw5	253	3.9
Gw6	233	4.4
Gw7	246	2.9
Gw8	210	1.7
Gw9	249	5.2
Gw10	256	5.5
Gw11	244	5.7
Gw12	238	7.1
Gw13	2253	18.3

The PRR provides insight into the percentage of the received packets. PRR depends on distance, fading sensitivity and collision. We ignore collision as we showed in Section 2.1 above that the load is concentrated at data rate 0 and that the channel is not saturated.

While all histograms from the indoor sender are for non-line-of-sight links in a suburban environment, histograms from an outdoor sender depend on the gateway placement and altitude, resulting in some links being line-of-sight and others non-line-of-sight in a suburban environment.

The RSSI distributions at gateways 4, 5, 6, and 7 follow well the expected distribution of gains for a Rayleigh channel, which appears in Figure 2.25—deep fades of -10 dB below the average gain (0 dB in Figure 2.25) are common. Gateways 4, 5, 6, 7 presents a PRR of 78%, 64%, 69%, 74%, and they are at 3.7 km, 3.9 km, 4.4 km, 2.9 km from the end devices, respectively. Although the distributions are truncated, with less than 75% of packets, it illustrates a shape roughly close to Rayleigh. However, RSSI distribution at Gateway 3 and Gateway 9 does not follow the expected distribution for a Rayleigh channel.

Gateways 3 is at 2.4 km from the end device and presents a PRR of 85%. The link between the node and the gateway is more likely to be a Line-Of-Sight (LOS), which results in less fading and attenuation to affect the packet power: the mean of the RSSI values for this gateway is around $-100dBm$ (see Figure 2.28), which is at least 10 dB more than the other gateways mean RSSI values that are more than 2 km away from the node (gateways 4 to 13). Note that the sensitivity of approximately -140 dBm for $SF11$ truncates the distribution because the frames experiencing high

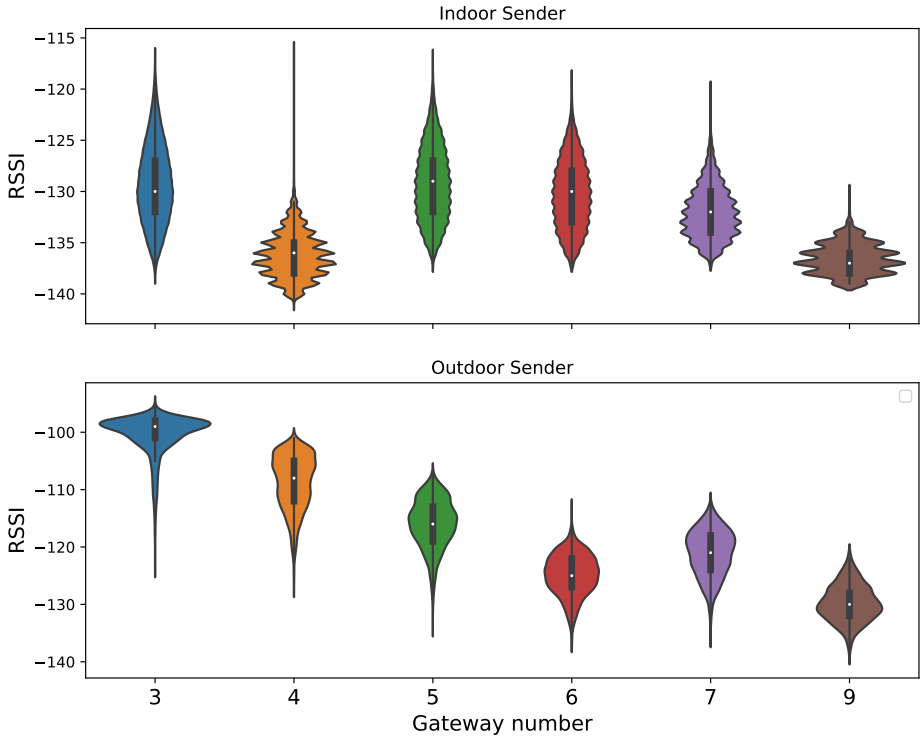

Figure 2.28 – Violin plots for measured RSSI at gateways 3, 4, 5, 6, 7, and 9 for an indoor sender and an outdoor sender, transmission power 14 dBm, *SF*11.

fading are lost. Gateway 9 presents a PRR of 23% and is at 5.2 km from the end device. This longer link faces severe fading and attenuation, which leads to high packet loss. With only 23% of received packets, the distribution is truncated; only a fourth of the expected distribution is visible, representing the start of the expected exponential distribution.

Gateways 10 to 13 present a PRR of less than 20%. The latter faces severe fading and distance attenuation and therefore exhibits the same result as gateway 9.

Gateways 1 and 2 are close and have a PRR of 96%. Packets, in this case, experience negligible fading and attenuation.

Figures 2.26, 2.27, and 2.28 reveal that the results from an indoor sender significantly differ from the outdoor sender. PRR values drop drastically from 85% to 52%, 78% to 28%, 64% to 37%, 69% to 7%, 74% to 7% for gateways 3, 4, 5, 6, and 7 respectively. The decrease in the PRR translates to a more truncated distribution, resulting in incomplete shape distribution that roughly follows Rayleigh distribution with missing parts.

Packets from an indoor sender face more obstacles and shadowing, leading to more attenuation affecting the received power of a packet. The increased attenuation introduces more variability between the received powers. This latter would randomize the outcome of the capture effect when a collision occurs.

Figure 2.28 displays the violin plots of the RSSI of the received values at gateways 3, 4, 5, 6, 7, and 9 from the indoor sender and the outdoor senders.

Violin plots include a marker for the median of the RSSI values, a box indicating the interquartile range, all inside a rotated kernel density plot on each side; it shows how the RSSI values are spread around the mean and where the majority of the values are concentrated.

Figure 2.28 exhibits the considerable difference between the channel gains when the sender is indoor vs. outdoor on the one hand and the channel gain from one gateway to another depending on distance in the suburban environment on the other hand.

While the mean RSSI ($RSSI_m$) for gateway 3 is -100 dBm when the sender is outdoor, it drops to -130 dBm when the sender is indoor, representing a considerable channel gain difference of -30 dB. We observe the same gain difference for gateway four, where $RSSI_m$ is -105 dBm for the outdoor sender and -135 dBm for the indoor sender. The gain gap between the values shrink as the gateway distance increases, but remains considerable, 15 dB for gateway 5 and 10 dB for gateway 6 and 7. Moreover, the difference between $RSSI_m$ values for the given gateways when the sender is outdoor is more remarkable than when the sender is indoor. For instance, the RSSI distribution for gateway 3 strongly differs when the sender is indoor or outdoor. While the values are concentrated in one area in a 10 dB margin, the values for the indoor sender are more spread out in a width of 40 dB, between -115 dBm to -140 dBm, which results in considerable variability between the RSSI values at the receiver. This variability would randomize the capture effect output when a collision occurs in favor of a stronger packet. We notice the same phenomena for gateways 5 and 6.

Finally, the measures confirm that the channel gains are always variable and that even for nodes with similar average channel gains,it would be very common to witness reception powers with a difference of 6 dB. In this case, the capture effect allows the gateway to receive one of the colliding frames [8].

2.7.3 Channel variability over time

This paragraph analyzes the channel more thoroughly by studying its time variability for several used frequency channels.

The set-up of this experiment is the same as for the previous experiment, where an outdoor and an indoor sender send packets to TTN gateways using one of the eight available frequency every time, using a pseudo-random policy with *SF*=11 and TP=14 dBm.

Figures 2.29 and 2.31 show the RSSI values of received packets in time, i.e., ordered by their reception time at gateways 1, 3, 4, 5, and 7 for the outdoor sender, and gateways 0, 1, 3, 4, and 5 for the indoor sender, respectively. The figures also reveal the central frequencies with which the packets were sent.

To get more insight into the overall aggregated distributions, Figures 2.30 and 2.32 illustrate the violin plots for gateways 1, 3, 4, 5, and 7 for the outdoor sender and gateways 0, 1, 3, 4, and 5

the outdoor sender, respectively.

In the following, we divide the analysis from the indoor and the outdoor sender since results at several gateways demonstrate distinct patterns.

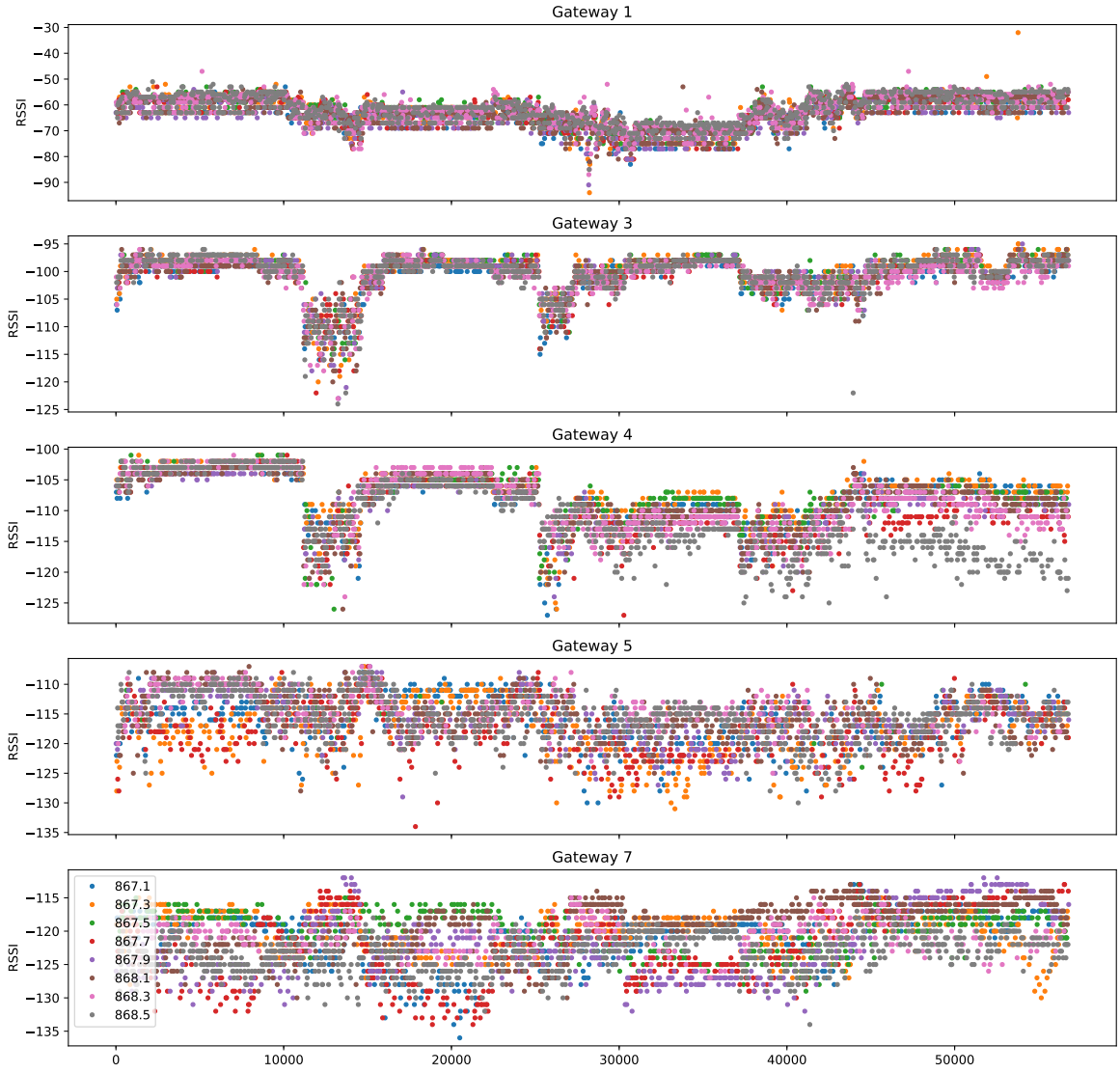

Figure 2.29 – Measured RSSI over time for gateways 1, 3, 4, 5, and 7 for an outdoor sender, transmission power 14 dBm, *SF*11.

When the sender is outdoor:

We distinguish three patterns. The first model is observed at gateway 1: the RSSI values from the eight sub-frequencies are close, the width of the variation is narrow, with a margin of almost 10 dB. When an increase or a decrease of the RSSI values arises during a period, it occurs for all the sub-frequencies. Moreover, the violin plot demonstrates three bumps, which corresponds to the three variations. In this use case, the channel is not Rayleigh, which is expected and explained since this gateway is only a few meters away from the sender, where it exhibits 96.5% of PRR, and RSSI values are close.

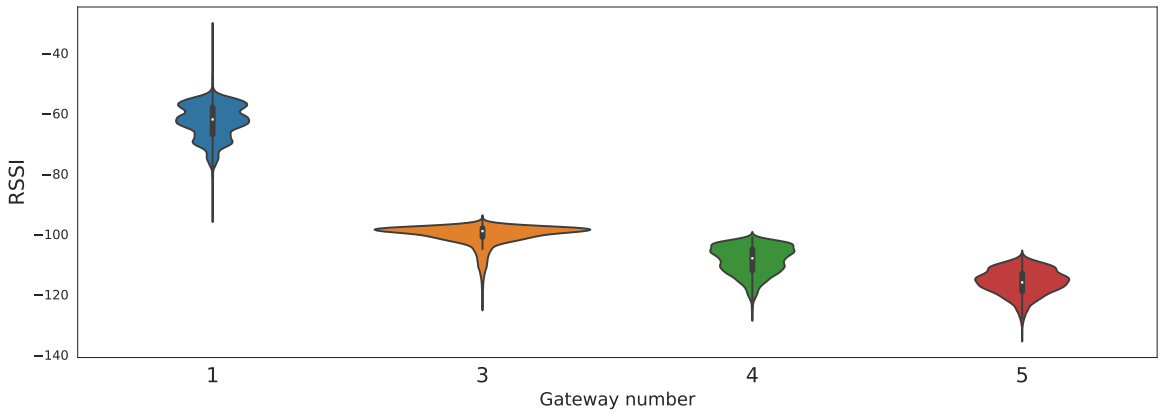

Figure 2.30 – Violin plots of gateways 1, 3, 4, 5, and 7 for an outdoor sender, transmission power 14 dBm, *SF*11.

We observe the second pattern in the RSSI variation through time for gateways 5 and 7. The values are scattered in a wider range from -135 dBm to -110 dBm with a margin spread of almost 25 dB. Aggregating the reception powers from the different frequency channels yields a distribution that closely resembles the expected one with a Rayleigh channel. The violin plot and RSSI distributions in Figures 2.30 and 2.29 confirm this behavior.

Finally, the last behavior in the RSSI variation of gateways 3 and 4: at gateway 3, RSSI values are scattered not most of the time, i.e., by a margin of 10 dB (between -95 dBm and -105 dBm). However, we notice a drop in the RSSI values, where values are scattered in a broader range of 20 dB (between -105 dBm and -125 dBm).

At gateway 4, we note that values at the beginning of the reception do not vary much, by about 5 dB. Then a drop of the values occurs, and consequently, values are scattered in a larger width. Then values rise and become again much less variable. In the last part, values drop and rise over a broader range, by as much as 20 dB.

This resulting RSSI variation model of the two gateways mixes two channels behaviors in one. The part where the values are widely scattered corresponds to a Rayleigh channel behavior, and the part where the values are concentrated and close together represents less challenged propagation environment. The violin plots and the aggregated distributions in Figures 2.30 and 2.29 confirm the channel mixture, Rayleigh and non-Rayleigh, for gateways 3 and 4. For instance, at gateway 3, where values were not scattered most of the time, the non-Rayleigh channel takes over all the resulting distribution, which is not a Rayleigh distribution. On the contrary, for gateway 4, where it was most of the time Rayleigh, but a noticeable part of the time was not Rayleigh, we can observe that aggregated RSSI distribution is the result of the overlap of two distribution patterns, a Rayleigh part and a non-Rayleigh part (the pick at -100 dBm).

When the sender is indoor:

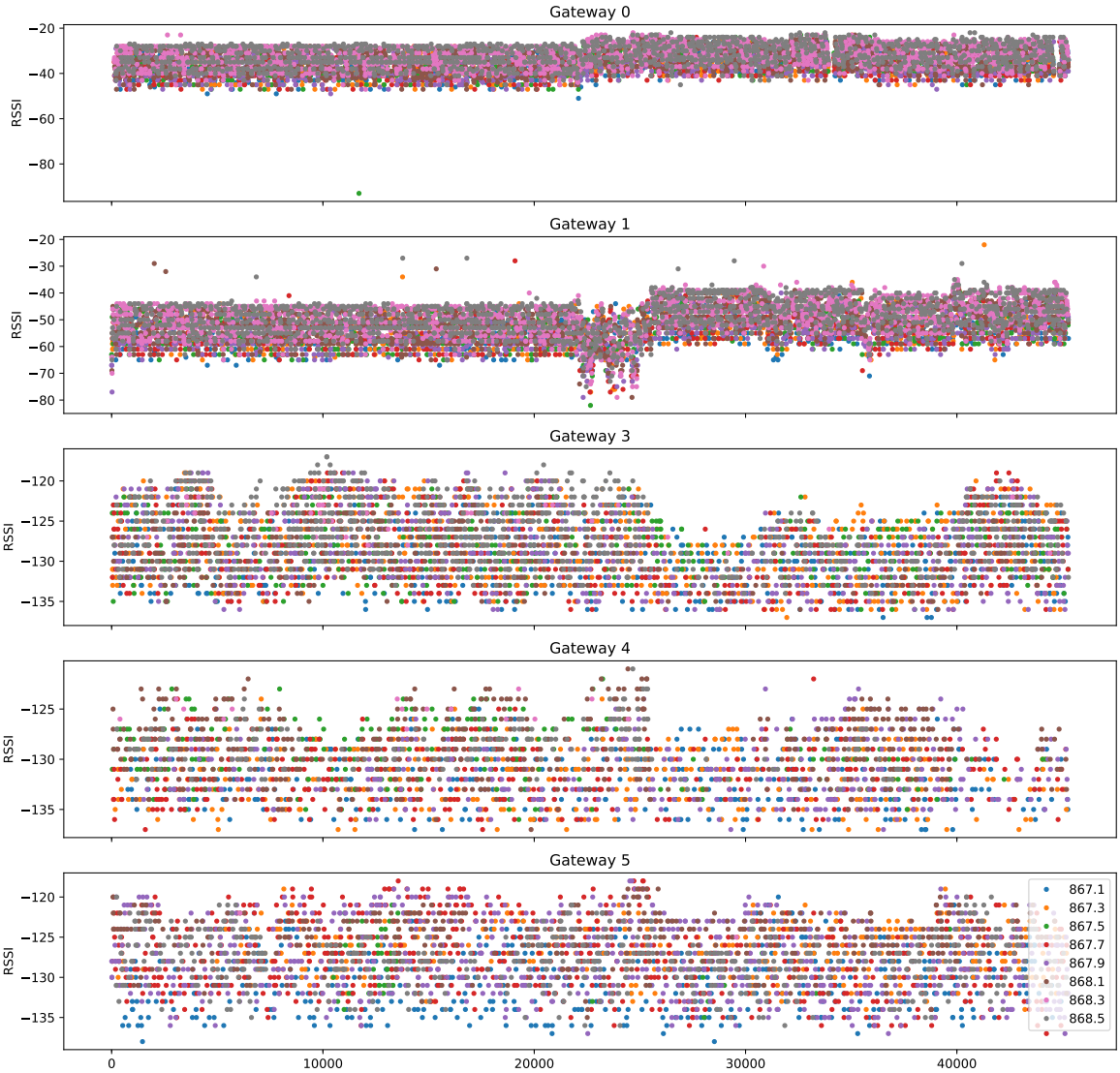

Figure 2.31 – Measured RSSI over time for gateways 0, 1, 3, 4, and 5 for an indoor sender, transmission power 14 dBm, *SF*11.

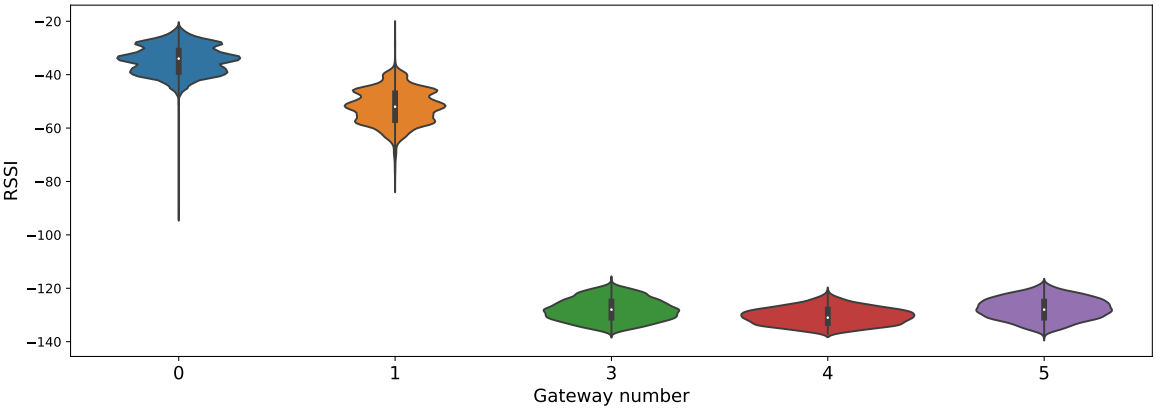

Figure 2.32 – Violin plots of gateways 0, 1, 3, 4, and 5 for an indoor sender, transmission power 14 dBm, *SF*11.

We observe two patterns. At gateways 0 and 1: RSSI values are close to one another. These gateways are in the vicinity of the sender and present a PRR of 95% resulting in a non-Rayleigh channel. In gateways 3, 4, and 5, RSSI values are widely scattered, which corresponds to a Rayleigh channel. The violin plots in Figure 2.32 confirm this observation. For instance, the distributions of gateways 0 and 1 presents three bumps, and the distributions of gateways 3, 4, and 5 exhibit a truncated distribution, as explained in the previous section. We perceive a noticeable shift in the RSSI mean between gateways 0 and 1. Mean RSSI of gateway 0 is almost -30 dBm, and the mean RSSI of gateway one is around -50 dBm, a margin of 20 dB is observed. This difference is due to the fact that gateway 0 was installed in the same office as the mote with a distance of 2 meters while gateway 1 was in another office almost 10 meters further away.

We can conclude from the two parts that in both cases, indoor and outdoor sender, gateways in the vicinity do not exhibit a Rayleigh channel. For the indoor sender, the wireless channel for gateways at several kilometers follows a Rayleigh distribution. For the outdoor sender, the behavior varies according to the suburban environment. For links of some kilometers, the aggregated channel can be Rayleigh or a mixture of non-Rayleigh and Rayleigh with about changes from one to other. This behavior should be considered when working with ADR as it is sensitive to channel quality. In this case, it is more beneficial to avoid poor channel conditions when it emerges and wait until it becomes better than sending and losing packets.

2.7.3.1 Over different frequency channels

Figure 2.33 represents RSSI distributions per couple (sub-frequency, gateway) where the gateways are 1, 3, 4, 5, and 7, and the eight sub-frequencies are the three in h13, 868.1, 868.3, 868.5 Mhz, the five in h1.5: 867.1, 867.3, 867.5, 867.7 Mhz, and 867.9 Mhz. Figure 2.34 shows the aggregated RSSI distribution for all frequency channels by gateway. Figure 2.33 shows that the propagation per sub-channel is not Rayleigh, while the aggregated distribution for the same gateways in Figure 2.34 would correspond to a Rayleigh channel. For instance, the distribution shapes vary from one (gateway, sub-frequency) to the other. While some present some similarities, like (Gateway3, 868.3), (Gateway3, 868.5), (Gateway4, 867.9), and (Gateway4, 868.1), some are entirely different like (Gateway4, 867.3), (Gateway4, 867.7), (Gateway7, 867.9) and (Gateway7, 868.1).

Figure 2.33 confirms the origin behind the wireless channel behavior, which is the frequency hopping policy. Indeed, in mobile networks, the mobility of the node makes the channel Rayleigh. In LoRaWAN, the nodes are fixed in most cases, and more precisely, in the experiments. However, frequency hopping, i.e., changing the frequency for every sent packet, results in a Rayleigh channel. Figures 2.29 and 2.31 explained previously, confirm this fact, where the RSSI values were scattered for the Rayleigh channel and not on the non-Rayleigh channel.

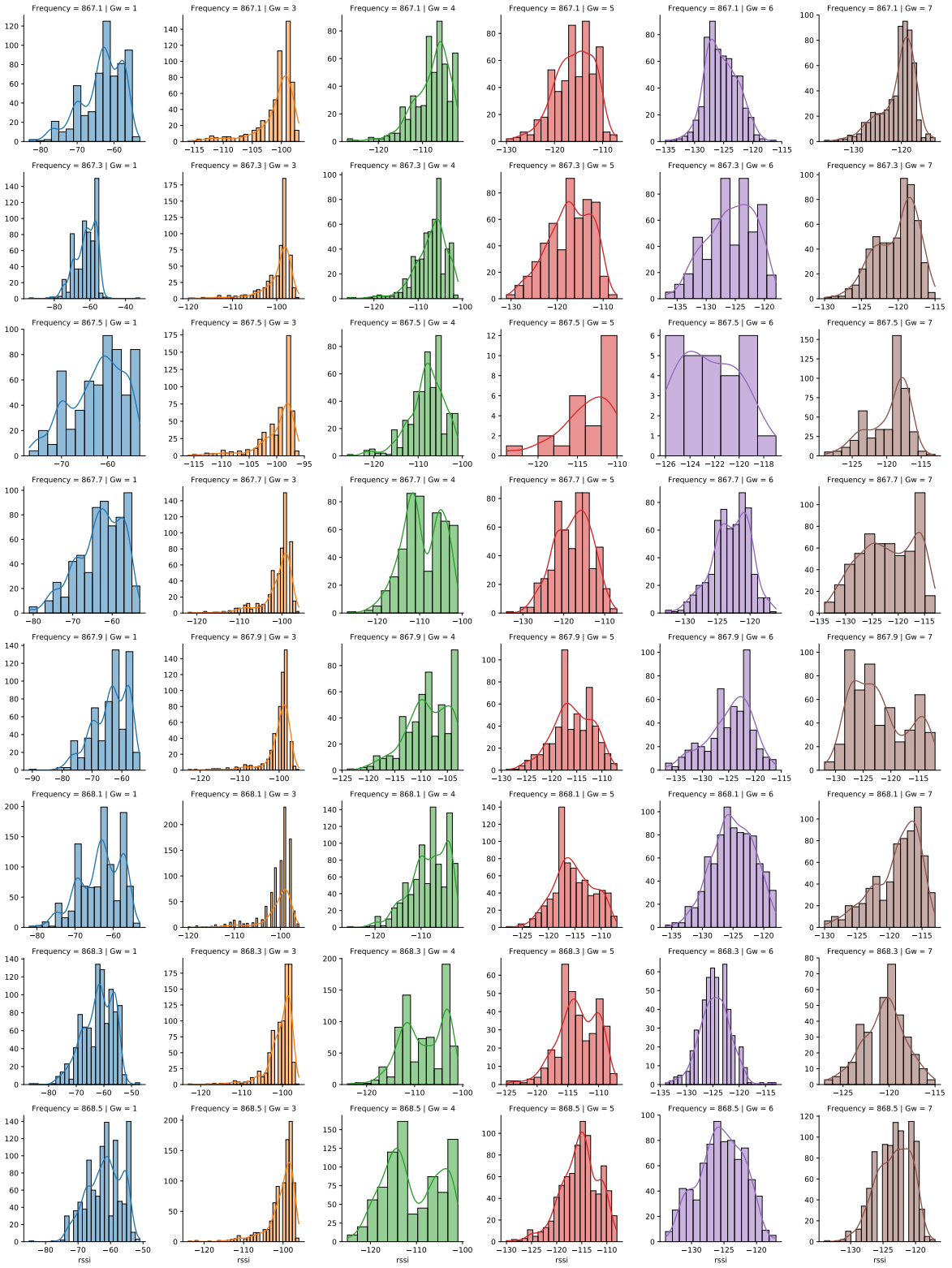

Figure 2.33 – RSSI distribution by sub-channel frequency for an outdoor sender for gateways 1, 3, 4, 5, 6, and 7, transmission power 14 dBm, *SF*11.

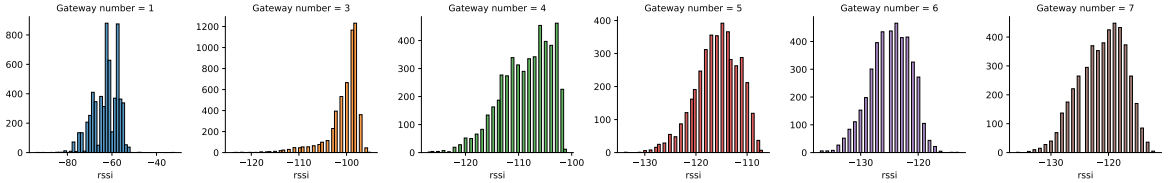

Figure 2.34 – Overall RSSI distribution for an outdoor sender at gateways 1, 3, 4, 5, 6, and 7, transmission power 14 dBm, *SF*11.

2.8 Conclusion

In this chapter, we present the results of extensive experiments in the TTN public LoRa network to evaluate the transmission quality of LoRa links by measuring PRR as a function of the payload length.

The results show that there is only a slight impact of the payload length on PRR, which means that the bit error rate due to the ambient noise at the receiver and collisions are not the only factors that impact the probability of packet reception. We find that successful reception requires effective preamble acquisition and that this step is the limiting factor: low channel attenuation favors the initial signal acquisition and remains for the rest of the packet. Our measurements show that the LoRa channel behaves like a slow fading Rayleigh channel, which also influences probability P_s of successful preamble reception. Our measurements of P_s show that it depends on *SF* and SNR, and often becomes a dominant factor of successful reception depending on the signal strength at a gateway.

These findings have important implications for the LoRaWAN application designer: to achieve a good level of data delivery, devices need to consider packet retransmissions because they have to cope with frame losses not only due to the ALOHA access method, but also to the channel variability. Moreover, it is always better to group past data with new measurements and send them in long packets instead of more numerous short packets because the actual frame size has little influence on transmission reliability.

In the second part of the chapter, we present the results and analysis of the experiments in the TTN with two types of senders: indoor and outdoor, to evaluate, study, and characterize the LoRaWAN wireless channel by displaying RSSI distributions, violin plots, and channel variability in time. The results show that the channel for gateways at several kilometers follows a Rayleigh channel, which results from the frequency hopping.

A difference in channel gain between indoor and outdoor sender is also noticed, around 30 db, which is a fundamental factor to consider. A degradation in link quality in time is to consider while designing the ADR algorithm that depends mainly of the quality of the channel.

Finally, the measures confirm that the channel gains are always variable. Even for nodes with similar average channel gains, it would be very common to witness reception powers with a difference of 6 dB. In this case, the capture effect allows the gateway to receive one of the colliding frames. This conclusion motivated us to investigate the capture effect mechanism at the gateways and to propose a novel enhanced technique inspired from IEEE802.11.

Chapter 3

Message in Message for Improved LoRaWAN Capacity

Contents

3.1 Introduction

Although the Aloha-like access method for class A provides the simplest and the lowest energy consumption access method, this advantage comes at the cost of low channel utilization, with only 18% at best of its theoretical channel utilization, which results in high packet loss in large-scale deployment [41].

The *capture effect* [42, 43, 44, 45, 46, 47] increases the channel utilization and, consequently, improves the Packet Delivery Rate (*PDR*). It consists of correctly decoding one frame in the presence of collision between two or multiple packets, with the condition of being 6 dB higher [8].

Haxhibeqiri et al. [34] adopted a simulation model based on the measurements of the interference behavior between two devices with a duty cycle of 1% to illustrate that when the number of devices rises to 1000 per gateway, the frame loss rate only raises to 32% (multiple channels, multiple SFs, and a payload size of 20 bytes). Nevertheless, this resulting loss rate is to be considered as low compared to 90% in pure unslotted ALOHA for the same load where it results from taking into account the capture effect giving the channel utilization of around 23%.
Message in Message (MIM) further enhances the rate of successful transmissions in case of collisions. In this technique, which is not implemented yet in current LoRaWAN gateways, the receiver may switch to receive a new arriving stronger frame during the reception of another frame. When the receiver is locked on a frame by receiving its preamble, and a new frame arrives with stronger power, it is propitious to switch to the stronger frame that has a higher probability of correct decoding. Several authors successfully applied MIM to 802.11 or 802.15.4 wireless LANs and showed its benefit of improving transmission reliability [45, 49, 50, 51, 52].

In this chapter, we explore MIM for LoRaWAN and evaluate the extent of improvement it can bring to its capacity. We develop an analytical model for channel utilization in LoRaWAN under multiple concurrent frames and validate its predictions with detailed simulations in NS-3.

Our performance analysis shows the improved channel utilization up to 35% in the scenario of a single LoRaWAN cell, which represents a considerable improvement with respect to the channel utilization of 23% for LoRaWAN with capture effect. Moreover, multiple gateways in a cell can significantly improve capacity with the channel utilization reaching over 40% with two gateways and 60% with four gateways.

In this chapter, Section 3.2 discusses the capture effect and introduces MIM. We then present the implementation of MIM in NS-3 and report on the evaluation based on simulations in Section 3.3. Section 3.4 discusses previous work, and Section 3.5 concludes the chapter.

3.2 Capture Effect and MIM

In wireless random access networks, simultaneous packet receptions are potentially prone to packet collisions resulting in either packet corruption, loss, or successful decoding. Depending on the corresponding reception power, the arrival time of the concurrent packets, and the receiver hardware capabilities, one packet can be correctly received and survive a collision. Therefore, the reception scheme defining how the receiver handles packet concurrency is the fundamental feature that directly impacts the network performance and its capacity.

Moreover, modern wireless radio receivers include more advanced mechanisms to tackle overlapping packet transmissions: for instance, they can foster the *capture effect* or can implement some form of *Message in Message* reception. These functionalities allow receiving at least a fraction of the colliding packets instead of losing them all.

We define the following terms useful to explain different reception schemes:

- **Received Signal Strength Indicator (*RSSI*)**, an indicator of received signal power.
- **Signal to Interference plus Noise Ratio (*SINR*)**, the difference in dB between the involved signal reception powers.
- **Capture Threshold**: the capture is possible if *SINR* is above this threshold.
- **Capture Window**: the capture is possible if the concurrent signal arrives during the time interval.

From the received signal power point of view, we will distinguish between two possible key scenarios:

- **Stronger First:** the stronger packet arrives before the weaker one.
- **Stronger Last:** the stronger comes after the weaker one.

We define five possible reception schemes:

Collision. Both simultaneously transmitted packets are lost.

Simple capture. The receiver can capture one frame according to the Stronger First scenario if it satisfies the Capture Threshold. The receiver locks on the stronger frame and keeps its reception even if any weaker frame arrives later. However, the receiver is unable to capture the stronger frame in the Stronger Last scenario: even if it arrives after the weaker one, both are lost regardless of the difference in power.

Advanced capture. It corresponds to the situation in which the reception is correct if the interfering frame arrives after the preamble of the transmitted frame with the same *RSSI* ($SINR \geq 0$ dB) [34].

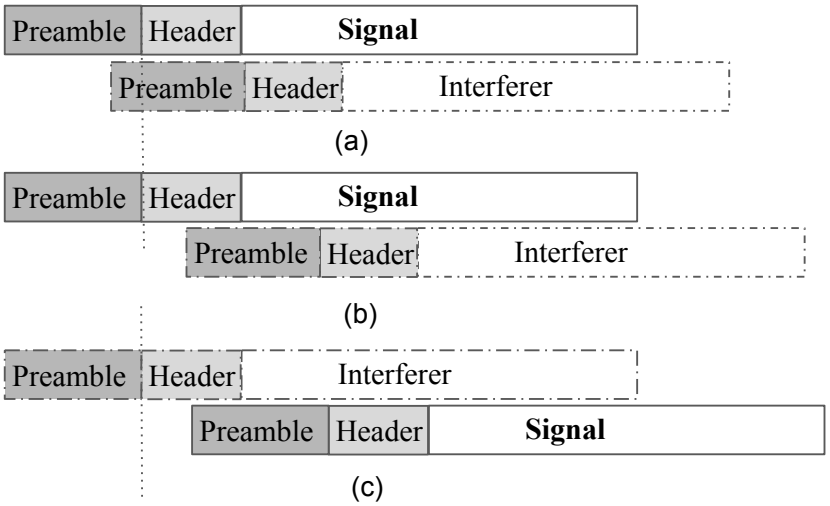

Figure 3.1 – Capture scenarios at the receiver: a) **Simple capture** if $SINR \geq 6$ dB, b) **Advanced capture** if an interferer arrives after the preamble duration and $SINR \geq 0$ dB, c) **Physical capture** when the receiver switches to the incoming stronger frame if it arrives during the header of the interferer and $SINR \geq 6$ dB. The continuous line denotes the correctly received frame.

Physical capture. The receiver can capture the stronger frame in the Stronger Last scenario only if it satisfies the Capture Threshold and it arrives during the Capture Window corresponding in 802.11 to the frame preamble [45, 49]. In this case, the receiver drops the reception of the ongoing weaker frame and locks on the stronger one.

Message in Message (MIM). This scheme enables the receiver to switch from the ongoing reception of a weaker frame to the newly arriving stronger frame as long as the latter frame dominates the former one by a sufficient margin θ_{MR} [44, 45, 49]. The receiver thus drops the ongoing reception and locks on the new frame. The signal of the weaker frame becomes interference to the ongoing reception. For a LoRaWAN gateway, MIM reception would be possible by keeping on monitoring the channel for a preamble even if the reception is active at a given *SF* just like the gateways keep on looking for frames transmitted at other *SFs*. To filter out the signal from the ongoing reception, its received power plus a margin defines the threshold power for the new incoming transmission to switch to. Formally, the receiver switches to another frame if the following condition is satisfied:

$$P_i > \theta_{\text{MR}} = \delta_{\text{MR}} P_l, \tag{3.1}$$

where P_i is the reception power of the new incoming frame, δ_{MR} is the capture threshold, and P_l is the power of the packet the receives is locked on.

3.2.1 Capture Effect and MIM in LoRaWAN

LoRa is a wireless network subject to a high collision rate due to its ALOHA access method that exacerbates the collision issue because there is no predefined scheduling nor the listening before

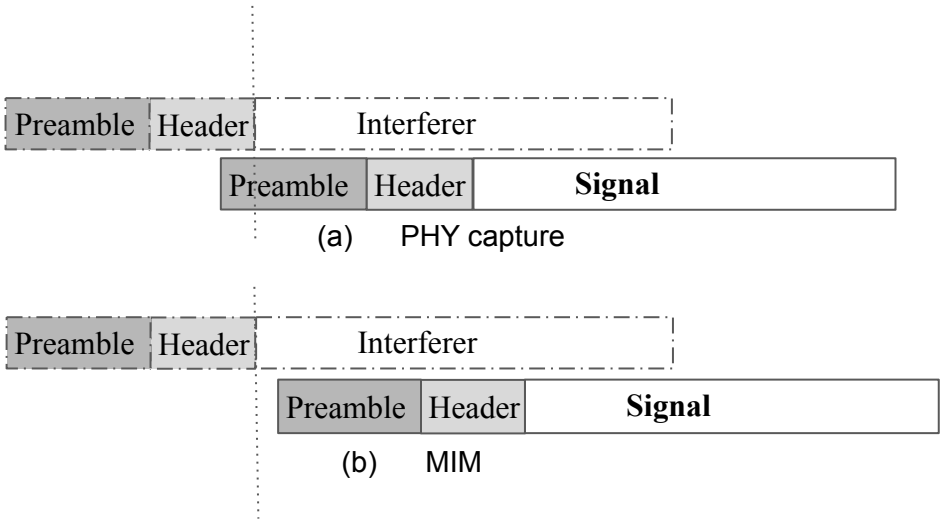

Figure 3.2 – **Physical capture** versus **MIM**: a) **Physical capture**: the receiver switches to the incoming stronger frame if it arrives during the header of the interferer and $SINR \geq 6$ dB, b) **MIM**: the receiver switches to the incoming stronger frame even though it arrives after the header of an interferer and $SINR \geq 8$ dB. Continuous line denotes the correctly received frame.

talk mechanism.

The difference of LoRa with the capture schemes defined for 802.11 or 802.15.4 is that we need to consider the arrival instant of the second frame with respect to the preamble and the PHY header (see Figure 3.1). We can observe **Simple capture** in Figure 3.1a, the **Advanced capture** in Figure 3.1b, and **Physical capture** in Figure 3.1c.

Figure 3.2 explains the difference between the **Physical capture** and **MIM**. The **Physical capture** enables the receiver to switch to the stronger frame when it arrives during the header and $SINR \geq 6$ dB while in MIM, the receiver switches to the incoming stronger frame even though it arrives after the header of an interferer and $SINR \geq 8$ dB. We use the value of 8 dB for the power margin triggering MIM reception, the same value as needed for MIM in 802.11 [47].

3.3 Evaluation with NS-3 Simulations

The goal of the evaluation is to investigate the impact of different reception schemes on the single-channel capacity with several scenarios and configurations. We opted for simulations because experimental validation would require a network with a large number of devices to observe collisions. Nevertheless, we carefully validated the NS-3 simulator to obtain meaningful results.

NS-3 is open-source software licensed under GNU GPLv2 [89]. It is a discrete-event network simulator, entirely written in c++ language, with Python binding. It exhibits a Linux-like architecture so that it attempts to be as realistic as possible in mimicking the real network behavior. NS-3 provides sets of several libraries of internet and non-internet-based networks. It benefits from the development community that encourages developers to contribute to the source code.

It provides an open emailing list, a tracker for error, and a wiki with user-contributed instructions. We have modified and extended the NS-3 LoRa module developed by Magrin et al. [90] with the capture schemes and MIM.[1] The module implements several features: Adaptive Data Rate (ADR), downlink traffic, multiple reception paths at the gateway, Duty Cycle (DC) limitation, co-spreading interference matrix, and retransmissions. Since our study focuses on the reception schemes at the gateway, the features are disabled except for DC limited to 1%.

3.3.1 LoRa Channnel Model for NS-3

We wanted our simulations as realistic as possible so we used an adequate channel model closely representing the real LoRa channel. A packet transmission is subject to both large scale and a small scale fading. For the large scale, we adopted the lognormal path loss as it is the most used for attenuation in suburban cities, also used by Magrin et al. [90], defined as:

$$L^{dB}(d) = L(d_0) + 10 * \eta * \log_{10}(\frac{d}{d_0}),$$

where $L(d_0)$ is the reference path loss based on measurements at distance d_0, η is the path loss or propagation exponent that determines at which rate the path loss increases with distance [17]. More specifically, L in suburban environments is given as:

$$\begin{aligned} L^{dB}(d) = 40(1 - 4 * 10^{-3} * h)\log_{10}(d) \\ -18\log_{10}(h) + 21\log_{10}(fr) + 80, \end{aligned}$$

where $h \in [0, 50]$ is the antenna elevation, fr is the frequency in MHz. For fr = 868 MHz and h = 15 m, we obtain:

$$L^{dB}(d) = 120.5 + 10 * 3.76 * \log_{10}(d).$$

In our previous work [91, 41], we showed through experimental validation on a testbed that the LoRa channel behaves like a Rayleigh fading channel. NS-3 includes the Nakagami-m model, a more generalized formula than Rayleigh: for $m = 1$, it corresponds to Rayleigh. The Nakagami probability density function is as follows:

$$f(x; m, w) = \frac{2m^m}{\Gamma(m)w^m} x^{2m-1} e^{-\frac{m}{w} * x^2},$$

[1] https://gricad-gitlab.univ-grenoble-alpes.fr/attiata/lorawan-ns3

where m is the fading depth parameter and w the average received power. For $m = 1$, the distribution is Rayleigh:

$$f_1(x; w) = \frac{x}{w^2} e^{-\frac{x^2}{2w^2}},$$

and the received power follows an exponential distribution.

3.3.2 Capture Schemes in LoRaWAN

Implementing the most relevant capture schemes that mimic the real physical behavior of the gateway is challenging yet fundamental for obtaining accurate simulation results, notably with LoRaWAN in which the capture impact is significant in increasing the throughput of the network. Below, we present the implementation of the several reception schemes described above in the NS-3 simulator.

We assume that a Signal (or frame) of Interest (SoI) may face multiple colliding packets depending on the network load. We use the following notation: I^i is the set of interferers transmitting at rate DRi that collide with SoI. I^i_k is the k^{th} interferer, $k \in \{1..n_I\}$, where n_I is the number of frames colliding with SoI. Its reception power is $P^{\text{rx}}_{I^i_k}$ and that of SoI, $P^{\text{rx}}_{\text{SoI}}$.

LoRaWAN Simple capture. The simulator computes $SINR$ between $P^{\text{rx}}_{\text{SoI}}$ and the received power of the strongest interferer denoted by k^*, $P^{\text{rx}}_{k^*}$ as:

$$SINR = \frac{P^{\text{rx}}_{\text{SoI}}}{P^{\text{rx}}_{k^*}}, \text{ where } P^{\text{rx}}_{k^*} = \max_k P^{\text{rx}}_k.$$

If $SINR \geq 6dB$ [92], then the SoI packet survives and can be decoded. The scheme is independent of the arrival timing of the concurrent packets and SoI.

LoRaWAN Advanced capture. In this scheme, the required power difference between the interferer and SoI goes from 6 dB to 0 dB if the interferer arrives after the end of the SoI preamble. Let $I^i_1 = \{I^i_{1,1}..I^i_{1,k}...I^i_{1,n_{1,I}}\}$ denote the subset of interferers that arrive before the SoI preamble and $I^i_2 = \{I^i_{2,1}..I^i_{2,k}...I^i_{2,n_{2,I}}\}$ those arriving after. k^*_1 and k^*_2 are the indices of the strongest interferer of I^i_1 and I^i_2, respectively. We define $SINR_1$ and $SINR_2$ as:

$$SINR_1 = \frac{P^{\text{rx}}_{\text{SoI}}}{P^{\text{rx}}_{k^*_1}}, \text{ where } P^{\text{rx}}_{k^*_1} = \max_{k_1} P^{\text{rx}}_{k_1}.$$

$$SINR_2 = \frac{P^{\text{rx}}_{\text{SoI}}}{P^{\text{rx}}_{k^*_2}}, \text{ where } P^{\text{rx}}_{k^*_2} = \max_{k_2} P^{\text{rx}}_{k_2}.$$

SoI survives collisions if and only if $SINR_1 \geq 6$ dB and $SINR_2 \geq 0$ dB.

LoRaWAN Physical capture. In the physical capture, the receiver can switch to an incoming packet depending on the arrival time and reception power of both packets. Let t_1 and t_2 denote

the respective arrival instants of the Locked-on-Packet (LoP) and the New-incoming-Packet (NiP), P_1^{rx} and P_2^{rx} are the received powers of LoP and NiP, respectively, $\tau_{\text{pr},1}$ and $\tau_{\text{hd},1}$ are the preamble and header durations of LoP, respectively. We define *SINR* as:

$$SINR = \frac{P_2^{\text{rx}}}{P_1^{\text{rx}}}.$$

The physical capture of NiP happens if and only if $SINR \geq 6$ dB and $t_1 + \tau_{\text{pr},1} < t_2 < t_1 + \tau_{\text{hd},1}$.

LoRaWAN MIM. Unlike physical capture, MIM has the advantage of being independent of any capture window, i.e., the arrival time of NiP with respect to LoP. It only depends on the capture threshold (*SINR*) that should be higher than 8 dB. Therefore, the receiver can switch to NiP if $SINR \geq 8$ dB, where:

$$SINR = \frac{P_2^{\text{rx}}}{P_1^{\text{rx}}},$$

with P_1^{rx} and P_2^{rx} the reception powers of LoP and NiP, respectively.

In MIM and the physical capture scheme, the receiver after locking on NiP, will perform advanced capture of NiP in the presence of other colliding packets. If it satisfies the required condition for successful reception with advanced capture, the receiver can correctly decode the packet. The fact that the receiver is locked on NiP that now becomes SoI, does not make it immune to collisions from other packets that can potentially arrive later. Only its high received power compared to other packets can guarantee its successful reception.

3.3.3 Simulation Setup

In the evaluation, we consider two scenarios: a) uniformly distributed nodes in a given range R and b) all nodes in the same place at a given distance R. In both scenarios, *SF* is the same for all nodes because we analyze the performance of a single channel characterized by the couple (frequency, *SF*). The first scenario corresponds to the conditions favorable to capture effect—nodes face different channel attenuation resulting in a difference in their received powers at the gateway. The second scenario is the worst case for capture effect—all nodes are subject to the same attenuation so their packets have similar reception powers.

Devices periodically generate a packet according to the configured application period respecting the duty cycle. All devices generate the same amount of traffic. We only consider uplink traffic with disabled ADR and retransmissions. Table 3.1 summarizes all simulation parameters.

3.3.4 Simulator Validation

We start with the validation of the simulator in a scenario with a given number of nodes uniformly distributed in a cell of radius $R = 2{,}500$ m around a single gateway using *SF12* and P of 14 dBm

Table 3.1 – Simulation parameters

Parameter	Value(s)[unit]
Number of devices	0 to 10000
Cell radius R	2,500, 7,500 m
Packet length	59 B
Transmission power P	14 dBm
Spreading Factor SF	12
Bandwidth	250 KHz
Frequency bands	868 MHz
Duty cycle	1%
SNR threshold for DRj	Table 1.7
Available reception paths	8
Enabled reception path	1
Path loss	Log Normal
Fading	Rayleigh fading
ADR	disabled
Retransmissions	disabled

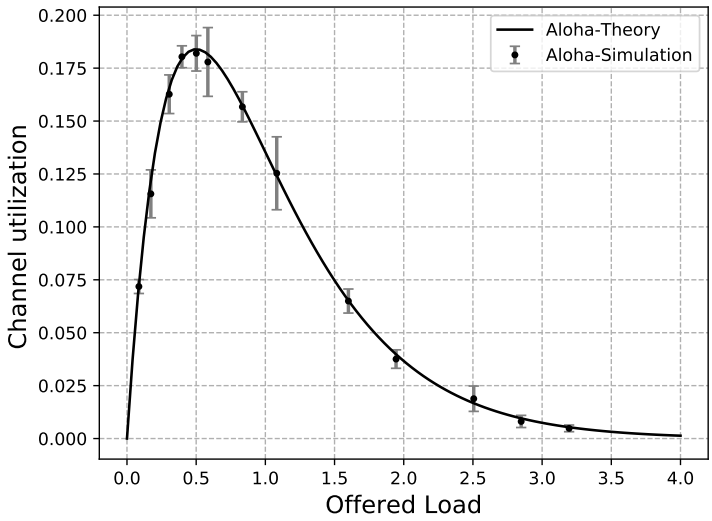

Figure 3.3 – Comparison of the theoretical ALOHA utilization with simulation.

under path loss attenuation without capture effect. Figure 3.3 presents the comparison of the theoretical ALOHA utilization with simulation results along with 95% confidence intervals showing good agreement with the theory.

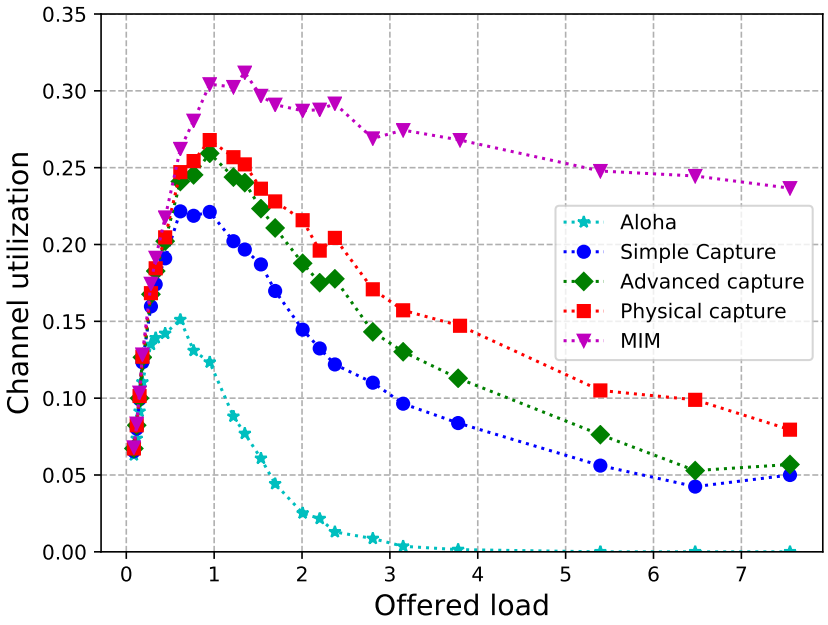

(a)

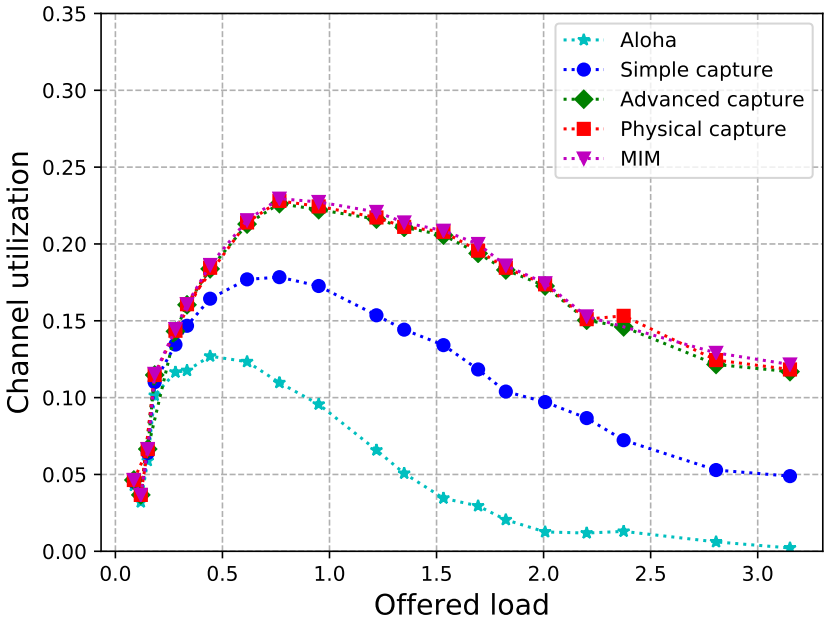

(b)

Figure 3.4 – Channel utilization vs. offered load in Erlang for *SF12*, $P = 14$ dBm at 7,500 m: a) uniformly distributed nodes, b) nodes at the same place.

3.3.5 Simulation Results for Different Reception Schemes

We have evaluated the reception schemes in a cell with the ranges $R = 2{,}500$ m and $R = 7{,}500$ m, using *SF12* and transmission power P of 14 dBm under path loss and Rayleigh fading. Figures 3.4 and 3.5 show the utilization as a function of offered load in Erlang for all the reception schemes. We can observe that MIM outperforms all other reception schemes. However, the difference between MIM and other schemes depends on the node distribution and the distance to the gateway. For instance, in Figures 3.4a and 3.5a under MIM, the gateway can receive more packets than with the other reception schemes provided the fundamental condition is satisfied: the gap in powers

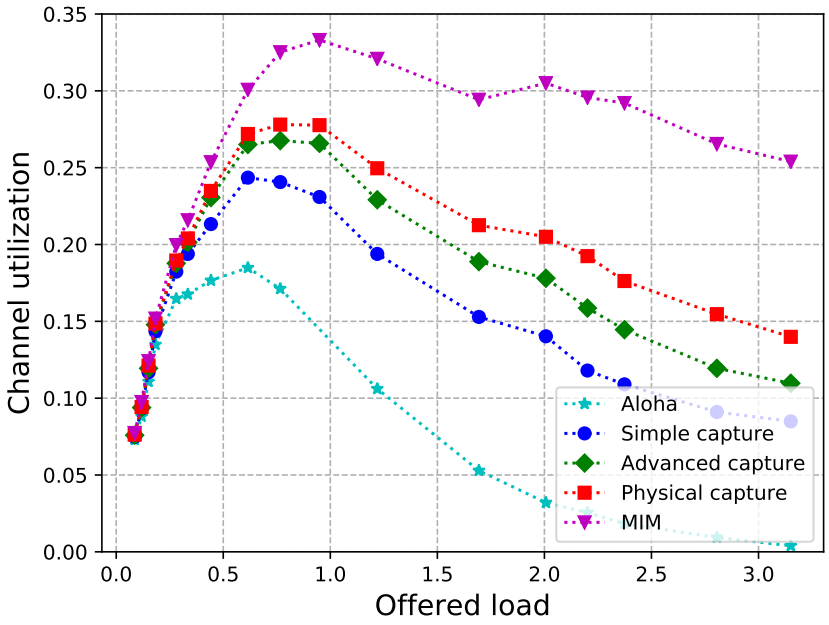

(a)

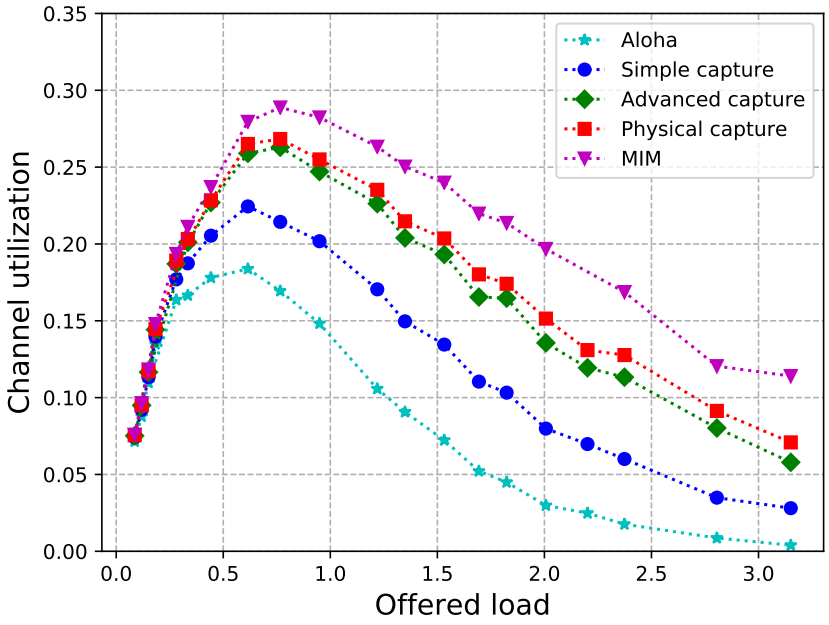

(b)

Figure 3.5 – Channel utilization vs. offered load in Erlang for *SF12*, $P = 14$ dBm at 2,500 m: a) uniformly distributed nodes, b) nodes at the same place.

between concurrent packets should be above 8 dB. As we may expect, at the distance of 7,500 m from the gateway, nodes suffer from important attenuation compared to the distance of 2,500 m.

For the second scenario of nodes at the same place presented in Figures 3.4b and 3.5b, all capture schemes exhibit almost the same performance because there is less opportunity to benefit from capture effect. Nevertheless,

For high channel load ($\nu_0 > 2$) corresponding to 5,000 nodes and above up to 21,000 nodes ($\nu_0 = 7$ in Figure 3.4a), MIM shows a high and almost stable channel utilization, compared to simple, advanced, and physical capture. The utilization of these schemes begins to drop after load

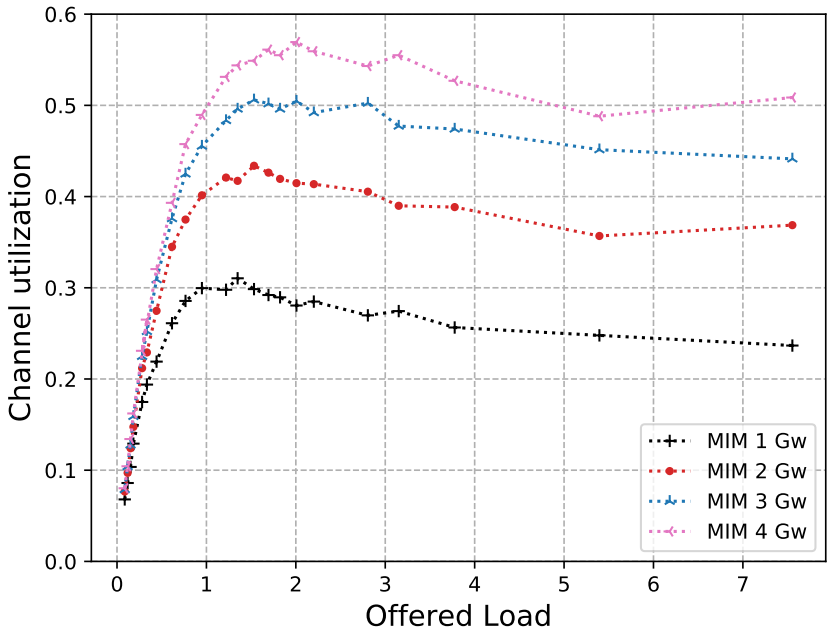

Figure 3.6 – Channel utilization vs. offered load in Erlang for multiple gateways under MIM. Nodes are uniformly distributed in a cell with radius $R = 7,500$ m, $SF = 12$, and $P = 14$ dBm. Gateways at the same place.

greater than $\upsilon_0 = 1$ due to collisions and concurrency.

We can conclude from these results that MIM obtains remarkable performance in usual conditions in which nodes are distributed over some area and it copes with the increased load better than other reception schemes.

Figures 3.6 and 3.7 explore a setup with multiple gateways under the MIM scheme and physical capture, respectively : nodes are uniformly distributed in a cell of radius 7,500 and gateways are at the same place, but we assume that the antennas are sufficiently far away from each other to achieve different small-scale fading. We can observe in Figures 3.6 and 3.7 that multiple gateways significantly improve the capacity of the cell with the channel utilization reaching over 40% for two gateways and 60% for four gateways in Figure 3.6 and peaks at 35% for two gateways and at 45% for four gateways in Figure 3.7. Interestingly, the overall channel utilization for three gateways with MIM outperforms four gateways with physical capture. For high load ($\upsilon_0 > 3$), two gateways with MIM outperform four gateways with physical capture, therefore increasing the efficiency and maximizing the capacity of the network.

Figures 3.8 and 3.9 present the results of the analytical model detailed in our paper [93] compared with the simulation results (95% confidence intervals) for a cell with a single gateway. In the simulation, we have adopted the same assumptions as in the analytical model: i) if there is any other frame that arrived before SoI, then we consider the latter lost and ii) the capture of SoI is successful if the power of the signal is equal to the sum of the power of all overlapping frames at DR_i, i.e., $SINR > 0$.

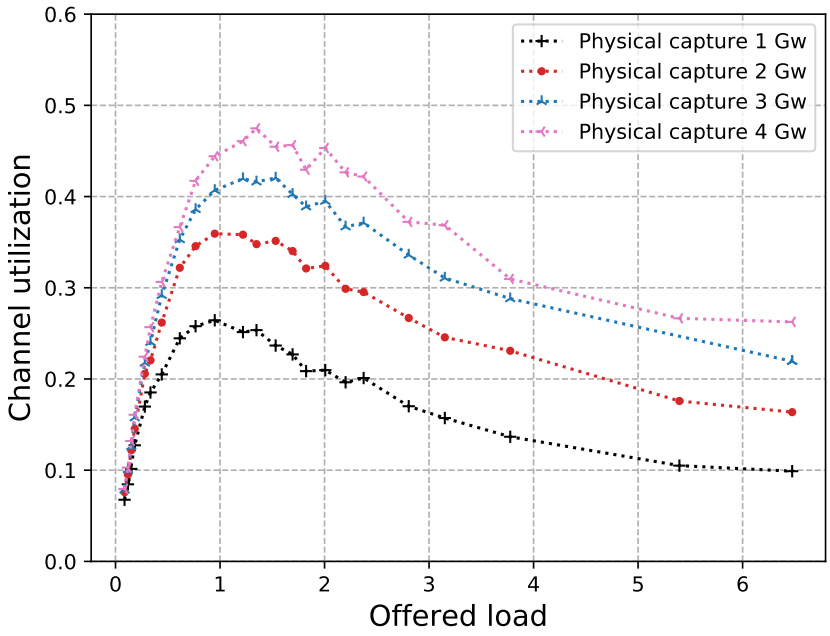

Figure 3.7 – Channel utilization vs. offered load in Erlang for multiple gateways under physical capture. Nodes are uniformly distributed in a cell with radius $R = 7,500$ m, $SF = 12$, and $P = 14$ dBm. Gateways at the same place.

Figure 3.8 corresponds to the scenario in which nodes are at the same place at distance $R = 2,500$ m and at distance $R = 7,500$ m in Figure 3.9. The simulation assumes the Rayleigh and path loss channel with all nodes using the same $SF = 12$ and $P = 14$ dBm. The figures also show the results for pure ALOHA for comparison.

We can notice that the simulation results perfectly fit the analytical model for $R = 2,500$ m and are very close to simulation for $R = 7,500$ m. The assumptions of the model are close to the previously presented advanced capture in which $SINR \geq 0$ with packets arriving after the preamble of SoI.

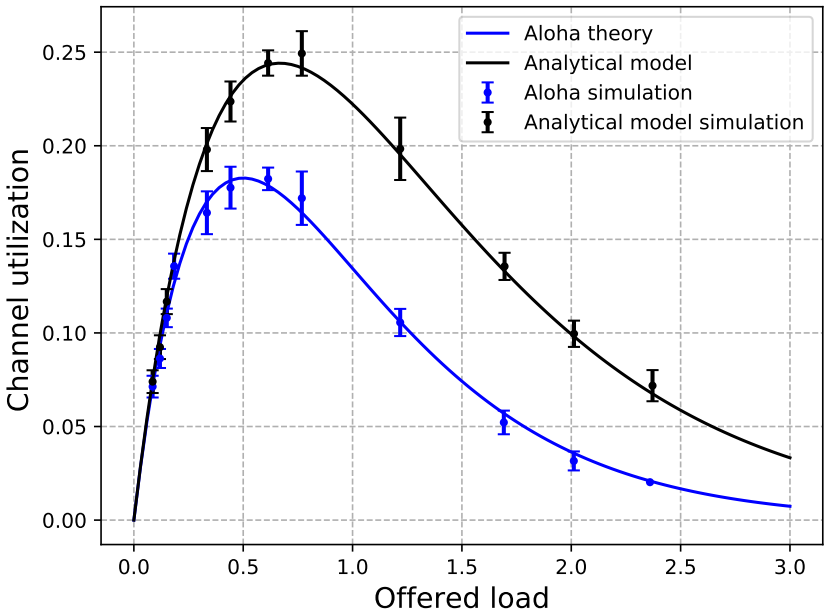

Figure 3.8 – Comparison of the analytical model results with simulation. Channel utilization vs. offered load in Erlang. Nodes at the same place at distance $R = 2,500$ m, single gateway.

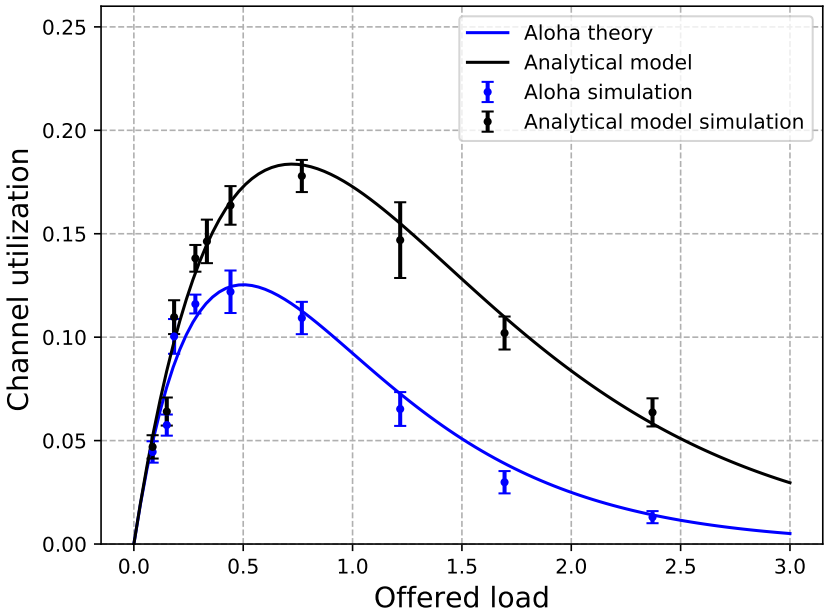

Figure 3.9 – Comparison of the analytical model results with simulation. Channel utilization vs. offered load in Erlang. Nodes at the same place at distance $R = 7,500$ m, single gateway.

3.4 Related work

Many studies examined the Lora capture experimentally and identified many reception schemes. Haxhibeqiri et al. [34] investigated physical capture in LoRa networks. They showed that the capture effect depends on two main parameters: i) the arrival instant of a transmitted frame (Signal of Interest, SoI) relative to the interfering frame and ii) the Received Signal Strength Indicators (*RSSI*) of the transmitted and interfering frames.

Rahmadhani et al. [94] studied LoRaWAN frame collisions and capture effect through experiments based on the application level side. They focus on the frame loss due to collisions between a weak and a strong frame. They distinguish four cases similar to the results of Haxhibeqiri et al. [34].

Magrin et al. [90] have implemented the capture effect in NS-3 as follows. For every interferer and a packet arriving with the same *SF* during the reception of SoI, they compute related energy and the sum all energy of different interferers to obtain *SINR*. Then, they compare the resulting *SINR* with the value from the collision matrix [92].

This approach is optimistic compared to a realistic operation of LoRa. In fact, if we consider a strong packet that interferes only during a short period with SoI, using this approach, resulting energy could be negligible with respect to total energy of SoI. However, in real world scenarios, this interferer can corrupt SoI, so the packet that should be considered lost is considered as successfully received. Such an approach could have been correct if the frequency band were wider, like in UMTS for instance, where the correction code, channel coding, and equalization techniques at the receiver could reconstruct/regenerate a packet from a correctly received part. However, such operation is not possible with LoRa for which, when we lose a packet because of a collision or the channel fading, it is lost in totality as we showed in our previous work [91].

Choir [95] leverages the frequency offsets introduced by the imperfect hardware nature of LPWAN to disentangle and decode concurrent colliding transmissions. This technique would allow to decode several packets simultaneously but there is no proof of whether it is applicable in a massive network. For instance, as the number of concurrent transmissions increases, it becomes more challenging to distinguish between the FFT peaks from different transmitters. Moreover, in presence of moving transmitters or scatterers, different propagation paths correspond to different frequency shifts, which makes things even more arduous, as several FFT peaks correspond to the same sender.

3.5 Conclusion

In an LPWAN context, we study the potential benefits of MIM, a relatively common reception scheme in WLAN networks. MIM allows a stronger signal to be received even if the receiver is locked on the reception of a weaker frame. MIM is promising for LPWANs because of the ALOHA access method for which collisions are extremely common. Moreover, nodes are naturally spread over a wide area and Rayleigh fading introduces additional variability to the reception power. Consequently, we expect that reception preemption may be frequent even with a significant power margin for triggering the switch.

In this chapter, before exploring the benefits of MIM, we have carefully defined the baseline performance, which corresponds to pure ALOHA and ALOHA with capture. Based on this foundation, we add MIM when there is a reception margin of 8 dB in favor of the frame arriving later. The performance gains are notable, especially when there is a variability between the channel gains experienced by nodes. Scalability is especially improved when there is a degree of macro-diversity like in the case of multiple gateways. We believe that the results are encouraging enough to justify an effort to implement MIM on real hardware. Actually, MIM reinforces the benefits of having contrasted reception powers between nodes, which calls for considering randomization of transmission powers [96].

Conclusion

This thesis explored many aspects of the LoRaWAN network, from network study analysis to experimental characterization and finally capacity improvement. After providing a general introduction, we have presented the state-of-the-art in the first chapter, then provided an experimental evaluation and characterization of the LoRaWAN link in the second chapter, followed by an investigation of one of its limitations by proposing, implementing, and evaluating MIM technique in a third chapter. In the following, we recapitulate the main contributions of the thesis and then outline the future research directions.

3.6 Contributions

We provided a description of the state of the art related to LoRa technology in the first part: we described the LPWAN properties and outlined the LoRa, Sigfox, NB-IoT and Ingenu networks and provided a comparison study. With a focus on LoRa and LoRaWAN, we detailed the physical layer characteristics and presented the MAC layer components and properties. The second part of the thesis presented our contributions, highlighted in the following:

Contribution 1: Monitoring LoRaWAN Real Traffic

We presented the analysis of a monitoring set-up we have configured, comprising a LoRaWAN gateway installed on the roof of the IMAG building. We save all the received traffic and process it to get relevant statistics about the actual state of the network. The resulting analysis shows that frequency band h1.5 is more loaded than h1.1; the most used data rate was 0 AND the channel was not yet saturated.

Contribution 2: Experimental characterization of LoRaWAN Link Quality

In the second contribution, we presented the results of extensive experiments in the TTN pub-

lic LoRa network to evaluate the transmission quality of LoRa links by measuring PRR as a function of the payload length. The results illustrate that there is only a slight impact of the payload length on PRR, signifying that there are other factors than collisions and bit error rate to affect the packet reception probability. We identify that successful reception requires effective preamble acquisition and that this step is a critical factor: indeed, low channel attenuation favors the initial signal acquisition and remains for the rest of the packet. The measurements depict that the LoRa channel behavior, like a slow fading Rayleigh channel, influences the probability P_s of successful preamble reception. Our evaluations of P_s demonstrate that it depends on *SF* and SNR and often becomes a dominant factor of successful reception. These findings have significant implications for the LoRaWAN application designer: In order to cope with frame losses caused by the ALOHA-like access method and the channel variability, devices need to consider retransmission to improve their data delivery rate. Moreover, it is always better to group past data with new measurements and send them in long packets instead of more numerous short packets because the actual frame size has little influence on transmission reliability.

Contribution 3: LoRaWAN channel characterization: Indoor vs. Outdoor sender

We investigated the wireless channel characterization by analyzing the RSSI distributions at several gateways placed in different placements at Grenoble city from two types of senders, indoor and outdoor. Results show that the behavior depends strongly on the distance that separates the sender from the gateway. For instance, the result illustrates that the LoRa channel for links of several kilometers behaves like a *slow fading Rayleigh channel*—an exponentially distributed Rayleigh channel gain affects the reception power of each transmission, which lies mostly constant during the transmission. Moreover, the channel gain dramatically differs when the sender is outdoor than when it is indoor, with a margin of 20 dB for links several kilometers from the sender, which depicts a notable illustration to consider before deploying a LoRa network. By illustrating the RSSI distributions for each sub-channel at several gateways, we showed that while originally, the Rayleigh fading channel model was for mobile nodes, the frequency hopping policy, i.e., changing the central frequency for every transmission, is behind the overall behavior of the channel when nodes are static.

Contribution 4: Message In Message for improved LoRaWAN Capacity

In the last contribution, we investigated the several reception schemes in LoRaWAN: for instance, collision, simple capture, advanced capture, and physical capture. We examined the potential benefits of the Message In Message approach, a frequent reception scheme in WLAN networks. MIM technique can enable a stronger signal's reception even if the receiver is locked on the

reception of a weaker frame. In a LoRaWAN cell, nodes are typically spread over a wide area, and Rayleigh fading introduces additional variability to the reception power, which favors the reception preemption at the gateway even with a significant power margin for triggering the switch.

We have established the baseline performance, which corresponds to pure ALOHA and ALOHA with capture. We have provided an NS3 simulation validation for an analytical model for channel utilization in LoRaWAN under multiple concurrent frames. We implemented MIM with a reception margin of 8 dB in favor of the frame arriving later. The performance gains are remarkable, especially when nodes experience variable channel gains in the receiver. Scalability is considerably improved with the deployment of multiple gateways, which represents a form of macro-diversity. Finally, we conclude the results are encouraging enough to justify an effort to implement MIM on real hardware.

3.7 Future Work

As most of the LoRaWAN traffic is uplink-oriented, we conducted all the experiments with motes configured with non-confirmed traffic. Thus, configuring and running experiments with confirmed traffic could generate different results.

As a continuity of the channel characterization study, an investigation of the coherence band of the wireless channel at one gateway could provide more insight into the variability of the channel over time and on what it depends. Moreover, using a machine learning approach like CNN with a long-term data set to predict the state of the channel and coherence band can help designers choose adequate physical parameters.

Further, in all our conducted experiments, motes were static, therefore characterizing the channel with mobile motes and studying its variability is considered in a future work.

We have implemented and evaluated Message In Message on an NS3 simulator. Implementing MIM on real hardware or an SDR-based solution and experimentally evaluate the approach would be interesting to show the benefits of MIM.

We have evaluated MIM in terms of channel utilization according to two configurations based on a variation of two parameters: distance and the distribution of the nodes. However, other parameters could also affect the channel utilization or the PRR: for instance, we raise the following questions for future work: what is the impact of nodes with confirmed traffic? What about the variation of the Transmission Power? What is the effect of the distribution of different gateways and their distances?

Finally, as MIM benefits better from variability between received power, in this case, the randomization of the Transmission Power could be beneficial and fairer to benefit from MIM.

Bibliography

[1] Nicolas Sornin, "868Mhz kerlink gateway setup," 2019. 9, 47, 48

[2] S. Li, U. Raza, and A. Khan, "How agile is the adaptive data rate mechanism of lorawan?," in *2018 IEEE Global Communications Conference (GLOBECOM)*, pp. 206–212, 2018. 9, 53, 54

[3] Kerlink, "Kerlink wirnet station." https://www.kerlink.com/product/wirnet-station/. 9, 65

[4] STMicroelectronics, "Discovery kit for LoRaWAN™, Sigfox™, and LPWAN protocols with STM32L0." https://www.st.com/content/st_com/en/products/evaluation-tools/product-evaluation-tools/mcu-mpu-eval-tools/stm32-mcu-mpu-eval-tools/stm32-discovery-kits/b-l072z-lrwan1.html. 10, 73, 74

[5] STMicroelectronics. 10, 73, 74

[6] E. C. Committee, "ERC Recommendation 70-03." https://docdb.cept.org/download/25c41779-cd6e/Rec7003e.pdf. 13, 42, 43

[7] Semtech, "Sx1276 137 mhz to 1020 mhz low power long range transceiver," 2015. 13, 39, 45

[8] C. Goursaud and J.-M. Gorce, "Dedicated Networks for IoT: PHY/MAC State of the Art and Challenges," *EAI Endorsed Transactions on Internet of Things*, vol. 1, 10 2015. 13, 55, 56, 91, 100

[9] D. Croce, M. Gucciardo, S. Mangione, G. Santaromita, and I. Tinnirello, "Impact of lora imperfect orthogonality: Analysis of link-level performance," *IEEE Communications Letters*, vol. 22, pp. 796–799, April 2018. 13, 55, 56

[10] A. Zanella, N. Bui, A. Castellani, L. Vangelista, and M. Zorzi, "Internet of things for smart cities," *IEEE Internet of Things Journal*, vol. 1, no. 1, pp. 22–32, 2014. 19

[11] K. Su, J. Li, and H. Fu, "Smart city and the applications," in *2011 International Conference on Electronics, Communications and Control (ICECC)*, pp. 1028–1031, 2011. 19

[12] A. Al-Fuqaha, M. Guizani, M. Mohammadi, M. Aledhari, and M. Ayyash, "Internet of things: A survey on enabling technologies, protocols, and applications," *IEEE Communications Surveys Tutorials*, vol. 17, no. 4, pp. 2347–2376, 2015. 19, 33

[13] Cisco, "Cisco Annual Internet Report (2018–2023)." https://www.cisco.com/c/en/us/solutions/collateral/executive-perspectives/annual-internet-report/white-paper-c11-741490.html. 19, 33

[14] U. Raza, P. Kulkarni, and M. Sooriyabandara, "Low power wide area networks: An overview," *IEEE Communications Surveys Tutorials*, vol. PP, no. 99, pp. 1–1, 2017. 20, 33

[15] IETF, "IETF." "https://www.ietf.org/". 20

[16] ETSI, "ETSI." "http://www.etsi.org". 20

[17] 3GPP, "Radio Frequency (RF) system scenarios,," Jan. 2016. 20, 104

[18] L. Alliance, "About the LoRa™ Alliance." 20

[19] WEIGHTLESS ALLIANCE, "Weightless alliance." 20

[20] dash7-alliance, "Dash7 alliance." 20

[21] Semtech, "Smart Cities Transformed Using LoRa® Technology, howpublished = "https://www.semtech.com/uploads/technology/LoRa/Semtech_SmartCitiesTransformed_WhitePaper_FINAL.pdf"." 20

[22] L. Alliance, "WHY LORAWAN® IS THE FOUNDATION FOR SMART BUILDING SUCCESS." https://lora-alliance.org/wp-content/uploads/2020/11/LA_WhitePaper_SmartBuildings_0520_v1.1_1.pdf. 20

[23] Semtech, "LoRa Technology:Mallorca Develops First LoRaWAN™ Smart Island)." 20

[24] Semtech, "Revolutionizing Smart Agriculture Using Semtech's LoRa Technology)." 20

[25] A. Berni and W. Gregg, "On the Utility of Chirp Modulation for Digital Signaling," *IEEE Trans. Commun.*, vol. 21, 1971. 20, 34, 39

[26] N. Sornin, M. Luis, T. Eirich, T. Kramp, and O.Hersent, "Lorawan specification v1.0.2," 2016. 20, 49, 52, 53

[27] The Thing Network, "The Thing Network." 21, 24, 63, 73, 86

[28] K. Mikhaylov, J. Petäjäjärvi, and T. Hänninen, "Analysis of Capacity and Scalability of the LoRa Low Power Wide Area Network Technology," in *European Wireless Conference*, pp. 1–6, May 2016. 21, 63

[29] O. Georgiou and U. Raza, "Low Power Wide Area Network Analysis: Can LoRa Scale?," *IEEE Wireless Commun. Letters*, vol. 6, no. 2, pp. 162–165, 2017. 21, 63

[30] B. Reynders, W. Meert, and S. Pollin, "Range and Coexistence Analysis of Long Range Unlicensed Communication," in *IEEE ICT*, (Thessaloniki, Greece), pp. 1–6, 2016. 21, 63

[31] M. C. Bor, U. Roedig, T. Voigt, and J. M. Alonso, "Do LoRa Low-Power Wide-Area Networks Scale?," in *International Conference on Modeling, Analysis and Simulation of Wireless and Mobile Systems*, (New York, NY, USA), pp. 59–67, ACM, 2016. 21, 63

[32] A. Augustin, J. Yi, T. Clausen, and W. M. Townsley, "A study of lora: Long range and low power networks for the internet of things," *Sensors*, vol. 16, no. 9, 2016. 21, 63, 81

[33] F. Adelantado, X. Vilajosana, P. Tuset-Peiró, B. Martínez, J. Melià-Seguí, and T. Watteyne, "Understanding the Limits of LoRaWAN," *IEEE Communications Magazine*, vol. 55, no. 9, pp. 34–40, 2017. 21, 63

[34] J. Haxhibeqiri, F. V. D. Abeele, I. Moerman, and J. Hoebeke, "LoRa Scalability: A Simulation Model Based on Interference Measurements," *Sensors*, vol. 17, no. 6, p. 1193, 2017. 21, 23, 63, 81, 100, 101, 113

[35] T.-H. To and A. Duda, "Simulation of LoRa in NS-3: Improving LoRa Performance with CSMA," in *IEEE ICC*, (Kansas City, USA), 2018. 21, 63

[36] T. Petrić, M. Goessens, L. Nuaymi, L. Toutain, and A. Pelov, "Measurements, Performance and Analysis of LoRa FABIAN, a Real-World Implementation of LPWAN," in *IEEE PIMRC*, pp. 1–7, Sept 2016. 21, 63, 81

[37] M. C. Bor and U. Roedig, "LoRa Transmission Parameter Selection," in *ACM DCOSS*, (Ottawa, ON, Canada), pp. 27–34, 2017. 21, 63

[38] K. Mikhaylov, J. Petäjäjärvi, and J. Janhunen, "On LoRaWAN Scalability: Empirical Evaluation of Susceptibility to Inter-Network Interference," in *2017 European Conference on Networks and Communications (EuCNC)*, June 2017. 21, 63, 82

[39] N. Blenn and F. A. Kuipers, "LoRaWAN in the Wild: Measurements from The Things Network," *CoRR*, vol. abs/1706.03086, 2017. 21, 63, 82

[40] Q. Lone, E. Dublé, F. Rousseau, I. Moerman, S. Giannoulis, and A. Duda, "WiSH-WalT: A Framework for Controllable and Reproducible LoRa Testbeds," in *IEEE PIMRC*, (Bologna, Italy), Sept. 2018. 21, 63, 73

[41] M. Heusse, T. Attia, C. Caillouet, F. Rousseau, and A. Duda, "Capacity of a LoRaWAN Cell," in *Proc. ACM MSWiM '20*, pp. 131–140, 2020. 23, 100, 104

[42] C. Lau and C. Leung, "Capture Models for Mobile Packet Radio Networks," *IEEE Trans. Commun.*, vol. 40, pp. 917–925, 1992. 23, 100

[43] J. Boer *et al.*, "Wireless LAN with Enhanced Capture Provision." US Patent 5987033, 1999. 23, 100

[44] C. Ware, J. F. Chicharo, and T. A. Wysocki, "Simulation of Capture Behaviour in IEEE 802.11 Radio Modems," in *Proc. IEEE VTC Fall 2001, Atlantic City, New Jersey, USA*, pp. 1393–1397, 2001. 23, 100, 102

[45] A. Kochut, A. Vasan, A. U. Shankar, and A. K. Agrawala, "Sniffing Out the Correct Physical Layer Capture Model in 802.11b," in *IEEE ICNP*, (Berlin, Germany), pp. 252–261, 2004. 23, 55, 100, 102

[46] K. Whitehouse, A. Woo, F. Jiang, J. Polastre, and D. Culler, "Exploiting the Capture Effect for Collision Detection and Recovery," in *Proc. the 2nd IEEE Workshop on Embedded Networked Sensors*, p. 45–52, 2005. 23, 100

[47] J. Lee, W. Kim, S.-J. Lee, D. Jo, J. Ryu, T. Kwon, and Y. Choi, "An Experimental Study on the Capture Effect in 802.11a Networks," in *Proc. of WinTECH '07*, p. 19–26, 2007. 23, 100, 103

[48] T. H. To, *Energy Saving Protocols for the Internet of Things*. PhD thesis, Université Grenoble Alpes [2020-....], 2020. 23

[49] J. Manweiler, N. Santhapuri, S. Sen, R. R. Choudhury, S. Nelakuditi, and K. Munagala, "Order Matters: Transmission Reordering in Wireless Networks," in *Proc. MOBICOM 2009* (K. G. Shin, Y. Zhang, R. L. Bagrodia, and R. Govindan, eds.), pp. 61–72. 23, 100, 102

[50] W. Wang, W. K. Leong, and B. Leong, "Potential Pitfalls of the Message in Message Mechanism in Modern 802.11 Networks," in *Proc. WiNTECH '14*, pp. 41–48, 2014. 23, 100

[51] G. Boudour, M. Heusse, and A. Duda, "An Enhanced Capture Scheme for IEEE 802.15.4 Wireless Sensor Networks," in *Proc. IEEE ICC*, (Budapest, Hungary), IEEE, June 2013. 23, 100

[52] G. Boudour, M. Heusse, and A. Duda, "Improving Performance and Fairness in IEEE 802.15.4 Networks with Capture Effect," in *Proc. IEEE ICC*, (Budapest, Hungary), IEEE, June 2013. 23, 100

[53] A. Zanella, N. Bui, A. Castellani, L. Vangelista, and M. Zorzi, "Internet of things for smart cities," *IEEE Internet of Things Journal*, vol. 1, pp. 22–32, Feb 2014. 33

[54] E. Morin, M. Maman, R. Guizzetti, and A. Duda, "Comparison of the device lifetime in wireless networks for the internet of things," *IEEE Access*, vol. PP, no. 99, pp. 1–1, 2017. 33

[55] LoRa™ Alliance, "A Technical Overview of LoRa and LoRaWAN," 2015. 34

[56] N. Sornin, "LoRaWAN 1.1 Specification," tech. rep., LoRa Alliance, Oct. 2017. 34, 35, 46

[57] SIGFOX, "Sigfox Technology Overview," 2018. 35

[58] Sigfox, "Sigfox Technical Overview," 2017. 35

[59] Y.-P. E. Wang, X. Lin, A. Adhikary, A. Grovlen, Y. Sui, Y. Blankenship, J. Bergman, and H. S. Razaghi, "A primer on 3gpp narrowband internet of things," *IEEE Communications Magazine*, vol. 55, no. 3, pp. 117–123, 2017. 36

[60] D. Flore, "3GPP Standards for the Internet-of-Things," GSMA MIoT, London, U.K., Feb. 2016. 36

[61] D. R. J. Schlienz, "Narrowband Internet of Things Whitepaper." 36

[62] O. R. W. Inc, "Light monitoring system using a random phase multiple access system." 36, 37

[63] INGENU, "An Educational Guide: How RPMA works, A white paper by INGENU." 36, 37

[64] Ingenu, "RMPA." 36, 37

[65] Q. M. Qadir, T. A. Rashid, N. K. Al-Salihi, B. Ismael, A. A. Kist, and Z. Zhang, "Low power wide area networks: A survey of enabling technologies, applications and interoperability needs," *IEEE Access*, vol. 6, pp. 77454–77473, 2018. 37

[66] K. Mekki, E. Bajic, F. Chaxel, and F. Meyer, "A comparative study of lpwan technologies for large-scale iot deployment," *ICT Express*, vol. 5, no. 1, pp. 1–7, 2019. 37

[67] Matt Knight, Bastille Networks, "Reversing LoRa, Exploring Next-Generation Wireless." 38

[68] Semtech, "SX1272/73 - 860 MHz to 1020 MHz Low Power Long Range Transceiver," 2017. 39, 46

[69] Semtech, "Sx12172/3/6/7/8 application note an1200.13 modem designer's guide," 2013. 43

[70] Semtech, "Application note an1200.22 lora modulation basics," 2015. 44, 45

[71] "Lora modem designer's guide," tech. rep., Semtech Corporation, July 2013. 46

[72] LoRa Alliance, "LoRa Alliance Geolocation Whitepaper," 2019. 48

[73] Semtech Corporation, "An In-depth Look at LoRaWAN® Class A Devices." https://lora-developers.semtech.com/uploads/documents/files/LoRaWAN_Class_A_Devices_In_Depth_Downloadable.pdf, 2019. 49

[74] Semtech Corporation, "An In-depth Look at LoRaWAN® Class B Devices." https://lora-developers.semtech.com/uploads/documents/files/LoRaWAN_Class_B_Devices_In_Depth_Downloadable.pdf, 2019. 50

[75] Semtech Corporation, "An In-depth Look at LoRaWAN® Class C Devices." https://lora-developers.semtech.com/uploads/documents/files/LoRaWAN_Class_C_Devices_In_Depth_Downloadable.pdf, 2019. 50

[76] A. I. Pop, U. Raza, P. Kulkarni, and M. Sooriyabandara, "Does bidirectional traffic do more harm than good in lorawan based lpwa networks?," in *GLOBECOM 2017 - 2017 IEEE Global Communications Conference*, pp. 1–6, Dec 2017. 55

[77] M. Centenaro, L. Vangelista, and R. Kohno, "On the impact of downlink feedback on lora performance," in *2017 IEEE 28th Annual International Symposium on Personal, Indoor, and Mobile Radio Communications (PIMRC)*, pp. 1–6, Oct 2017. 55

[78] A. I. Pop, U. Raza, P. Kulkarni, and M. Sooriyabandara, "Does bidirectional traffic do more harm than good in lorawan based lpwa networks?," in *GLOBECOM 2017 - 2017 IEEE Global Communications Conference*, pp. 1–6, Dec 2017. 55

[79] M. Capuzzo, D. Magrin, and A. Zanella, "Confirmed traffic in lorawan: Pitfalls and countermeasures," in *2018 17th Annual Mediterranean Ad Hoc Networking Workshop (Med-Hoc-Net)*, pp. 1–7, June 2018. 55

[80] L. Angrisani, P. Arpaia, F. Bonavolontà, M. Conti, and A. Liccardo, "Lora protocol performance assessment in critical noise conditions," in *2017 IEEE 3rd International Forum on Research and Technologies for Society and Industry (RTSI)*, pp. 1–5, Sept 2017. 55

[81] C. Orfanidis, L. M. Feeney, M. Jacobsson, and P. Gunningberg, "Investigating interference between lora and ieee 802.15.4g networks," in *2017 IEEE 13th International Conference on Wire-*

less and Mobile Computing, Networking and Communications (WiMob), pp. 1–8, Oct 2017. 55

[82] T. Voigt, M. Bor, U. Roedig, and J. Alonso, "Mitigating inter-network interference in lora networks," in *Proceedings of the 2017 International Conference on Embedded Wireless Systems and Networks*, EWSN ’17, (USA), pp. 323–328, Junction Publishing, 2017. 55

[83] M. Lauridsen, B. Vejlgaard, I. Z. Kovacs, H. Nguyen, and P. Mogensen, "Interference measurements in the european 868 mhz ism band with focus on lora and sigfox," in *2017 IEEE Wireless Communications and Networking Conference (WCNC)*, pp. 1–6, March 2017. 55

[84] C. Orfanidis, L. M. Feeney, and M. Jacobsson, "Measuring phy layer interactions between lora and ieee 802.15.4g networks," in *2017 IFIP Networking Conference (IFIP Networking) and Workshops*, pp. 1–2, June 2017. 55

[85] B. Vejlgaard, M. Lauridsen, H. Nguyen, I. Z. Kovacs, P. Mogensen, and M. Sorensen, "Interference impact on coverage and capacity for low power wide area iot networks," in *2017 IEEE Wireless Communications and Networking Conference (WCNC)*, pp. 1–6, March 2017. 55

[86] STMicroelectronics, "B-L072Z-LRWAN1." www.st.com, 2018. 73, 86

[87] S. Corporation, "Semtech SX1276." 73

[88] J. Markkula, K. Mikhaylov, and J. Haapola, "Simulating LoRaWAN: On Importance of Inter Spreading Factor Interference and Collision Effect," in *IEEE International Conference on Communications (ICC)*, 2019. 86

[89] NS-3 Consortium, "NS-3 Network Simulator," 2019. 103

[90] D. Magrin, M. Centenaro, and L. Vangelista, "Performance Evaluation of LoRa Networks in a Smart City Scenario," in *IEEE ICC*, May 2017. 104, 113

[91] T. Attia, M. Heusse, B. Tourancheau, and A. Duda, "Experimental Characterization of LoRaWAN Link Quality," in *Proc. IEEE GLOBECOM*, pp. 1–6, 2019. 104, 113

[92] C. Goursaud and J. M. Gorce, "Dedicated Networks for IoT: PHY/MAC State of the Art and Challenges," *EAI Endorsed Transactions on Internet of Things*, vol. 15, 10 2015. 105, 113

[93] T. Attia, M. Heusse, and A. Duda, "Message in message for improved lorawan capacity," in *30th International Conference on Computer Communications and Networks, ICCCN 2021, Athens, Greece, July 19-22, 2021*, pp. 1–9, IEEE, 2021. 110

[94] A. Rahmadhani and F. Kuipers, "When LoRaWAN Frames Collide," in *Proc. WiNTECH '18*, pp. 89–97, 2018. 113

[95] R. Eletreby, D. Zhang, S. Kumar, and O. Yagan, "Empowering Low-Power Wide Area Networks in Urban Settings," in *Proc. SIGCOMM*, pp. 309–321, ACM, 2017. 113

[96] Y. Birk and Y. Revah, "Increasing Deadline-Constrained Throughput in Multi-Channel ALOHA Networks via Non-Stationary Multiple-Power-Level Transmission Policies," *Wireless Networks*, vol. 11, pp. 523–529, July 2005. 114